ELUCIDATING PATHOLOGICAL MECHANISMS OF JOINT DEGENERATIVE DISORDERS

A Dissertation
Presented to
The Academic Faculty

by

Giuliana E. Salazar-Noratto

In Partial Fulfillment
of the Requirements for the Degree
Doctor of Philosophy in Biomedical Engineering

Georgia Institute of Technology
and Emory University

August 2018

ELUCIDATING PATHOLOGICAL MECHANISMS OF JOINT DEGENERATIVE DISORDERS

Approved by:

Dr. Robert E. Guldberg, Advisor
George W. Woodruff School of
Mechanical Engineering
Georgia Institute of Technology

Dr. Nick J. Willett
Department of Orthopaedics
Emory University

Dr. Greg Gibson
School of Biological Sciences
Georgia Institute of Technology

Dr. S. Clifton Willimon
Orthopaedics
Children's Healthcare of Atlanta

Dr. Johnna S. Temenoff
Wallace H. Coulter Department of
Biomedical Engineering
Georgia Institute of Technology

Date Approved: May 29, 2018

To Giuliana D. Noratto Dongo, Katherine A. Salazar Noratto, Gino A. Salazar Noratto, Adonel A. Salazar Mendoza, Doris T. Dongo Montoya and C. Eva Mendoza de Salazar—my family, who has supported me and loved me unconditionally.

ACKNOWLEDGEMENTS

When I think about how many people have been part of this journey, I am amazed at how truly collaborative this thesis work turned out to be. First of all, I need—and want—to thank my advisor, Robert (Bob) E. Guldberg. He has often been more positive about my data and excited about my projects than myself, and his encouragement and positivity were just what my projects needed sometimes. I specially need to thank Bob for being supportive of the iPSC project I pitched to him and of me going to Ireland for a whole year to learn the technology in Frank Barry's lab. This single decision made the difference in the world for my dissertation. I am happy that Bob chose me as one of his graduate students and will be forever thankful for the trust that he placed on me to carry out these projects.

I need to thank the members of my committee as well. I will always appreciate the genuine excitement and interest that Greg Gibson had for my projects, and science in general. He truly opened up his lab for me, and became an amazing mentor in more ways than one. I enjoyed talking to him about science and about life nuances, such as us becoming American citizens. I am happy to have worked with him, and I do sincerely hope that we keep in touch in the future. I met Nick J. Willett as a post-doc in Bob's lab when I first joined the lab, and soon after, Nick became a professor in Emory University. Therefore, I believe that our relationship has leaned more towards peers than with my other committee members. This is why it was so special to me, because I learned from Nick things that I couldn't have from other people. I was able to discuss and disagree with Nick more openly, which gave me the confidence to do the same with senior

professors, and that helped me grow as a scientist. I need to also thank Johnna Temenoff, who pushed me to think more critically of my projects and what contribution I was actually making to the scientific field. It is because of her that Aim 3 became what it did, and I will be eternally grateful for that, because I do think that it helped me become a better scientist. Finally, I need to thank Clifton Willimon, who provided me with patient samples for my JOCD projects and expertise about JOCD as a disease. I truly appreciate the time and effort he gave me considering that he is a very busy surgeon. He made time to meet with me, even if it was at 6 am, and to call me on my phone when I had questions. He was also constantly worried that I needed more patient samples and recruited several staff members at Children's Healthcare of Atlanta to help me. In that sense, I also have to thank Dr. David Busch for being another JOCD doctor who provided me with patient samples and Margaux Johnson, who was the person responsible for coordinating the patient sample collection and until she came around the project was stagnant.

I need to thank my labmates for being the best labmates I could have asked for. Tanushree Thote, Alice Lin, Ashley Allen, and Lauren Priddy were the senior girls (and now doctors) in the lab when I joined, and I learned a lot from them. I also learned about how to be a female scientist, which is something I had never thought would be different from a regular scientist, but I learned that females do still have it difficult in a male-dominated field and that the experiences that we have are not often what our male counterparts would experience. I thank them for fighting the good fight, and I hope to do the same. Marian Hettiaratchi and Marissa Rhuele were great back-row desk-mates, and I am very thankful to have become great friends with them as well. It meant a lot to me

that Marian teleconferenced from Canada to watch my defense, and that Marissa became a close confidant of mine. I will miss Marissa's and mine walks from and to work.

David Reece was a fun labmate to have and his upbeat and friendly personality always lightened up the day. Brett Klosterhoff was also a great labmate, who would be genuinely interested in people's projects and provide feedback and suggestions. His dancing and karaoke skills were also on point! I had a lot of fun hanging out with him and his wife Kayla. Then, there were Albert Cheng, Brennan Torstrick and Olivia Burnsed. We were all the same year, and we made of the lair a real chaos, especially Albert and Brennan—and it was all great fun! I am very happy that I had three other people to share my experiences with and that those two guys became like brothers to me. Albert, especially, was a great, close friend, who helped me in more ways than I could imagine.

Lastly, I also would like to thank Ryan Akman, Gilad Doron, Angela Lin, and Laxmi Krishnan for their friendliness and readiness to help, especially during surgeries, and Casey Vantucci for her crazy friendship. And of course, I need to thank Hazel Y. Stevens for all the help she has provided me. More than scientifically, it has been emotional help. She has truly helped me finished up my dissertation, by ordering materials at late hours of the night and reading my papers and chapters. She has been like a (lab) mother to me these past couple of months, and I am eternally grateful to have had her in my life and my lab life. The Guldberg lab will definitely never be the same without her! Moreover, I would like to take this opportunity to thank Eric O'neil, who is Andres Garcia's lab manager, but who helped me nonetheless with lab and protocol-related questions in the absence of Hazel.

I had several undergraduate students work with me in these projects that I need to thank. Destiny Cobb was my first undergraduate student, and I have to thank her for teaching me how to be a better manager and mentor for future students. Nica De Nijs was an amazing undergraduate, who helped me a lot with the first project and while I was in Ireland. She remained in Atlanta in charge of culturing JOCD skin fibroblasts, and there is no one else in the world I would have trusted to do this job. She is a real hard-worker and she deserves the best. Mohib Hasain and Catriana (Cat) Nations were my last students, and they helped me with the last project in particular. I specially need to thank Cat for all the help she provided me this last month. Even when things were wrapping up, there was a lot to do and she stayed many nights until 3 am or later with me just to help me finish. She also provided me with a constant supply of coffee and some snacks, for which I was really grateful. Her dedication to the JOCD project was astounding, and I will always appreciate the help and time she gave me.

The third project of this thesis work was carried out in collaboration with Frank Barry's lab in the National University of Ireland Galway, and I need to thank him and his lab. When I pitched the JOCD project to Bob, he was highly skeptical and it was Frank Barry's support and enthusiasm that convince him that this was a project worth pursuing. Therefore, I have to thank Frank not only for hosting when I was in Ireland learning about iPSCs, but really for believing in this project from the very beginning; participating in the National Science Foundation/Science Foundation Ireland grant I wrote and helping me give form to this idea. I also would like to thank Mary Murphy who was also a mentor while I was in Ireland and was always interested in the work I was doing and provided valuable feedback.

I would like to thank Katya McDonagh and Stephanie Boomkamp, post-doctoral fellows at the time in the Regenerative Medicine Institute (REMEDI), for helping me with the iPSCs. Culturing iPSCs is a difficult task, especially when the medium formulations required daily changes (not longer the case for future iPSC scientists), and I do not think I could have made it without the iPSC community in REMEDI. Katya and Stephanie taught me best practices for iPSC culture and taught me what I could get away with dong or not doing. Most importantly, they helped me feed my iPSCs when I needed a break from the long 12-hour-plus feeding days, or when I injured my shoulder. Besides labwork, Katya and Stephanie were my best friends in Galway, and I have countless fond memories of our infamous steak and wine dates.

Sean Gaynard helped me with the mesenchymal stem cell aspect of the third project, and I am immensely grateful that, busy as he was writing his own dissertation, he came in the weekends to help me run flow for multiple hours in a day. Cathy Brougham helped me with adipogenesis, but most importantly, she helped me as a labmate and a friend. I truly do not know what I would have done without the support of Cathy and Claire Dooley in the lab. They helped me ship my cells and they would help me in assays for which I wasn't an expert in. Claire, especially, helped me stained the iPSCs for pluripotency when I was swamped with other work. These girls were the labmates I needed in Ireland, and they were also my best friends. I will never forget about Monday dinner nights turned shots/wine night outs, or the Irish lock-ins. Cathy was particularly working long hours as well to finish her thesis work, and I am grateful that she was there at late hours and on weekends with me, and that we would go out after lab in very classy Irish style (me with my backpack).

Living in Ireland taught me many things and allowed me to mature as a scientist and person. The lesson that I perhaps value the most is that, despite weather or workload, one should always have a good amount of crazy fun! Irish fun was my kind of crazy fun, and I am grateful for the experience and the people who contributed to this experience. I am also thankful to Silvia Rosati, Swarna Raman and Patrizio Mancuso for being my labmates and friends in Ireland.

Besides REMEDI and the Barry lab, the Gibson lab was my other foster lab. Greg Gibson opened up his lab to me and allowed me to make it my home, and I am grateful for that. I am also thankful to Dalia Arafat for helping me with the technical aspect of Fluidigm, as well as Monica Pena-Rojas who taught me the JMP software and was involved in the original JOCD project collaboration with Children's Healthcare of Atlanta. I am thankful to the Drissi lab and Hicham Drissi specifically because, even though he was not involved in my project or was a collaborator, he took the time to meet with me in multiple occasions to talk about the third project (JOCD) and took genuine interest in my career as a scientist.

The scientific work in this thesis could not have been possible without the IBB core labs. I specially want to thank Aqua Asberry (histology), Andrew Shaw (optical microscopy), and David Small (mass spectrometry). In the Emory core labs, I would like to thank Hong Yi who carried out the TEM work, which was not presented in this thesis. I would also like to thank Laure Paige (BioE coordinator) for helping me get through the logistics of these last couple of months, even though I was not part of the BioE program.

At this point, I would like to thank my friends, which truly became my Atlanta family. I was lucky to part of the 2012 Biomedical Engineering (BME) Cohort, which in my opinion was the most friendly, fun, and collaborative. Cheryl San Emeterio (née Lau) was the first person who talked to me and became my friend in the program, and she introduced me to the rest of our squad: Elizabeth (Betsy) Campbell, Candice Hovell, Claire Olingy (née Segar), and Efrain Cermeño. I cannot begin to imagine my life in Atlanta without these people. They have all been supportive through tough times and essential to all the fun activities and memories I experienced in Atlanta and during my Ph.D. Betsy will always be the voice of reason to me (and an amazing gin friend), and Efrain my dancing and drinking buddy. Melissa Alvarado-Velez and Juliana Soto-Giron were also my best friends, and I am thankful for having them through the fun and tough times of this Ph.D. journey. Finally, the lair people, who are the graduate students of the Guldberg and Garcia labs, have also been an important part of my life here.

Before thanking my family, I do need to thank two more people who I believe have played an essential role in my accomplishments. Firstly, Linda Jo Huff (née Martinez) was my sophomore (high school) math teacher. I connected with her more than I had with any other teacher, and it was with her help that I won multiple scholarships for college, because her letters of recommendation assured the committees that she had faith on me beyond any reasonable doubt that I was going to make a difference in the world. I can only hope that I do not disappoint Mrs. Huff. Secondly, I would like to thank Dr. Kristen Maitland, who is a professor in BME at Texas A&M University, my undergraduate institution. Dr. Maitland never taught me a single course, and yet she helped me write my NSF Graduate Research Fellowship Program Application and polish

it. I do believe that she helped me win the NSF fellowship, and it was because she genuinely wanted to help this undergraduate student, me. She also taught me something that was very empowering and I will never forget: that I should not let people tell me that I have gotten where I am because I am a female or a minority. My identities do not cancel out my accomplishments, which were earned with hard work and sweat. I believe that it is people like Dr. Maitland that will change the science world for the better, and I will always be thankful that she changed my world.

Finally, my family. I am grateful for all the love and support my family has always provided me. I have a big family, with more than 15 cousins, and they all have always believed in me and have been proud of every accomplishment along the way, no matter how small. My uncle Gino Noratto flew from Peru for my defense presentation, and that meant the world to me. I know that all of my other uncles and aunts would have loved to be here as well, and I also know that I would not be who I am today without my family. I am thankful that my sister, Katherine (Kati) Salazar-Noratto, grew up with me, because I know now that I will always have a friend in her no matter what happens. Her support and her constructive criticisms are things I really value in our friendship. My brother, Gino Salazar-Noratto, is the best person I know in this world, and he always believes the best of me. His love and understanding have carried me through many situations and especially this Ph.D. journey. I am also thankful for my dad, Adonel Salazar Mendoza, for always trying his best.

My mom, Giuliana Noratto Dongo, is the strongest woman I know, and after finishing this Ph.D. journey, I am simply in awe at how she was able to do her own Ph.D. as a single mother with three (very difficult) children. She is my hero, because since I

was little she taught me that “si no puedes es porque no quieres” (if you can’t do something, you must not really want it). Her resilience and constant drive to better herself are characteristics I admire. It is because of her that I am strong, confident, and a female scientist. It is because of her that I believe all dreams are attainable and that we, as humans, can do anything in the world as long as we set out minds to it. It is, really, because of her that this thesis work has been accomplished. I thank my mother for all of her support—especially her emotional support through turbulent times during this journey—and for coming to take care of me when I needed her to and helping me analyze data when I was overwhelmed.

TABLE OF CONTENTS

LIST OF TABLES

LIST OF FIGURES

LIST OF SYMBOLS AND ABBREVIATIONS

ANOVA	Analysis of variance
BM-MSC	Bone marrow-derived mesenchymal stem cell
BMP	Bone morphogenetic protein
cDNA	Complementary deoxyribonucleic acid
DMOAD	Disease-modifying osteoarthritis drug
DNA	Deoxyribonucleic acid
EB	Embryonic body
ECM	Extracellular matrix
ELISA	Enzyme-linked immunosorbent assay
EPIC-μCT	Equilibrium partitioning of an iconic contrast agent via micro-CT
ER	Endoplasmic reticulum
ERSD	Endoplasmic reticulum storage diseases
FDA	The Food and Drug Administration
GAG	Glycosaminoglycans
H&E	Hematoxylin and Eosin
IHC	Immunohistochemistry
iMSC	Induced pluripotent stem cell-derived mesenchymal stem cells
IL	Interleukin
iPSC	Induced pluripotent stem cell
JOCD	Juvenile Osteochondritis Dissecans
MCL	Medial collateral lligament
MIA	Monosodium iodoacetate

MMP	Matrix metalloproteinase
MMT	Medial meniscus transection
MSC	Mesenchymal stem cell
NBF	Neutral buffered formalin
NO	Nitric oxide
OA	Osteoarthritis
OCD	Osteochondritis Dissecans
PTIC	Protein transport inhibitor cocktail
QRO	Quantile range outlier
RA	Rheumatoid arthritis
rER	Rough endoplasmic reticulum
RNA	Ribonucleic acid
ROS	Reactive oxygen species
RT-PCR	Real time polymerase chain reaction
RT	Room temperature
SD	Standard deviation
SEM	Standard error of the mean
sGAG	Sulfated glycosaminoglycans
TEM	Transmission electron microscopy
TNF	Tumor necrosis factor
TUN	Tunicamycin

SUMMARY

Joint degenerative disorders impose a large burden on lifestyle and the healthcare system. The goals of this thesis were to elucidate pathological mechanisms in osteoarthritis (OA) and juvenile osteochondritis dissecans (JOCD) in order to improve understanding of these diseases, and to provide well-characterized platforms for therapeutic development and testing. OA is the leading cause of disability in the U.S., and it is a disease of the joint that affects multiple tissues. Despite breakthroughs in molecular events (e.g. mechanisms in cartilage degradation), its pathological mechanisms are still largely unknown. There are currently no FDA-approved disease modifying OA drugs (DMOADs), despite promising preclinical data. In order to bridge the gap in knowledge between preclinical and clinical studies, we characterized molecular events that occur in the rat medial meniscus transection (MMT) model of post-traumatic OA as the disease develops and progresses. Our results indicated that pathological events in the articular cartilage and synovium of the MMT model are similar to known human OA development. Our results also suggested feedback interactions between joint tissues during disease progression.

Second, we investigated the mechanisms of action of micronized dehydrated human amnion/chorion membrane (AmnioFix Injectable, MiMedx, USA) in order to elucidate potential disease-modifying mechanisms of this therapeutic. Results showed that AmnioFix does not have a direct influence on the gene expression of articular cartilage or tissue from the osteophyte-forming region of the joint. Instead, AmnioFix acted through the synovial membrane, modulating its microenvironment to a favorable

chondro-protective profile. These results further supported the importance of tissue interactions in the MMT model and in OA, and also provided a new view point concerning disease-modifying approaches for OA.

JOCD is an increasingly common disorder that affects children and adolescents with an open physis. JOCD results in the partial or complete fragmentation of a necrotic osteochondral body from the parent bone, which permanently affects the joint and alters its mechanics. Therefore, JOCD patients have a higher probability of developing OA at an early age. JOCD presents a unique challenge, as treatment strategies are limited to surgical interventions at advanced stages. Although there a number of hypotheses about the etiology of JOCD, its pathological mechanisms are yet to be investigated. In this thesis, we established induced pluripotent stem cell (iPSC)-derived models of JOCD chondrogenesis and endochondral ossification in order to study its pathology. Our results demonstrated that cells from JOCD patients have a lower chondrogenic capacity than normal, control cells. Results also showed that although endochondral ossification is successfully accomplished, there may be irregularities in its process. We also established ER-stress induction models in order to dissect mechanistically how JOCD-iPSC-derived mesenchymal stem cells (iMSCs) responded to ER stress. Our results showed that JOCD cells have a different response to ER stress, which could lead to cell death should the ER stressor persist. We propose that this pathological feature could lead to the onset of clinical JOCD.

Taken together, this thesis significantly contributed to the knowledge gap of OA and JOCD pathomechanisms. This work provided new insights into development of joint degeneration in the MMT model and established a well-characterized baseline to evaluate

mechanistic effects of potential therapeutic agents in this OA-like model. It also investigated mechanisms of action of AmnioFix, which may be leveraged to develop more specific DMOADs. Most importantly, this thesis presented pioneering work on patient-specific iPSC-based disease modeling. This is the first study to elucidate pathomechanisms of JOCD and to establish JOCD-specific *in vitro* models for future therapeutic testing.

CHAPTER 1. SPECIFIC AIMS

1.1 Introduction

As the population ages and lives longer, joint degenerative disorders impose a larger burden in the healthcare system. Osteoarthritis (OA) is the most common form of musculoskeletal disability, affecting approximately 30 million people in the US alone [1]. It is forecast that one in four people will develop OA in their lifetime [2]. Due to its complexity and the many interactions in the joint space, the pathological events that take place in OA development remain largely unknown. Therefore, current available treatments are limited to pain management and eventual total joint replacement.

When OA affects the working or pediatric populations, the burden on lifestyle and the healthcare system increases. Juvenile OsteoChondritis Dissecans (JOCD) affects children and adolescents, and often progresses to early onset OA. The etiology of JOCD is not fully understood, but it is believed to be a combination of factors such as biomechanical overuse, trauma, and genetic predisposition. Unfortunately, molecular pathological mechanisms are virtually unknown. Previous research has been primarily focused on retrospective clinical studies, which has also hampered the development of effective therapeutics for this disorder and the prevention of its progression to OA. Current treatments are limited to invasive surgical interventions to salvage the necrotic lesion at advance stages of this disorder.

The **overall objective** of this thesis is to elucidate pathophysiological mechanisms of OA and JOCD models in order to fill gaps in knowledge as well to provide the field

with well-characterized platforms for future therapeutic development and testing. We approached this objective through the following specific aims:

1.2 Specific Aim I

Investigate localized molecular events of disease progression in an *in vivo* post-experimental model of post-traumatic OA

The rat medial meniscus transection (MMT) model is a frequently used model of post-traumatic OA and is of high clinical relevance. This model replicates many characteristics attributed to human OA, such as cartilage degeneration, osteophyte and focal lesion formation, and cartilage fibrillation. However, this model has not yet been characterized at the molecular level. The microenvironment that treatments encounter upon delivery is unknown and thus mechanisms of action for the therapeutic in question cannot be properly assessed. The *objective of this aim* was to characterize the MMT OA model at the molecular level (gene expression), for multiple tissues, regions of interest within the joint, and timepoints. *Our hypothesis* was that the MMT model replicates some of the observed human OA pathomechanisms, such as degradation and remodeling of the extracellular matrix (ECM) of the articular cartilage and chondrocyte dedifferentiation.

1.3 Specific Aim 2

Elucidate therapeutic mechanisms of micronized dehydrated amnion/chorion membrane as a potential disease-modifying OA drug

In a previous study, intra-articular delivery of micronized dehydrated human amnion/chorion membrane (AmnioFix Injectable, MiMedx, GA, USA) showed a

chondro-protective effect in the MMT post-traumatic OA animal model [3]. AmnioFix is hypothesized to act through the synovial membrane. However, it is unknown how AmnioFix modulates the microenvironment of the synovial membrane or the joint space, if at all. As an ECM-based treatment, AmnioFix Injectable contains a cocktail of growth factors and cytokines, and so, in order to dissect its potential disease-modifying attributes, in-depth molecular analyses need to be performed. The *objective of this aim* was to elucidate the mechanisms of action (via microarray gene expression) of AmnioFix Injectable in the MMT model, in multiple tissues of different regions and at multiple timepoints. *We hypothesized* that AmnioFix does indeed act through the synovial membrane, down-regulating ECM degradation markers in the synovium, which protects the articular cartilage from a faster degradation rate.

1.4 Specific Aim 3

Develop patient-specific iPSC-derived *in vitro* models of JOCD in order to elucidate pathological mechanisms

iPSCs allow an endless supply of patient-specific cells and to be able to study multiple aspects of the same disease by differentiating multiple tissues. Because JOCD occurs in the still-developing pediatric population, its onset has been theoretically linked with aberrations in the differentiation of the secondary physis. Previous research has studied JOCD primary chondrocytes, but not chondrogenic differentiation or endochondral ossification, which occur in the affected joints around the time JOCD develops. Moreover, other diseases under the OCD umbrella (familial and equine) have

been directly associated with ER dysfunction, yet there are no studies to this date that have investigated this pathological feature in JOCD patients.

The objective of this aim was to develop and study patient-specific iPSC-derived *in vitro* models of JOCD of chondrogenesis and endochondral ossification (both considered important processes in JOCD) and of ER-induced stress. *Our overarching hypothesis* was that JOCD patients have a suboptimal bone matrix synthesis and assembly due to impaired ER-stress-related responses, which may lead to a higher susceptibility to clinical JOCD. These models did not only shed light in our understanding of JOCD pathology, but also provided the field with well-characterized platforms for testing of therapeutic interventions.

1.5 Significance and Scientific Impact

The burden of joint diseases is continually increasing as the population lives longer and the incidence of co-morbidities (e.g. obesity) increase. The lack of effective disease-modifying therapeutics is in part due to a gap in knowledge concerning the pathological mechanisms of these diseases and the relevance of pre-clinical models. The work described in this thesis is significant because it provides novel information that may help bridge this gap for OA and JOCD. It also presents innovative tools and platforms to test new therapeutic interventions for these diseases.

OA is a complex multi-tissue joint disease with various sub-phenotypes. Therefore, the models in which potential drugs are tested should be thoroughly characterized in order to understand the mechanisms of action of the therapeutic and to infer for which OA cases it may be most efficacious. This thesis is the first to utilize

microarray gene expression technology to characterize the molecular events of OA development in multiple tissues and regions of interest in the MMT post-traumatic model. This work will provide the scientific community with a baseline to determine whether the MMT model is appropriate for testing the therapeutic in question. Furthermore, by studying molecular events in the MMT model, we shed light on tissue interactions and the complexity of OA-like development in this model.

This work has also isolated molecular events that occur in the MMT model as a response to ECM-based therapeutic AmnioFix Injectable. AmnioFix is currently considered a potential disease-modifying treatment, and by utilizing our microarray gene expression tool, we were able to suggest mechanisms that may be leveraged to create a more specific therapeutic than AmnioFix. This thesis introduces the scientific community to a perspective concerning the treatment of OA. Conventional approaches often seek to treat or inhibit pro-inflammatory pathways within the joint; instead, we suggest the approach of modulating the microenvironment of the joint towards a phenotype that promotes wound healing mechanisms.

While OA is an active area of research within the musculoskeletal field, research about the development and pathology of JOCD is very limited. This work is the first to investigate JOCD differentiation mechanisms, in chondrogenesis and endochondral ossification, as well as JOCD-specific mechanistic response to ER stress. By developing JOCD-specific iPSC-derived *in vitro* models, not only did this thesis introduced cutting-edge technology to the field, but it also became the first work to elucidate possible pathological molecular events in JOCD. Early therapeutic interventions in JOCD are conservative and with a high rate of failure (34% to 50%, [4-7]). The observations

presented in this work may help in the development of treatments and thus possible prevention of OA in these patients. This work has also significantly contributed by being the first to introduce JOCD-specific *in vitro* models, both of differentiation and of ER-stress induction.

CHAPTER 2. BACKGROUND

2.1 Osteoarthritis

OA is the most common cause of musculoskeletal pain and disability worldwide, with almost $200 billion per year impact on healthcare costs in the U.S. [1, 8, 9]. Although typically viewed as a result of bodily "wear and tear", OA is now considered a multifactorial disorder and to affect multiple tissues within the joint cavity. OA can be divided into subtypes, some of which might have a more biochemical, inflammatory or genetic signature than others, but all of which eventually converge into the common phenotype [10]. OA is a full organ disease, and it is characterized by the progressive breakdown of the articular cartilage, the formation of bony outgrowths at the joint margin (osteophytes), subchondral bone sclerosis, hypertrophy of the joint capsule and inflammation of the synovial membrane (synovitis) [11, 12]. Despite improved understanding, the consequences of pathological events in OA are still poorly understood. This is in part due to the heterogeneity of the disease and the complexity of interactions among the different tissues within the joint space. Many questions remain about missing links (unknown processes) and how the known processes come together to mediate the pathogenesis of OA.

Currently, there are no FDA-approved DMOADs in the market. Therapeutic interventions are targeted towards symptomatic management via pain control, viscosupplementation (via intra-articular injections of hyaluronic acid) and joint replacements [3, 9, 12]. Knee replacements alone cost nearly $30 billion annually in the U.S., and they are primarily attributed to knee OA [13]. Total joint replacements are only

expected to last 15 to 20 years; therefore, doctors do not recommend these surgeries to patients younger than 50 years old. This younger population has to endure OA symptoms for longer periods of time despite their advanced stage, and when given the replacement surgery, they outlive the implants and need revision surgeries. Although OA is typically associated with old age, with approximately 37% of the US population over 60 years of age affected [12, 14, 15] and 45% adults expected to suffer from it by the age of 85 [16], it also afflicts the young (Figure 1). Degenerative joint diseases impose a larger and longer-term burden on the healthcare system when they affect working or pediatric populations. Younger people may develop OA as a result of injury, overuse or as a secondary effect of another joint disorder.

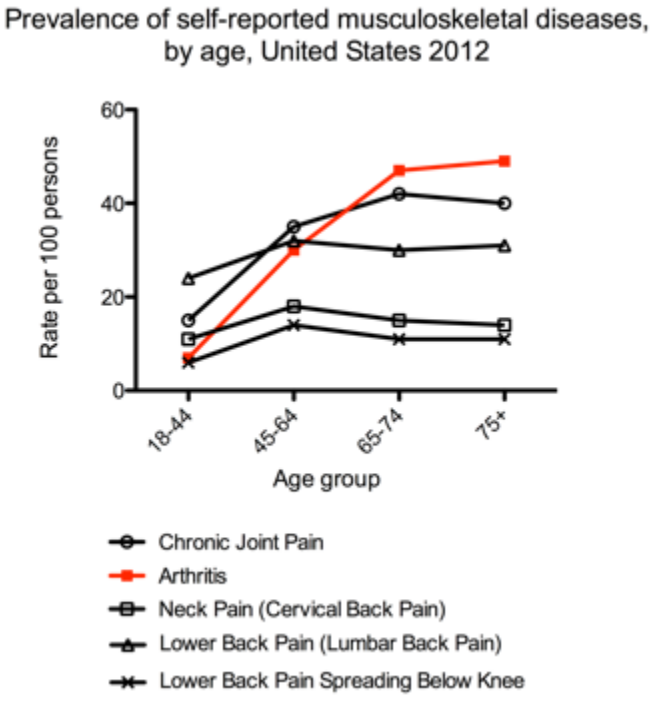

Figure 1. Prevalence of self-reported musculoskeletal disease by age group, reported by the National Health Interview Survey (NHIS): Adult sample (July 2nd, 2013).

2.1.1 Biological and molecular pathomechanisms

2.1.1.1 Cartilage

Key events occurring in cartilage during pathogenesis of OA include an imbalance of metabolic and degradative signals, driven by cytokine cascades and the production of inflammatory mediators [17]. Moreover, altered biomechanics, such as those seen in joint malalignment, obesity or advanced stages of OA, induce and potentiate further biochemical changes. Mechanical stress, by both static and intermittent compression, increases nitric oxide (NO) production by chondrocytes as well as nitric oxide synthase expression [17]. NO contributes to articular cartilage damage: it inhibits collagen and proteoglycan synthesis, activates matrix metalloproteinases (MMPs), and increases susceptibility to other oxidant injury [17]. Furthermore, two important pathogenic events characteristic of OA chondrocytes, premature senescence and apoptosis, appear to results from NO and other oxidative injury [17-21]. As a result, it has been postulated that OA is a disease of premature aging of the joint; mechanically driven, and chemically, particularly reactive oxygen species (ROS)-mediated [17].

2.1.1.2 Synovium

Accumulating evidence indicates that inflammation has a critical role in OA pathogenesis, and that this inflammation is distinct from that in rheumatoid arthritis and other autoimmune diseases: it is chronic, comparatively low-grade [12]. Because of this feature and its low synovial fluid leukocyte counts, OA is classified as a non-inflammatory arthritis. Yet, synovitis occurs even in early OA and can be sub-clinical, as arthroscopic studies suggest that localized proliferative (thickening) and inflammatory

changes of the synovium occur in up to 50% of OA patients – many of whom do not appear to have active inflammation [11, 17, 22]. Unlike rheumatoid arthritis, synovial inflammation of OA is mostly confined to areas adjacent to pathologically damaged cartilage and bone [23], which suggests that synovitis is a response to cartilage injury.

Once cartilage breakdown has begun, the synovial cells phagocytose the breakdown products released into the synovial fluid, resulting in the synovial membrane becoming hypertrophic and hyperplasic [11]. The activated synovium then releases pro-inflammatory cytokines and catabolic mediators, which further alter the balance of cartilage matrix degradation and repair and lead to excess production of the proteolytic enzymes responsible for cartilage breakdown [11]. In this sense, the synovium and the cartilage enter a positive feedback loop, in which destructive molecules are produced in a vicious autocrine and paracrine fashion [17]. This inflammatory response is amplified by activated synovial T cells, B cells and infiltrating macrophages [11].

To counteract this inflammatory response, the synovium has shown to produce anti-inflammatory cytokines, which decrease the release of pro-inflammatory cytokines and MMPs and inhibit the apoptosis of synovial cells, thus contributing to synovial hypertrophy [11]. Unfortunately, persistence of the stimuli (injured cartialge) greatly complicates the resolution of this inflammatory response in the synovium.

2.1.1.3 Bone

Given the intimate contact between the cartilage and bone, alterations of either tissue will modulate the properties and function of the other joint component [24]. Marked alteration in the contour of the adjacent articulating surfaces in OA result in

modification in joint congruity that contribute to an adverse biomechanical environment for both the bone and the cartilage itself [24]. Then, cellular processes of remodeling and modeling occur in the bone as an adaptation to mechanical loads and damage.

Bone changes in OA can be divided into distinct patterns based on the anatomic location and mechanisms involved in their pathogenesis [25]. These alterations include progressive increase in subchondral plate thickness, modification in the architecture of subchondral trabecular bone, formation of new bone at the joint margins (osteophytes), development of subchondral bone cysts, bone marrow lesions, and advancement of the tidemark associated with vascular invasion of the calcified cartilage [24-27].

Osteophytes are commonly thought to develop from mesenchymal cells in or near the periosteum [28, 29], as a repair response to help stabilize degrading joint surfaces [25], even though osteophytes also cause obvious negative effects such as pain and loss of movement [30]. In this process, periosteal mesenchymal cells begin to proliferate at the joint margin and subsequently differentiate into chondrocytes that undergo hypertrophy and then endochondral ossification to create an enlarging skeletal outgrowth at the joint margin [25].

Osteophyte formation is thought to be initiated and accelerated by the local production of growth factors, particularly from the inflamed synovium. Apart from mediating synovial activation, macrophages in the synovial lining can produce several growth factors in high quantities, including chondroosseous-forming factors (e.g. transforming growth factor-β, and bone morphogenetic protein-2 and -4) [30]. In several models of experimental arthritis, selective depletion of macrophages from the synovial

lining prevents osteophyte formation [30-32]. Thus, synovial macrophages are crucial intermediaries in the formation of osteophytes.

2.2 Juvenile osteochondritis dissecans

JOCD is an increasingly common cause of pain and dysfunction among skeletally immature and young adult patients (typically ages 6 to 19), and progresses to early onset OA [33-36]. Increased incidence is in part due to earlier and increasingly competitive athletic endeavors and improved advanced imaging technology and diagnostic guidelines [37-39]. The majority of JOCD lesions (61.7% [40]) are found in the knee, most commonly in the medial femoral condyle. A study found that out of all JOCD lesions, 35.3% progressed to surgery, and out of that percentage, 58.5% were knee JOCD [40].

JOCD is hypothesized to initially involve the formation of an avascular lesion in the subchondral bone with secondary effects in the overlaying articular cartilage [33, 34, 41]. During late stages of this musculoskeletal disorder, the lesion becomes unstable and separation of an osteochondral fragment (loose body) ensues (Figure 2). Lesions early in their course are associated with poorly defined symptoms: variable pain and swelling. As the lesion progresses, catching, locking and pain are constant. The etiology of JOCD is not fully understood but believed to be a multifactorial combination of biomechanical overuse and genetic predisposition. However, previous research has been primarily limited to retrospective clinical studies, and no study to date has thoroughly characterized the pathological mechanisms associated with the onset and progression of JOCD [34]. An improved understanding of the pathobiological mechanisms of JOCD may facilitate the

development of more effective treatment options and ultimately prevent the development of OA at an early age in these patients.

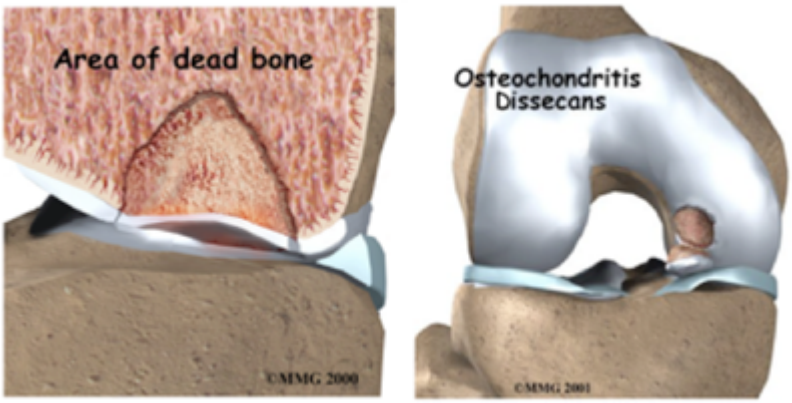

Figure 2. Osteochondritis Dissecans results in the formation of a loose body in the joint space. Osteonecrosis of the subchondral bone and degradation of the overlaying articular cartilage are key characteristics. Source: www.eorthopod.com (osteochondritis dissecans).

2.2.1 Diagnosis and Classification

Osteochondritis dissecans (OCD) has been traditionally subdivided into two types, juvenile (JOCD) and adult, on the basis of physeal closure [35]. Currently, there exist several classification systems for OCD based on radiographs, MRI findings, and arthroscopically. The MRI and arthroscopic gradings have been shown to be highly correlated [42], yet further research and collaboration is still needed to reach a consensus to accurately describe OCD lesions [42, 43]. Imaging methods fail to provide conclusive evidence on the subchondral fragment stability unless the osteochondral fragment has dissecated [36].

Recognizing the need for a more standardized and universally accepted systems, the International Cartilage Repair Society (ICRS) published an OCD classification system (Table 1), applicable to both JOCD and adult OCD. This classification is based on superficial assessment of the articular cartilage surface, and is used widely as a basis to determine the course of patient treatment.

Table 1. ICRS OCD grading score [44]. Grades I and II are considered stable lesions, while III and IV are unstable.

Stage	Characteristics
I	Stable lesions with a continuous but softened area covered by intact cartilage
II	Lesions with partial discontinuity that are stable when probed
III	Lesions with a complete discontinuity that are not yet dislocated ("dead *in situ*")
IV	Empty defects and defects with a dislocated fragment or a loose fragment within the bed

*Subgroups ICRS OCD I-IVB are lesions greater than 10 mm in depth

JOCD cases are typically classified into ICRS OCD grade I/II (stable lesions). Despite the stable and normal appearance of articular cartilage, however, there is a controversy about conservative treatment of JOCD, where healing is reported in up to 50% of cases [5, 39]. The cause of treatment failure in these JOCD cases is still unclear, and may be attributed to the initial diagnosis and classification system from which clinician determine the appropriate treatment option. Kijowski *et al* showed that previously described MRI for describing OCD instability has a higher specificity for

adult (100% sensitivity, 100% specific) but not juvenile lesions of the knee (100% sensitivity, 11% specific) [45].

Moreover, Yonetani *et al.* demonstrated that JOCD lesions in 8 symptomatic patients had pathological instability despite stability at the articular surface [35]. Arthroscopically, the surface of the JOCD lesions appeared normal and stable. Cylindrical biopsy (articular cartilage and bone) samples were obtained, and the extent of damage was histologically evaluated. It was found that all biopsy specimen had undergone separation between the cartilage and the subchondral bone, and that fibrous and fibro-cartilage tissue filled in the separation site [35]. Therefore, there is a clear need for an improved understanding and classification method for JOCD patients exclusively. In spite of similarity, studies have demonstrated that there are physical features in adult OCD, which are absent in JOCD. These distinct differences may be explained by the level of skeletal maturation, and are sufficient to warrant separate diagnosis and classification for JOCD.

In a recent epidemiology study, Weiss *et al* showed that progression to surgery for OCD of the knee, elbow, and ankle strongly correlated with patient age at the time of diagnosis [40]. Patients aged 12 to 19 years were 8.2 times more likely to progress to surgery for all OCD lesions than patients aged 6 to 11 years [40]. This drastic difference even among skeletally immature patients further supports the need for a better system of JOCD classification in order to accurately diagnose a stage and its most appropriate treatment. While imaging technology has helped push forward JOCD diagnosis, it has shown its limits, and the implementation of biological markers may steer towards an improved precise medicine.

2.2.2 Treatment

The management of JOCD is controversial. A number of factors need to be taken into account when choosing the appropriate course of treatment: skeletal maturity, fragment size, fragment location, and fragment stability [36, 46]. A lesion is classified into 3 main groupings: articular cartilage intact, articular cartilage separated (unstable), and fragment completely loose. The designated classification influences the surgical treatment, as shown in Figure 3.

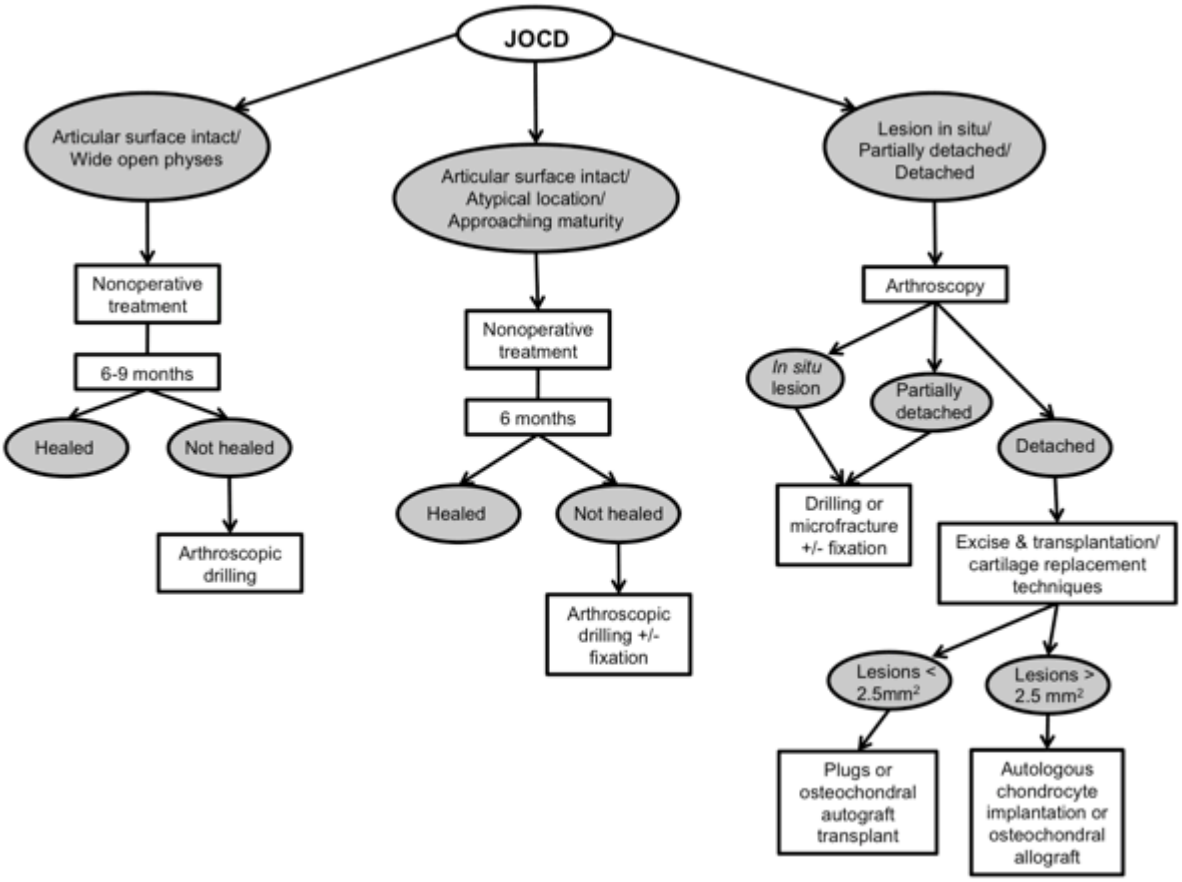

Figure 3. Decision-making algorithm for treating JOCD of the knee [47, 48].

Reportedly, non-operative treatment of JOCD is very successful in properly selected patients. However, thanks to the implementation of advanced imaging techniques with a higher sensitivity for diagnosis and outcome evaluation of JOCD, new studies have started to report a much higher rate of failure. Wall *et al.* showed 34% failure after non-operative treatment using MRI, while Cahill *et al* reported 50% failure using more sensitive bone scintigraphy and radiographs [4-6]. Pain and/or mechanical symptoms or lack of evidence of healing on radiographs or MRI that persist represent failed non-operative treatment and indicate the need for surgery in up to 50% of patients with stable JOCD lesions [4]. With non-operative treatment, an estimated 5% cumulative incidence at 5 years after diagnosis developed symptomatic OA; 10% at 10 years, 20% at 25 years, and 30% at 35 years [49]. Depending on the age at which JOCD was diagnosed, this could mean developing OA as early as 15 years of age.

Bone marrow stimulation techniques, in particular arthroscopic drilling, is recommended for stable lesions with intact cartilage. The goal of this technique is to create channels for vascular ingress stimulating local revascularization [36]. This technique has been successful in skeletally immature patients, with healing rates of 75% and higher [7, 50]. In patients with unstable or partially detached (ICRS OCD grade III) lesions, fixation with pins or screws is the treatment of choice. Despite success rate, patient morbidity associated with intra-articular fragment fixation and complications have been reported in a number of cases [36]. Once the lesion has reached ICRS OCD grade IV, the loose osteochondral fragment is excise and salvage procedures include perichondral/periosteal autografts, autogeneous cell transplantation, abrasion chondroplasty, osteochondral autografts, and osteochondral allografts depending on the

size and appearance of the lesion [46]. Unfortunately, most of these treatment options result in the formation of fibrocartilage covering over the exposed defect rather than true hyaline cartilage [36, 39, 46]. The long-term results from these procedures have yet to be clearly determined [46], but fragment excision procedures have reported 79% degenerative findings at a mean 11 year follow-up [51]. Advanced OCD lesions cause mechanical disruption of joint motion, loose body formation, mechanical wear, and attrition of associated surfaces on the tibial plateau or the meniscus [39]. In short, they lead to the onset of OA.

2.2.3 Etiology

2.2.3.1 Repetitive trauma

Repeated microtrauma is the most recognized cause of OCD, because of the rising incidence of this disorder among athletes. Aichroth *et al.* demonstrated 60% of the patients with OCD in his study were involved in high-level, competitive sports [52]. A multicenter study conducted by the European Pediatric Orthopeadic Society found nearly 55% of the patients with OCD were either regularly active in sports or performed "strenuous athletic activity" [53].

The classic location of OCD in the posterolateral portion of the medial femoral condyle suggests that indirect trauma is more likely the cause [54]. Repeated impingement of the tibial spine on the lateral aspect of the medial femoral condyle during internal rotation of the tibia has also been suggested to be a contributing factor [54, 55]. However, this theory would only explain lesions in that particular location.

2.2.3.2 Ischemia

Ischemia has been proposed as a potential cause of OCD. Enneking *et al.* found the vascular supply to the subchondral bone to have poor anastomoses to surrounding arterioles [54, 56]. It has been suggested that this propensity for ischemia could lead subchondral none to form sequestra, making it particularly vulnerable to traumatic insult, resultant fracture, and potential separation [54]. However, this hypothesis has met a number of opposing arguments. Rogers and Gladstone studied the vascularity of the distal part of the femur and found numerous anastomoses to intramedullary cancellous bone [57]. Milgram demonstrated revascularization in 50 OCD lesions that were only partially attached [58]. Furthermore, a few studies have shown a lack of osseous necrosis upon examination of intact OCD lesions [35, 59], which may suggest that necrosis found in OCD may be secondary to the actual detachment of the lesion rather than the underlying etiology of formation [51]. Moreover, a number of research scientists believe the ischemia hypothesis to be less likely in JOCD cases, because these young patients probably have a good distal femoral blood supply (for knee OCD cases) [34].

2.2.3.3 Genetics

While an initial study by Petrie in 1977 found no clear genetic etiology for OCD [60], several cases since then have been reported in which symmetric lesions in multiple joins were present [61, 62] and in sets of monozygotic and dizygotic twins [62-68]. Furthermore, a new study by Gornitzky *et al.* found that the proportion of pediatric patients with OCD (JOCD specifically) with positive family history was 14% [69].

2.2.3.4 Epiphyseal abnormalities

It has been hypothesized in the past that an aberrant development of only a portion of the epiphyseal growth plate may lead to OCD formation [51, 70, 71]. The concept is as follows: a single or repetitive insult to the endochondral epiphyseal growth plate occurs at an unspecified time (this is where the hypothesis of trauma may converge) [51]. With skeletal development, the uninjured region of endochondral epiphyseal ossification continues to ossify unhindered creating an ever enlarging OCD, whereas the injured region either completely stops ossification or temporarily stops [51]. In support of this theory, current unpublished data from the ROCK (Research in OsteoChondritis of the Knee) study group shows MRI signal (T2 fat saturation) for the epiphysis appears disrupted at the margins of the OCD lesion [51]. In addition, Laor *et al.* found a statistically significant frequency of discontinuity of the epiphysis overlaying JOCD lesions and postulated that the chondroosseous irregularities observed might be the result of disruption of normal process of endochondral ossification from the epiphysis [37].

Abnormal epiphysis ossification may also be the result of disruption of local vasculature. In the epiphyseal ossification center, the newest bone formation occurs at the chondroosseous junction of the growing epiphyseal ossification center. Thus, the immediate subchondral bone can be considered a "metaphyseal equivalent." As such, disruption in the vascular supply to the secondary physis would result in persistent cartilage extending deep and central to the chondroosseous border of the developing epiphysis [37]. Increased width of overlying chondroepiphysis would be observed, just like what was found in all of Laor's JOCD subjects [37]. Furthermore, results of studies in veterinary literature suggest that vascular injury to the epiphysis is responsible for the development of osteochondral lesions that progress to OCD in animals such as rabbits,

birds, and foals [37, 72-75]. Transection of blood vessels within epiphyseal cartilage canals in foals resulted in necrosis of vessels and chondrocytes, which led to a focal delay in endochondral ossification and pathological cartilage fracture [75]. However, it is unclear whether the initial insult in children would be located within the overlaying chondroepiphysis or the metaphyseal-equivalent portion of the developing secondary center of ossification [37].

2.2.4 Biological and molecular pathomechanisms

It has been shown that chondrocytes isolated from detached JOCD fragments maintain similar cell viability and proliferative activity to those from normal healthy cartilage [41, 76, 77]. CD166, a MSC surface marker, was detected in chondrocytes packaged in normal cartilages and JOCD chondrocytes, suggesting similar regenerative potential between these groups [41]. However, compared with normal chondrocytes isolated from control samples, both JOCD loose body- and cartilage biopsy-derived chondrocytes showed intracellular accumulation of matrix proteins that affected their morphology [77]. Histological assessment of JOCD biopsies showed abnormal ECM composition, which may be explained by the retention of matrix proteins intracellularly. This feature has also been observed in familial [78] and equine OCD [79], and in endoplasmic reticulum storage diseases (ERSD) [77]. All ERSD, including type II collagenopathies, show a critical accumulation of misfolded proteins that result in defective protein trafficking causing a phenotype characteristics of disease [77]. These disease similarities may suggest a direct role of the endoplasmic reticulum (ER) in the pathogenesis of JOCD.

Furthermore, JOCD is a disorder of the articular cartilage as well as the subchondral bone; however, no study to date has explored the mechanisms in JOCD endochondral ossification or the involvement of JOCD osteoblasts in the pathological mechanisms of the disorder. Osteoblasts are highly specialized cells that synthesize bone. They are key players in bone remodeling, and their misregulation may contribute to failure to heal the initial bone lesion in JOCD.

CHAPTER 3. REGIONAL GENE EXPRESSION ANALYSIS OF MULTIPLE TISSUES OF THE MEDIAL MENISCUS TRANSECTION MODEL OF POST-TRAUMATIC OSTEOARTHRITIS

3.1 Abstract

The objective of this study was to characterize local disease progression of the medial meniscus transection (MMT) model of post-traumatic OA at the molecular level, in order to establish a baseline for therapeutic testing at the preclinical stage and possibly discern molecular events that may further elucidate OA pathogenesis. Weight-matched male Lewis rats underwent MMT or sham surgery on the left limb with the right leg as contralateral control. At 1 and 3 weeks post-surgery, tissues were harvested from different areas of the articular cartilage (medial and lateral tibial plateaus, and medial osteophyte region) and synovium (medial and lateral), and analyzed separately. RNA was extracted and used for microarray gene expression (RT-PCR) analysis.

Results showed that gene expression changes due to surgery were isolated to the medial side of the joint. In the articular cartilage, gene changes in chondrocyte phenotype preceded changes in tissue composition genes. Differences in inflammatory markers were only observed at the osteophyte region at 3 weeks post-surgery. In the synovium, there was surgical noise at week 1, which dissipated at 3 weeks post-surgery. At this later timepoint, meniscal instability resulted in elevated expression of matrix degradation markers and osteogenic markers in the synovium and cartilage. These results suggest feedback interactions between joint tissues during disease progression. Regional tissue expression differences found in MMT joints indicated similar pathophysiology to human OA, and provided novel insights about this degeneration model. The

examination of gene expression at a localized level in multiple tissues provided a well-characterized baseline to evaluate mechanistic effects of potential therapeutic agents on OA disease progression in the MMT model.

3.2 Introduction

There is a need for full characterization of pre-clinical models, with a view to comparison to human OA pathophysiology and to establish a baseline for therapeutic testing in these systems. Preclinical animal models of OA include experimentally accelerated but naturally occurring joint degeneration, transgenic mouse models, and surgically or chemically induced OA [80]. Unfortunately, none of these models can fully replicate the features and symptoms of human OA. Nevertheless, the impact of preclinical research will depend largely on the choice of the most appropriate model of OA for the specific process under investigation [80]. The disconnect between positive results in preclinical studies and failed clinical trials supports the need for better understanding of currently available preclinical models at the biological and molecular level in order to evaluate more accurately the therapeutic mechanisms of the tested treatment.

The rat MMT model is a frequently used model of post-traumatic OA, and is of high clinical relevance. The transection of the meniscus at its narrowest point alters the mechanical stability of the knee joint and induces OA-like progressive damage: cartilage degeneration involving chondrocyte and proteoglycan loss, osteophyte and focal lesion formation, collagen degradation and cartilage fibrillation [81]. The MMT model is known for localized degeneration primarily restricted to the medial tibial plateau. However,

despite being the industry standard for therapeutic testing, local disease progression events have not been thoroughly characterized in this model and assessment of therapeutic outcomes is largely limited to classical histology or microCT (morphological analyses) as endpoint readouts [81].

To date, a single study has reported on changes in the articular cartilage transcriptome of the rat MMT model. 20 genes differentially expressed between MMT and sham groups were identified, and the study concluded that the model paralleled key features of OA pathology, namely articular cartilage extracellular matrix (ECM) remodeling, angiogenesis, and chondrocyte cell death [82]. In this study, articular cartilage from both medial and lateral sides of the tibial plateaus and femoral condyles were collected from each animal, and then the cartilage tissue from 5 animals was pooled to create a single sample [82]. Cartilage collection from the entire joint and pooling of samples is standard for gene expression analyses in OA small animal models [82-84]. Yet this practice may mask identification of localized events in such models, and fails to account for inter-individual variability. With advances in microarray RT-PCR technology, we are now able to analyze tissues of much lower cell concentration.

The objective of this study was to characterize the gene expression changes in MMT, sham and control groups for each side of the articular cartilage of the tibial plateau, for the osteophyte region, and for each side of the synovium. This study is the first to elucidate localized disease progression in the rat MMT model and to identify genetic regulation in osteophyte and synovial tissues in an OA preclinical model.

3.3 Materials and methods

3.3.1 MMT model

The Georgia Institute of Technology Institutional Animal Care and Use Committee approved all experimental animal procedures (IACUC protocol #A14023). 48 Weight-matched male Lewis rats (300-325 g) were acclimated for 1 week before surgeries. A small incision was made through the skin on the medial aspect of the femoro-tibial joint of the left limb. The medial collateral ligament (MCL) was exposed by blunt dissection and transected to visualize the joint space and medial meniscus. In the MMT group (24 animals), the meniscus was transected completely at its narrowest point; while in the sham group (24 animals), the meniscus was exposed but left intact. The inclusion of the sham group enabled distinction of gene expression changes due to joint instability from those simply due to surgery. The skin was closed with 4.0 silk sutures and then stapled using wound clips. MMT and sham surgeries were randomized.

Rats were euthanized via CO_2 inhalation at 1 and 3 weeks post-surgery (n=12 per group per timepoint), and tissues were harvested and analyzed in a blind manner. The naïve right limbs were used as contralateral baseline controls. 9 animals were allocated for gene expression experiments and 3 for histology per group (power analysis: α=0.05, β=0.05).

3.3.2 Microarray gene expression experiment

From each leg, 3 samples of cartilage tissue were collected: the medial tibial plateau region, the lateral tibial plateau region, and the osteophyte region at the joint

margin of the medial side of the tibia (Figure 4). Tissue from the osteophyte region was only collected from MMT and sham groups at 1 and 3 weeks post-surgery due to insufficient tissue in naïve controls. Moreover, 2 samples of synovial membrane were also collected for all groups, from the medial and lateral sides of the joint, distal of the meniscus and directly adjacent to the tibial plateau (Figure 4).

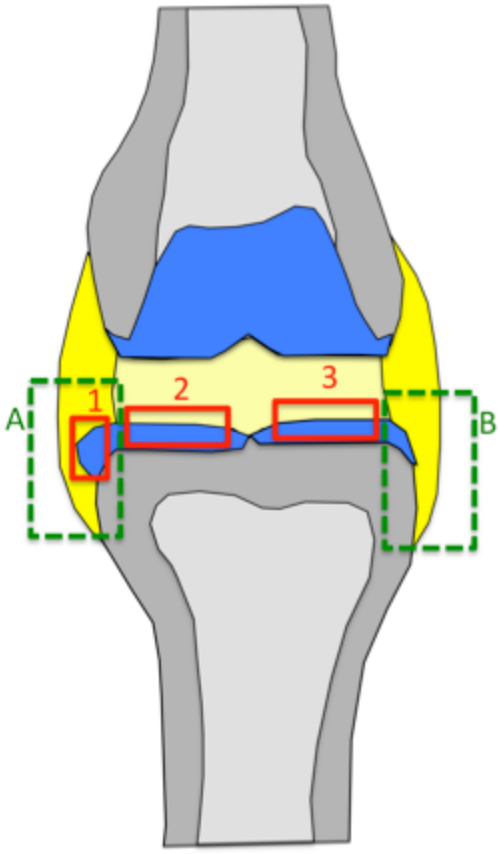

Figure 4. Representation of an operated left leg in which the medial meniscus has been transected (MMT rat model). At the indicated timepoint, 3 samples from the articular cartilage were harvested for each leg: 1) perceived osteophyte region (sham and MMT only), on the joint margin of the medial tibial plateau where osteophytes are known to develop; 2) medial tibial plateau, and 3) lateral tibial plateau. Additionally, 2 samples of synovium were collected from each leg: A) distal medial synovial membrane and B) distal lateral synovial membrane.

Total RNA from cartilage tissues was extracted using the RNeasy MinElute Clean-up Kit with QIAzol Lysis Reagent. Total RNA from synovium was extracted using the RNeasy Lipid Tissue Mini Kit with QIAzol Lysis Reagent. RNA quality and concentration for all samples were determined using the Nanodrop ND-1000 Spectrophotometer (ThermoFisher). Normalized RNA was converted to cDNA via the RT^2 First Strand Kit. All reagents were from Qiagen unless otherwise stated.

RNA expression was quantified using the Taqman real-time PCR Fluidigm Dynamic Array Integrated Fluidic Circuits (BioMark, Fluidigm). Our cDNA samples were tested against 40 genes (TaqMan gene expression assays, ThermoFisher, Table 2), which were selected from human OA literature. AccuRef rat universal cDNA (Gene Scientific) and ultrapure water were used as positive and negative controls, respectively, to ensure run fidelity. The Ct values greater than 37 were treated as 37, namely as null (lower Ct values correspond to higher expression since they represent the PCR cycle at which a threshold level of product is observed).

Table 2. Taqman Gene Expression assays utilized for the characterization of the MMT model. Assays were all purchased from Thermo Fisher Scientific. When available, selected assays were that of the best coverage, recommended by the company.

Category	Taqman Gene Expression Assay
ECM composition markers	*Col1a1* (Rn01463848_m1), *Col1a2* (Rn00670295_m1), *Col2a1* (Rn01637087_m1), *Acan* (Rn00573424_m1), *Fn1* (Rn00569575_m1), *Fmod* (Rn00589918_m1), *Tnn* (Rn01491027_m1)
ECM remodeling markers	*Mmp2* (Rn01538170_m1), *Mmp3* (Rn00591740_m1), *Mmp9* (Rn00579162_m1), *Mmp12* (Rn00588640_m1), *Mmp13* (Rn01448194_m1), *Adamts4* (Rn02103282_s1), *Adamts5* (Rn01458486_m1), *Ctsk* (Rn00580723_m1), *Spp1* (Rn00681031_m1), *Timp1* (Rn01430873_g1), *Inhba* (Rn01538592_m1)
Chondrogenesis markers	*Sox9* (Rn01751070_m1)
Chondrocyte hypertrophy markers	*Frzb* (Rn01746979_m1), *Grem1* (Rn01509832_m1), *Col10a1* (Rn01408030_m1), *Tgm2* (Rn00571440_m1)
Osteogenesis markers	*Bglap* (Rn00566386_g1), *Bmp2* (Rn00567818_m1), *Runx2* (Rn01512298_m1), *Sp7* (Rn_02769744_s1), *Sparc* (Rn_01470624_m1)
Vascularization marker	*Vegfa* (Rn01511602_m1)
Inflammation markers	*Tnfα* (Rn01525859_g1), *Tgfβ1* (Rn00572010_m1), *IL1b* (Rn00580432_m1), *IL6* (Rn01410330_m1), *IL10* (Rn01483988_g1), *IL17a* (Rn01757168_m1), *Ccl2* (Rn00580555_m1), *Ccl3* (Rn_01464736_g1), *Cxcr2* (Rn02130551_s1), *Ptgs2* (Rn01483828_m1)
Catabolic factors	*Epas1 (Rn00576515_m1), Sod2 (Rn00690588_g1)*
Cell apoptosis marker	*Casp8* (Rn00574069_m1)
Housekeeping genes	*Ppia* (Rn00690933_m1), *Rplp1* (Rn03467157_gH), *Rpl13a* (Rn00821946_g1)

3.3.3 Gene expression statistical analyses

Ct values were subtracted from 37 in order to invert them: this converts the data to a more intuitive scale in which higher values now represent higher levels of RNA transcription for each gene. To calculate the relative gene expression (ΔCt), Ct values were normalized by the geometric mean of three housekeeping genes: *Ppia*, *Rplp1* and *Rpl13a* (Equation 1). The raw Ct values of these housekeeping genes were not statistically different across different tissue types (cartilage and synovium), regions of interest (medial, lateral or osteophyte regions), or timepoints (1 and 3 weeks) (data not shown). In order to correct experimental differences observed between biological replicates and runs, the medians of each replicate experiment were median centered by subtracting the median normalized relative expression level across all conditions in a given replicate experiment for that same experiment. This step does not affect the fold induction, but it provides a correction for the difference in background or control level between independent biological repeats [85]. The Quantile Range Outlier (QRO) test was performed to remove any outliers. All statistical calculations were performed with JMP Genomic software (SAS Institute, Cary, NC, USA).

$$\Delta Ct = Ct_{target} - Ct_{housekeeping\ gene}$$

Equation 1. Equation for the relative expression of a target gene (ΔCt).

3.3.3.1 Principal component analysis (PCA) and unsupervised clustering analysis.

Scripts from JMP Genomic software were used to perform both analyses. In the weighted average proportions of the PCA models, a residual (unexplained) variance higher than 60% was considered as too noisy and to have too many potential confounding

variables in the sources of variability (surgery, timepoint, batch effect) to draw conclusions.

3.3.3.2 Differential expression

Volcano plots were used to compare the gene expression profile of groups. A volcano plot is a one-way ANOVA between two groups for multiple comparisons. Each gene (observation) is represented by a point on the graph. Significance was determined using Bonferroni correction (0.05 (p-value) divided by the number of observations).

For each individual gene expression, two-way ANOVA was performed to determine the statistical significance of the differences between the means for each treatment (surgical group) and time groups. Tukey's *post hoc* comparison was performed to compare the means of parametric cases in which one-way ANOVA assumptions were fulfilled. Kruskal-Wallis *post hoc* test was used for non-parametric cases. P-values less than 0.05 were considered statistically significant. Analyses were carried out using JMP Genomic software and graphed in it or in GraphPad Prism, version 7 (San Diego, CA).

3.3.4 Immunohistochemistry

In order to validate gene expression results, immunofluorescent staining of full-joint histological sections was carried out for specific markers: Collagen type 2 (sc-52658), Mmp13 (ab75606), and Osteopontin (sc-21742). Briefly, control, sham and MMT full-joints were fixed in 10% neutral buffered formalin, trimmed, and decalcified in ImmunoCal decalcifying agent (StatLab). Samples were processed, embedded in paraffin, then sectioned at 5μm thickness. Antigen retrieval (sodium citrate buffer),

permeabilization (0.1% Triton-X) and blocking were performed on the sections, before incubation overnight in primary antibody at 4°C. Secondary antibody (Cell Signaling 4409 and 4412) was incubated for 1 hour at room temperature, followed by counterstaining with DAPI (ThermoFisher S36938).

3.4 Results

3.4.1 Articular cartilage gene expression

3.4.1.1 Tibial plateau region.

There were at least a half dozen innate significant gene expression differences between the medial and lateral sides of the tibial plateau, in the control (unoperated) group at both 1 and 3 weeks after surgery (Figure 5). There were no significant differences in gene expression for the lateral side among surgical groups (MMT, sham, and control) at any timepoint, indicating that the lateral side is not affected by surgery (Figure 6A). Changes in gene expression in the medial side of the tibial plateau were, however, affected by the surgery, as expected (Figure 6B and Figure 7).

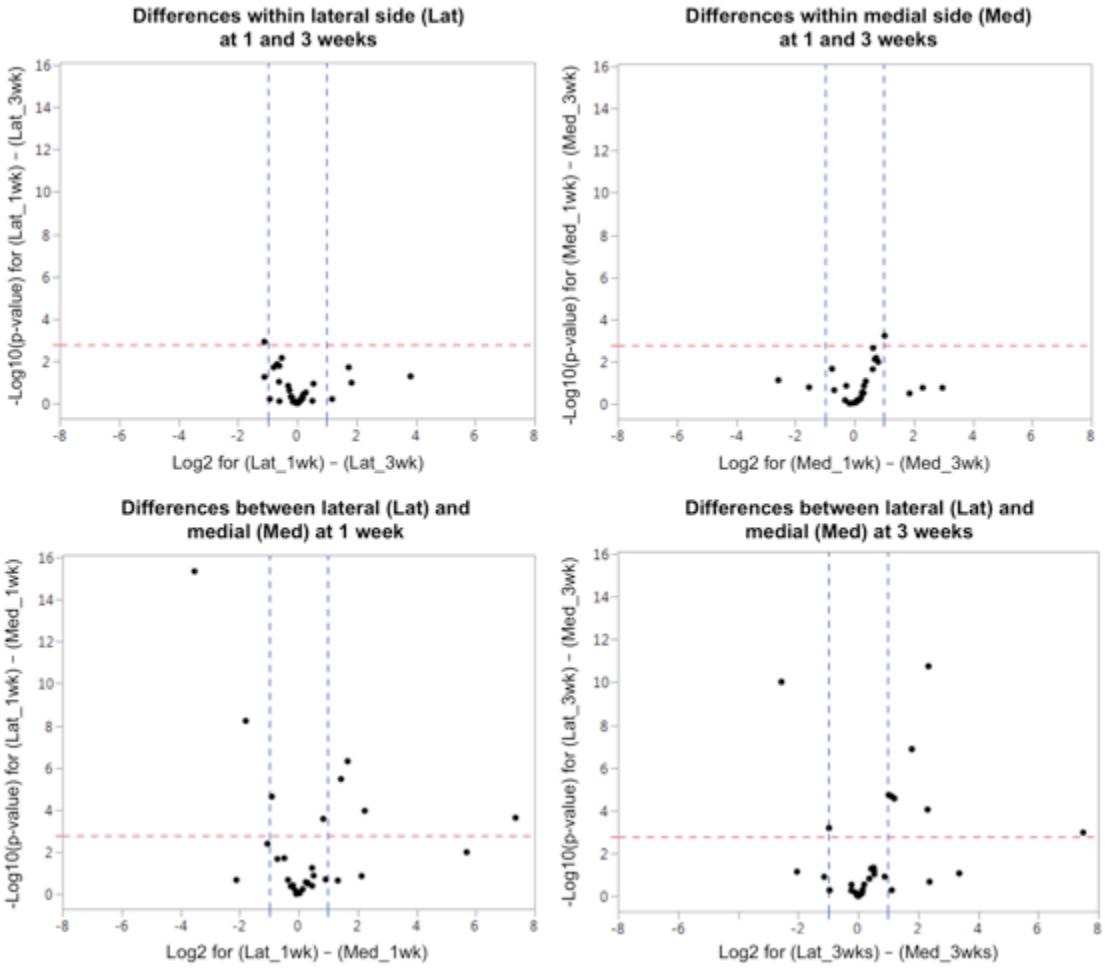

Figure 5. Volcano plots of the (unoperated) control group of the tibial plateau. There are no significant temporal differences in gene expression within a side (medial or lateral). There are, however, significant differences between sides at each timepoint. The dotted blue lines in the x-axis indicate 2 fold difference (1 in log2 scale), and the dotted red line indicates significance threshold for Bonferroni correction of p-value of 0.05 in –log10 scale. These results show that there are innate differences between the lateral and medial sides of the tibial plateau.

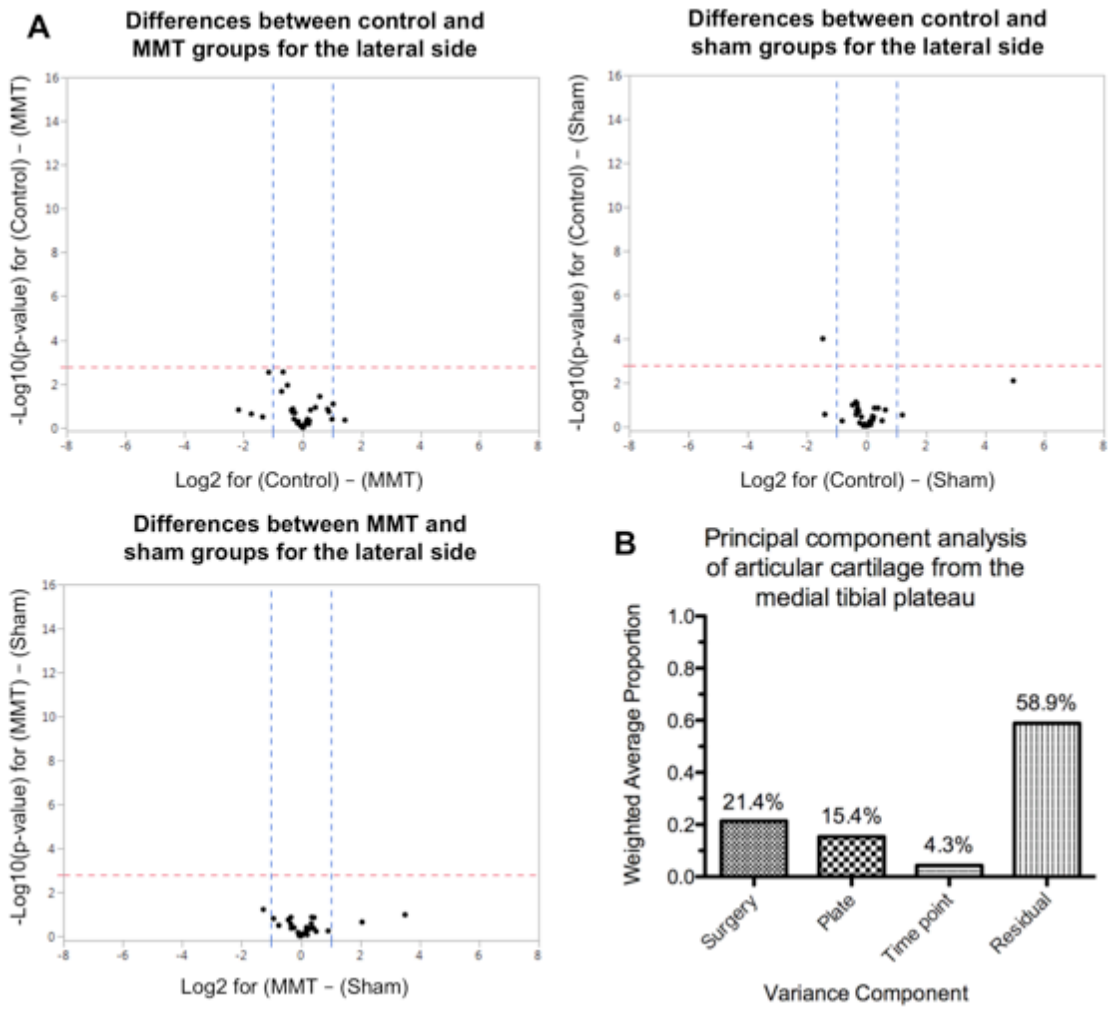

Figure 6. Volcano plots of the lateral side of the tibial plateau for all surgery groups. The lateral side is not affected by surgery. The dotted blue lines in the x-axis indicate a 2 fold difference (1 in log2 scale), and the dotted red line indicates the significance threshold for Bonferroni correction of p-value of 0.05 in –log10 scale. The one point at 10^{-4} in the control vs sham plot is borderline significant given the multiple conditions within the experiment, and is not indicative of a systematic transcriptional response. B. Principal component analysis (PCA) of the medial tibial plateau. Differences in the gene expression profiles of the medial side, however, are largely driven by surgery type.

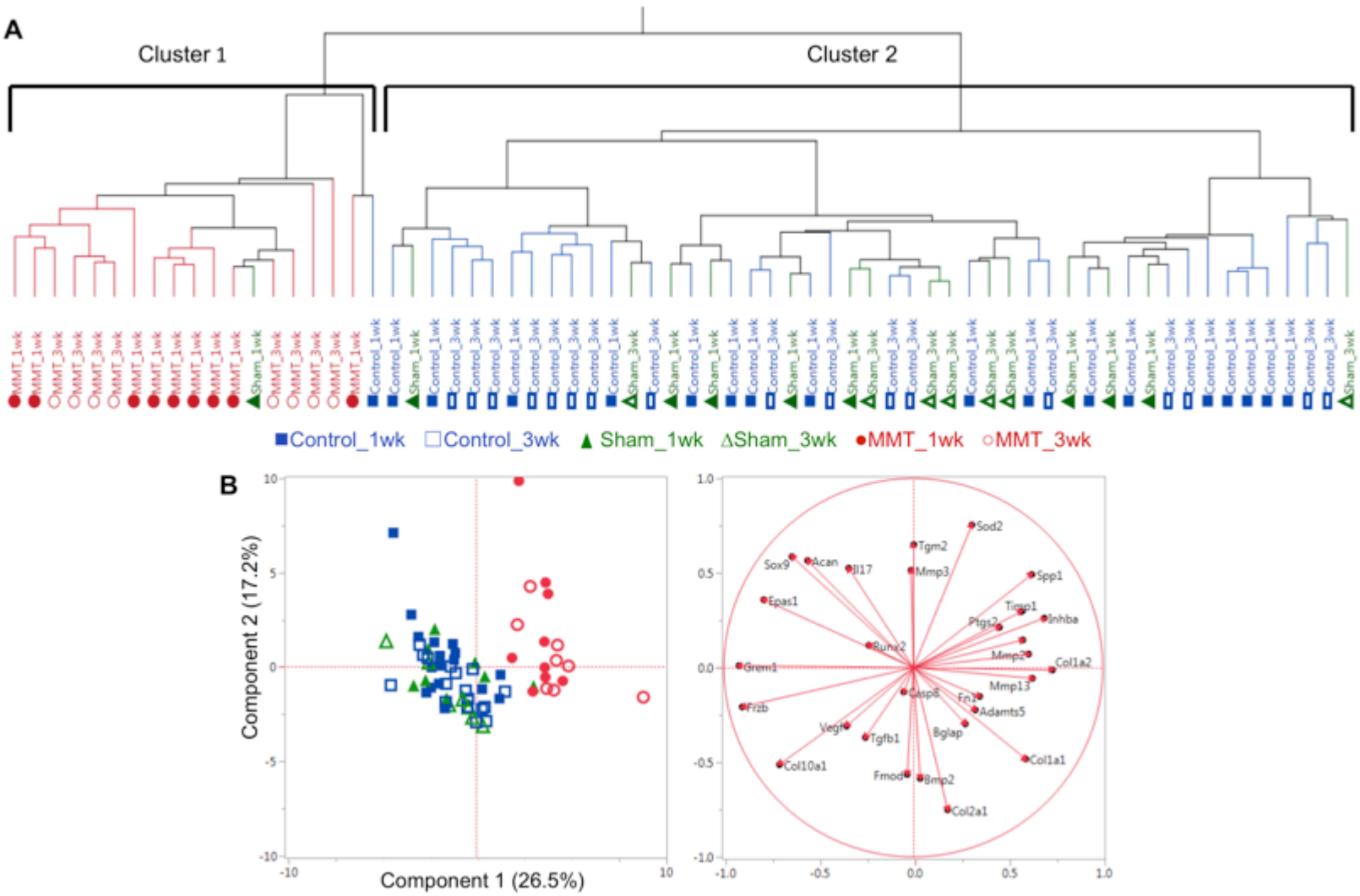
A
Cluster 1
Cluster 2
Control_1wk
Control_3wk
Sham_1wk
Sham_3wk
MMT_1wk
MMT_3wk
B
Component 2 (17.2%)
Component 1 (26.5%)
Sod2
Tgm2
Sox9
Acan
Il17
Mmp3
Spp1
Epas1
Timp1
Ptgs2
Inhba
Runx2
Mmp2
Grem1
Col1a2
Mmp13
Casp8
Fn1
Frzb
Adamts5
Vegfa
Tgfb1
Bglap
Col1a1
Col10a1
Fmod
Bmp2
Col2a1

Figure 7. A. Dendogram shows clustering of groups based on their gene expression profile. Control at week 1 and 3 cluster with sham at week 1 and 3, while MMT forms another group altogether. B. Principal component analysis (PCA) plots confirm clustering of control and sham groups away from the MMT group. There are no temporal differences within groups.

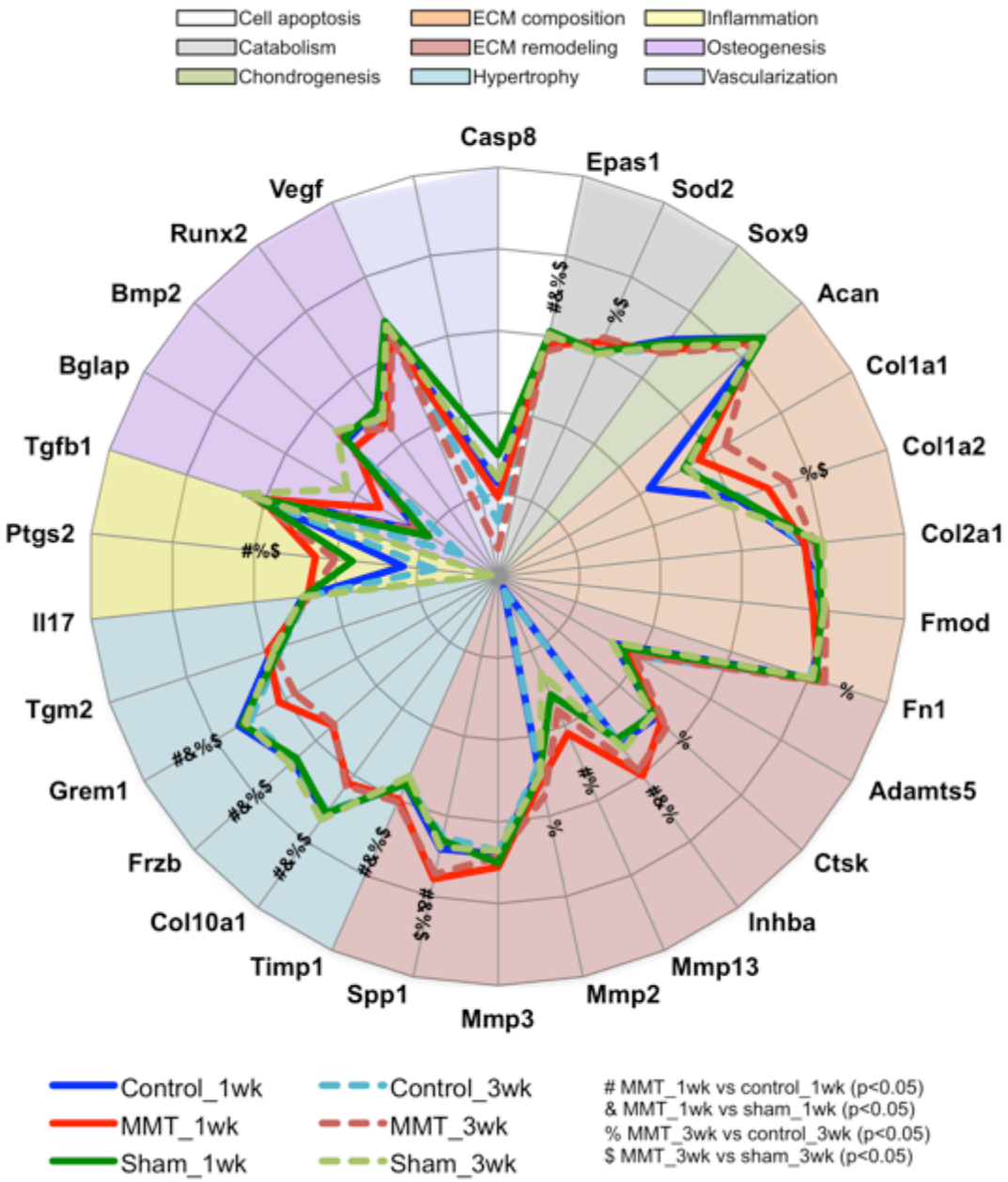

Figure 8. Radar plot of averaged (mean) ΔCt expression of individual genes in the unoperated, control medial tibial plateau cartilage (control), the MMT medial tibial plateau cartilage (MMT) and the sham medial tibial plateau cartilage (sham), at different timepoints. Statistical comparisons were carried out for each individual

gene as described in the methods. # indicates significant ($p<0.05$) difference between MMT and control at week 1; & between MMT and sham at week 1; % between MMT and control at week 3; and $ between MMT and sham at week 3. There were not statistical differences between timepoints within surgical groups.

3.4.1.1.1 Medial tibial plateau.

A clustering analysis showed that the gene expression profiles of control and sham samples were similar enough to be grouped into one cluster, while the MMT samples belonged to a different cluster entirely (Figure 7). This was confirmed with a PCA (Figure 1), which showed that MMT samples cluster separately from the control and sham groups. There were no temporal differences (week 1 vs. 3) within each cluster. Overall, expression of 14 genes was significantly different in the MMT group, when compared to control and sham groups (Figure 8 and Figure 9). There were no significant differences between the control and sham groups.

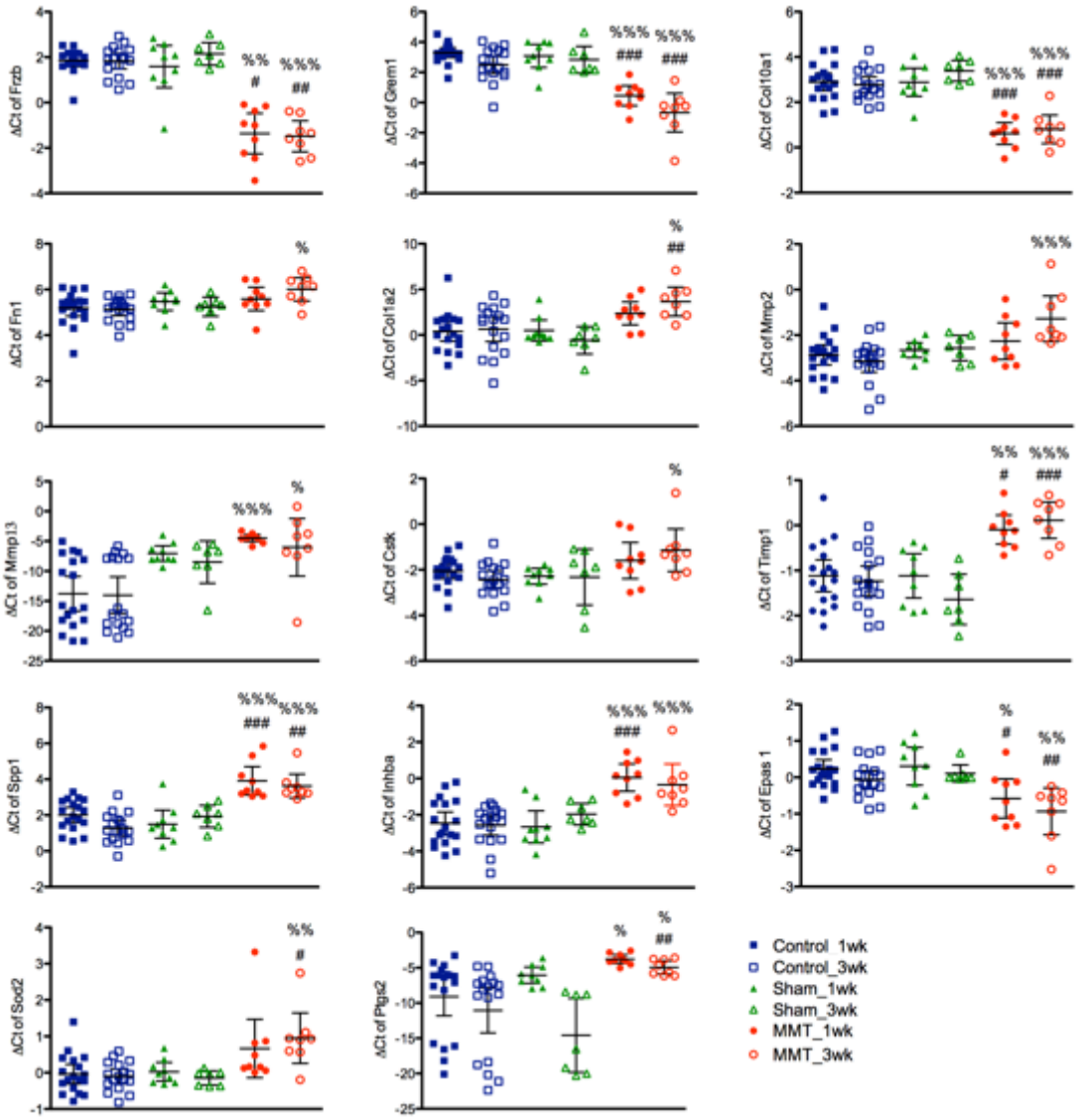

Figure 9. Significantly differently expressed genes of articular cartilage of the medial tibial plateau for all groups, graphed as means ± 95% confidence interval. % indicates statistically significant group difference vs. control ($p<0.05$), %% = $p<0.005$, %%% = $p<0.001$; and # group difference vs. sham ($p<0.05$), ## = $p<0.005$, ### = $p<0.001$.

Chondrocyte hypertrophy genes were differentially regulated as early as 1 week in the MMT group: *Frzb*, *Grem1*, *Col10a1*. *Frzb* (Frizzle-related protein) and *Grem1* (Gremlin 1) are Wnt-pathway antagonists, and were downregulated at weeks 1 and 3. The Wnt pathway is associated with articular chondrocyte dedifferentiation [86]. Its activation in *vivo* and *in vitro* leads to reprogramming of articular chondrocytes toward catabolism or loss of stable phenotype with subsequent loss of tissue structure and function [87]. *Col10a1* (type 10 collagen) was also underexpressed in the MMT group, observed at both week 1 and 3.

Gene expression of key cartilage extracellular matrix (ECM) protein markers, *Col2a1* (type II collagen) and *Acan* (aggrecan), was not significantly different among groups. However, *Fn1* (fibronectin) and *Col1a2* (type I collagen) were overexpressed by week 3 in the MMT model.

Markers for matrix degradation proteins and their inhibitors were also differentially expressed in the MMT group. *Mmp13* (metalloproteinase) is considered the primary collagenase in OA, and it was overexpressed at weeks 1 and 3, while *Mmp2* and *Ctsk* (cathepsin k) were elevated at week 3 only. *Timp1* and *Inhba* are inhibitors of these matrix degradation s, and they were both overexpressed at weeks 1 and 3. *Timp1* is a metalloproteinase inhibitor which acts on Mmps (relevant to this study, Mmp2, Mmp3, Mmp9, Mmp12, Mmp13). *Inhba* has shown to inhibit aggrecanase-mediated cleavage of aggrecan in human and rat articular cartilage [82].

Spp1 (osteopontin) is a matrix remodeling marker and was overexpressed as early as week 1 in the MMT model. *Spp1* has been implicated in a number of physiological and

pathological events, including maintenance or reconfiguration of tissue integrity during inflammatory processes [88].

Known catabolic factors in OA were dysregulated in the MMT model. *Epas1* encodes hypoxia-inducible factor-2alpha (HIF-2α), a known catabolic factor in the osteoarthritic process. HIF-2α regulates the expression of several matrix-degrading enzymes, and its overexpression is associated with increased chondrocyte apoptosis and OA cartilage destruction [89]. In this study, however, we observed a lower expression of *Epas1* at weeks 1 and 3. *Sod2* (superoxide dismutase 2) is also a marker for catabolism in the articular cartilage, and it was overexpressed in the MMT group at weeks 1 and 3. *Sod2* is a mitochondrial enzyme that converts superoxide to hydrogen peroxide, acts in oxidative stress response, and may affect aging [82].

Lastly, *Ptgs2* (prostaglandin-endoperoxide synthase 2 encoding cyclooxygenase 2 [COX-2]) is an inflammatory response gene whose product converts arachidonate to inflammatory prostaglandins [82]. *Ptgs2* was significantly overexpressed in the MMT group at weeks 1 and 3.

3.4.1.2 Osteophyte region.

There was significantly more RNA extracted from tissue collected from the joint margin (osteophyte) region in the MMT than the sham at 3 weeks (Figure 10). This difference in RNA concentration was not observed for any other tissue, for either groups or timepoints. A PCA showed that regardless of surgical group, tissue from this osteophyte region was distinctively different from that which had been collected from the articular tibial plateau (Figure 10). We observed significant overexpression of osteogenic

markers and underexpression of chondrogenic markers. There were 20 significantly differentiated genes in the MMT osteophyte region when comparing it to the MMT medial articular cartilage region (Figure 11).

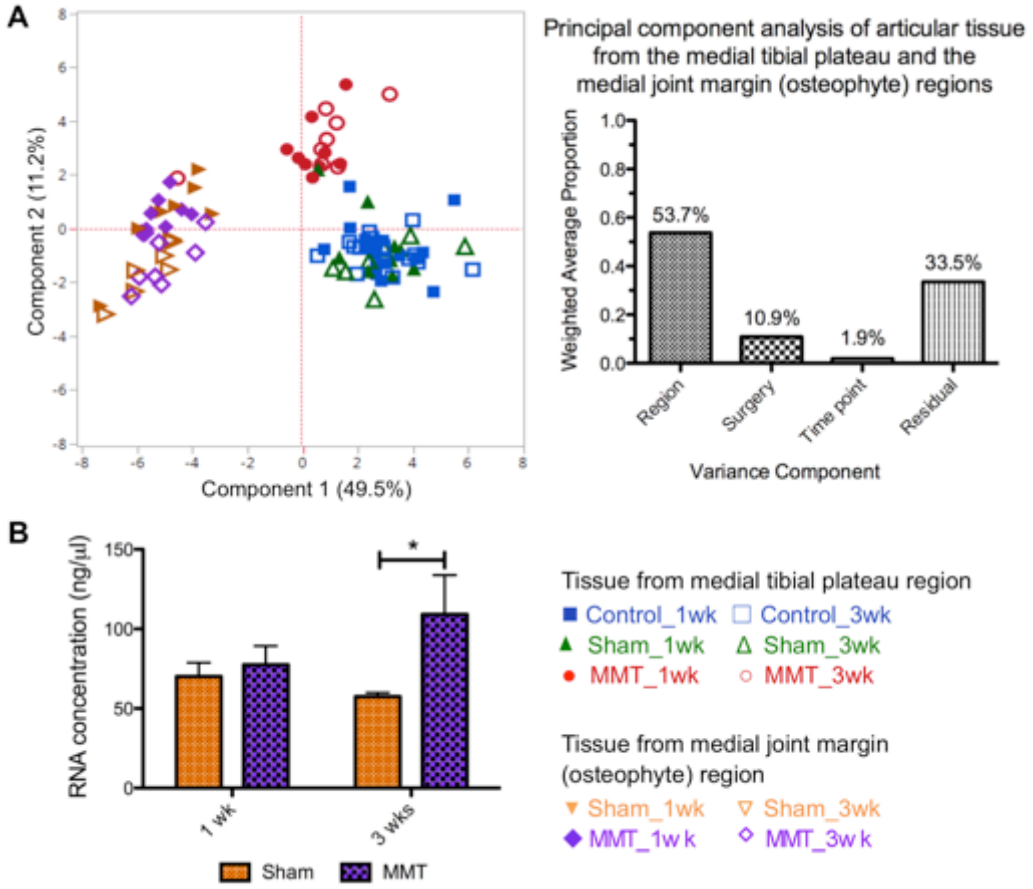

Figure 10. A. Principal component analysis (PCA) of tissue from the medial tibial plateau region (control, sham and MMT groups) and osteophyte region (sham and MMT groups) for all timepoints. The significant difference in gene expression profiles is mainly due to the region from which tissue was collected (53.7%). Tissue from the osteophyte (sham and MMT) is fundamentally different from the tissue from the articular cartilage of the medial tibial plateau. B. There is more tissue (and therefore RNA extracted) from the MMT group at the osteophyte region at week 3. Concentrations from nanodrop are graphed as means ± standard error of the mean (SEM). * indicates significant difference ($p<0.05$) between the two groups.

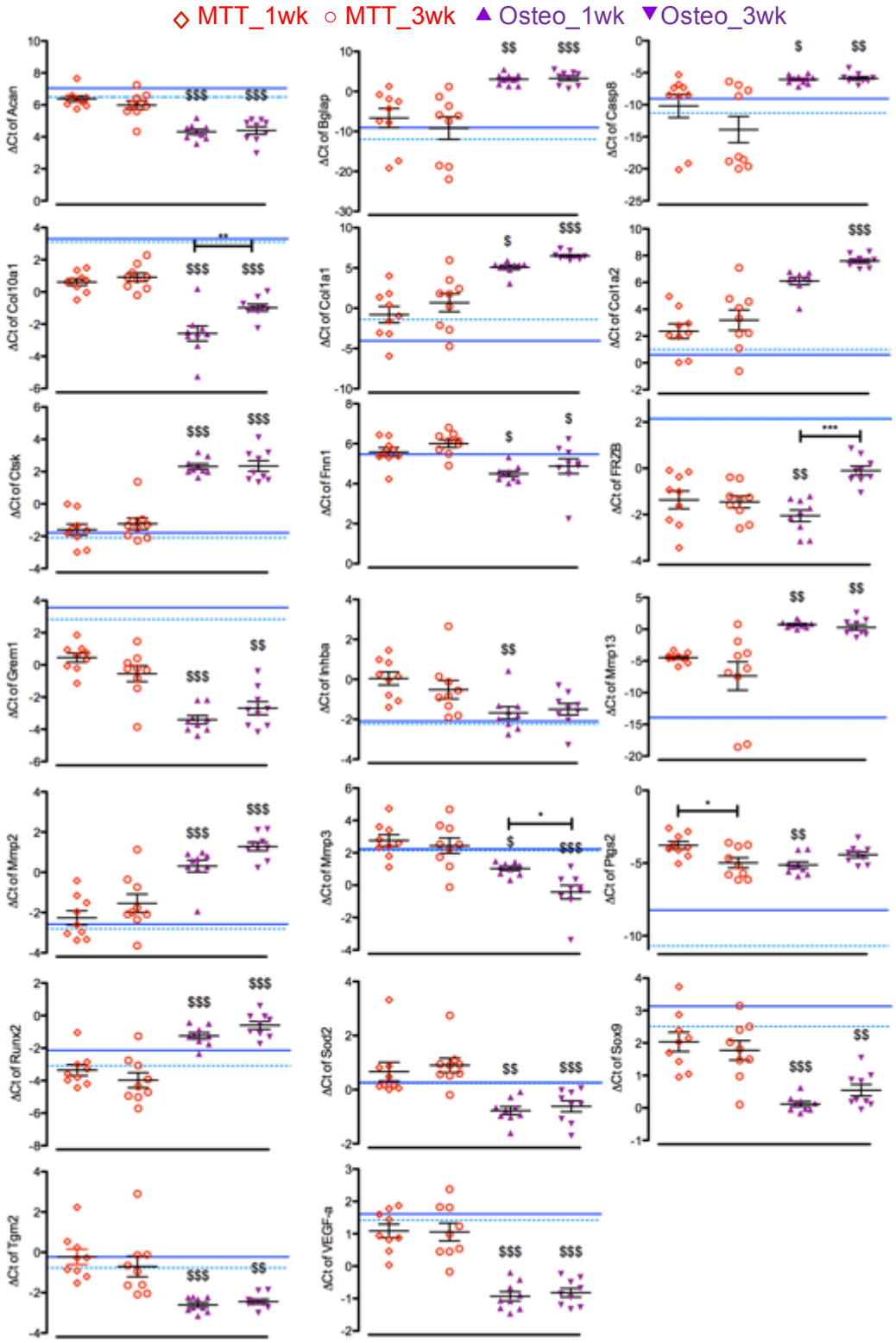

Figure 11. Significantly differently expressed genes of the articular cartilage from the medial tibial plateau of MMT animals (MMT group) vs. tissue from the

osteophyte-developing region of MMT animals (osteo group), graphed as means ± SEM. The solid blue lines is the mean expression for the articular cartilage from the medial tibial plateau of control at 1 week post-surgery, unoperated animals; while the dashed light blue line is at 3 weeks post-surgery. $ indicates significance between the MMT and osteo groups at the indicated timepoint at a p-value<0.05 ; $$ at a p-value<0.01; and $$$ at a p-value<0.001.

The osteophyte region generally expressed a higher degree of osteogenic genes and ECM markers related to osteogenesis than the MMT medial tibial plateau region. Col1a1, Col1a2, Runx2, and Bglap (Osteocalcin) were significantly higher expressed in the osteophyte region as early as week 1.

Chondrocyte hypertrophic markers were also differentially regulated in the osteophyte region when compared to the medial tibial plateau region of the MMT group. At week 1 and 3, Col10, Tgm2 (transglutaminase-2) and Grem1 were significantly underexpressed. Frzb was significantly underexpressed in the osteophyte region at week 1, but at week 3 it went up to similar levels of that of the MMT medial tibial plateau, though still lower than the control/sham medial tibial plateau.

Chondrogenic and ECM-remodeling markers were also altered depending on the region of interest within MMT group. Acan and Fn1 were significantly underexpressed in the osteophyte region. Sox9, a marker of chondrogenesis, had significantly lower expression levels in the osteophyte region at week 1 and 3. Inhba and Mmp3 were significantly underexpressed in the osteophyte region at week 1, while Mmp2, Mmp13 and Ctsk were significantly overexpressed in the osteophyte region at both time points.

Catabolic factor Sod2 was lower expressed in the osteophyte region at week 1 and 3 when compared to the medial tibial plateau in the MMT model. Apoptosis marker Casp8 was higher expressed at both timepoints. In the osteophyte region, Ptgs2 was

significantly lower at week 1 than the MMT medial tibial plateau and comparable to the control medial tibial plateau. Interestingly, Vegf was significantly underexpressed in the osteophyte region as early as week 1.

Given that the tibial plateau cartilage is dissimilar to the osteophyte tissue, we proceeded with comparisons exclusively within the osteophyte tissue of sham vs. MMT at the different timepoints. We found that 6 genes were differentially expressed between these 2 groups (Figure 12 and Figure 13).

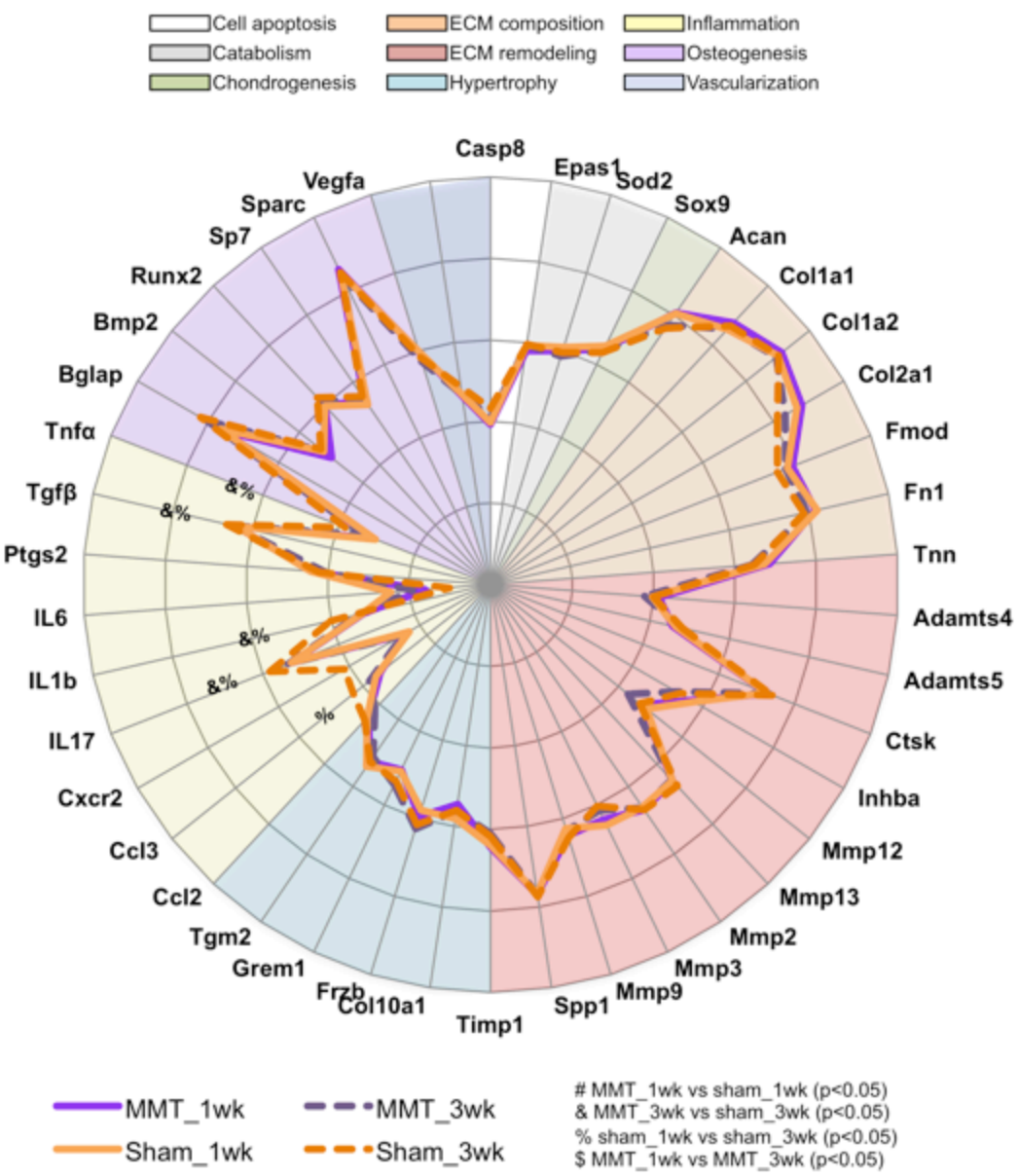

Figure 12. Radar plot of averaged (mean) ΔCt expression of individual genes in the sham osteophyte tissue (sham) and the MMT osteophyte tissue (MMT), at different timepoints. Statistical comparisons were carried out for each individual gene as described in the methods. # indicates significant (p<0.05) difference between MMT and sham at week 1; & between MMT and sham at week 3; % between week 1 and 3 for the sham group; and $ between week 1 and 3 for the MMT group.

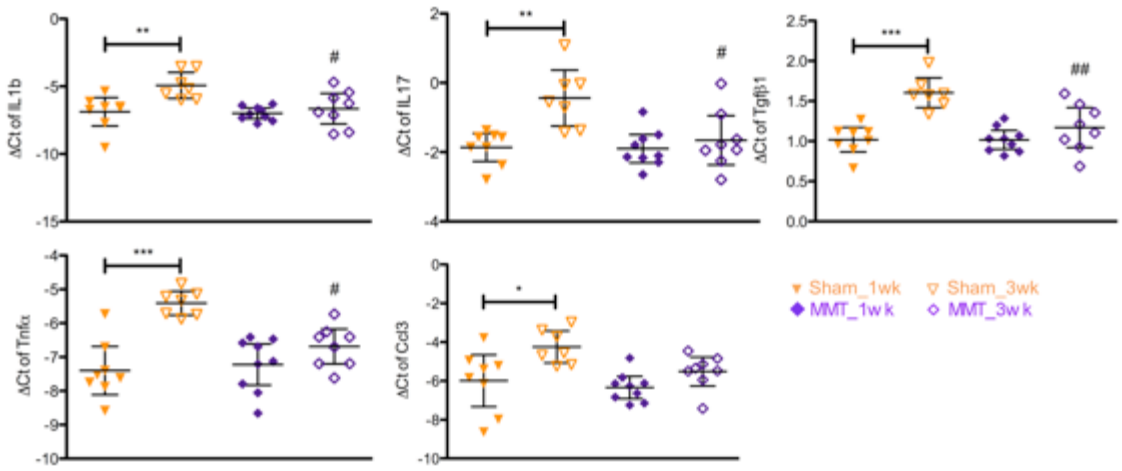

Figure 13. Significantly differently expressed genes of the osteophyte region between the sham and MMT groups for both timepoints, graphed as means ± 95% confidence interval. # indicates statistically significant group difference vs. sham ($p<0.05$), ## = $p<0.005$; and * between timepoints of the same group ($p<0.05$), ** = $p<0.005$.

The inflammatory genes *IL1b* (interleukin), *IL17*, *Tgbβ* (transforming growth factor-β) and *Tnfα* (tumor necrosis factor-α) were significantly underexpressed in the MMT group at week 3 compared to the sham. In the sham group, their expression at week 1 was comparable to that of the MMT, but at week 3, these genes were significantly overexpressed compared to the sham at week 1 and MMT at week 3. *Ccl3* (c-c- motif chemokine-3), another gene involved in inflammation, showed a similar trend; however, no differences were observed at week 3.

3.4.2 Synovial membrane gene expression

In the control group, medial and lateral sides of the synovial membrane had one significantly differentially expressed gene (Figure 14). Unlike the cartilage samples, however, there were significant differences in the lateral side samples among surgical procedures (data not shown), though we note that latent unknown variables beyond

surgery type, microarray plate number (batch effect), and timepoint contribute to a large residual variance (Figure 14). On the other hand, on the medial side, a small number of significant changes were observed in gene expression among groups are largely driven by the surgery type (Figure 14). Therefore, we focus only on the differences in the medial side of the synovium.

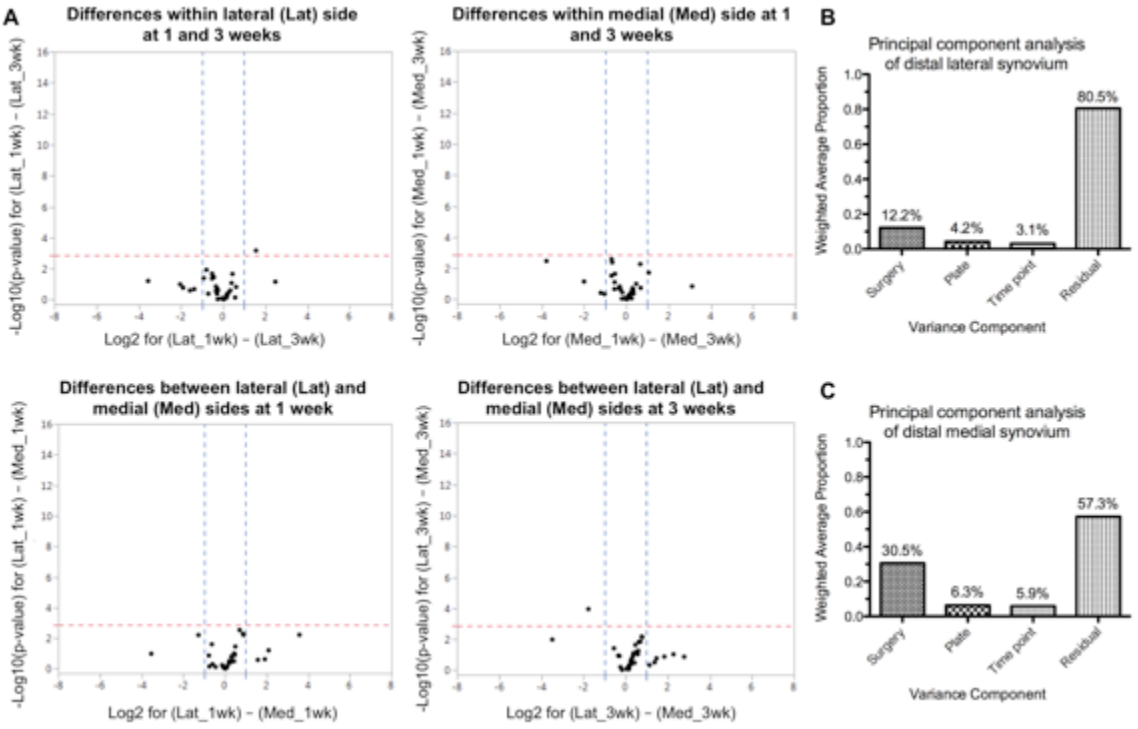

Figure 14. A. Volcano plots of the unoperated, control group of the distal synovial membrane. There are very few (1 or 2) significant differences in gene expression within a side (different timepoints) and between sides at a specific timepoint. The dotted blue lines in the x-axis indicate 2 fold difference (1 in log2 scale), and the dotted red line indicates significance threshold for Bonferroni correction of p-value of 0.05 in –log10 scale. B. Principal component analysis (PCA) of the distal lateral synovial membrane. Differences in gene expression profiles for the lateral side of the synovium are largely unexplained (80.5%). C. PCA of the distal medial synovial membrane. Differences in gene expression profiles for the medial side of the synovium can be attributed to surgical procedures.

3.4.2.1 Medial synovial membrane.

Our cluster analysis showed that there were temporal differences in the sham group (Figure 15). Sham samples at week 1 cluster with the MMT samples (both timepoints). At week 3, however, sham samples are equally split between the control cluster and the MMT cluster. The PCA further confirms this clustering and shows that expression of Mmps is a key driver of principal component 1 (Figure 15). Overall, there were 16 genes that were differentially expressed among groups (Figure 16 and Figure 17). There were no statistical differences between the sham and MMT groups at week 1, but this was not the case at week 3.

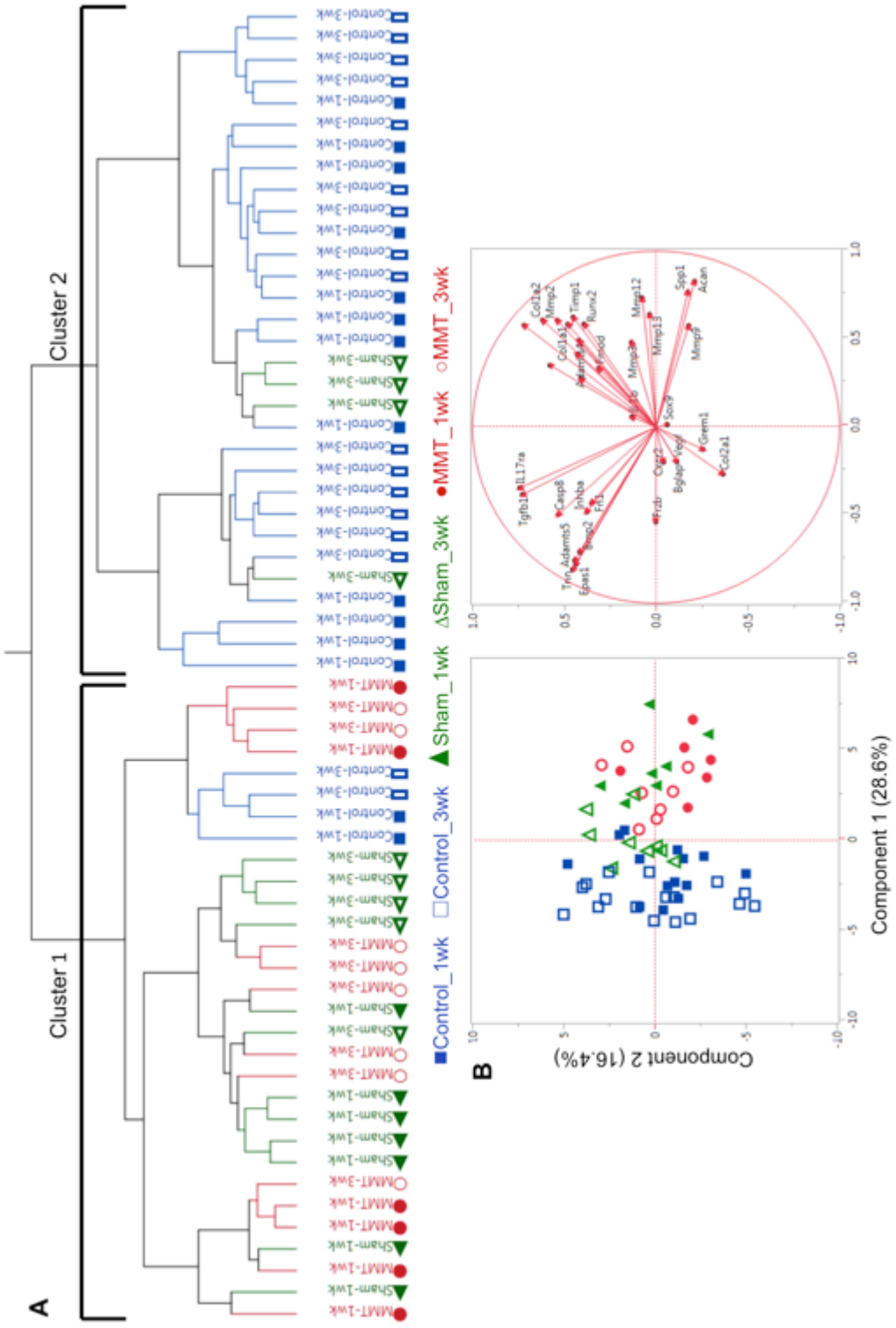

Figure 15. A. Dendogram shows clustering of groups based on their gene expression profile. Sham at week 1 clusters with MMT at week 1 and 3, while at 3 weeks post-surgery, sham clusters with both MMT and control groups. B. PCA confirms this clustering and

shows that this difference is largely driven by ECM remodeling genes and osteogenic markers. These results suggest a surgical effect that dominates at week 1

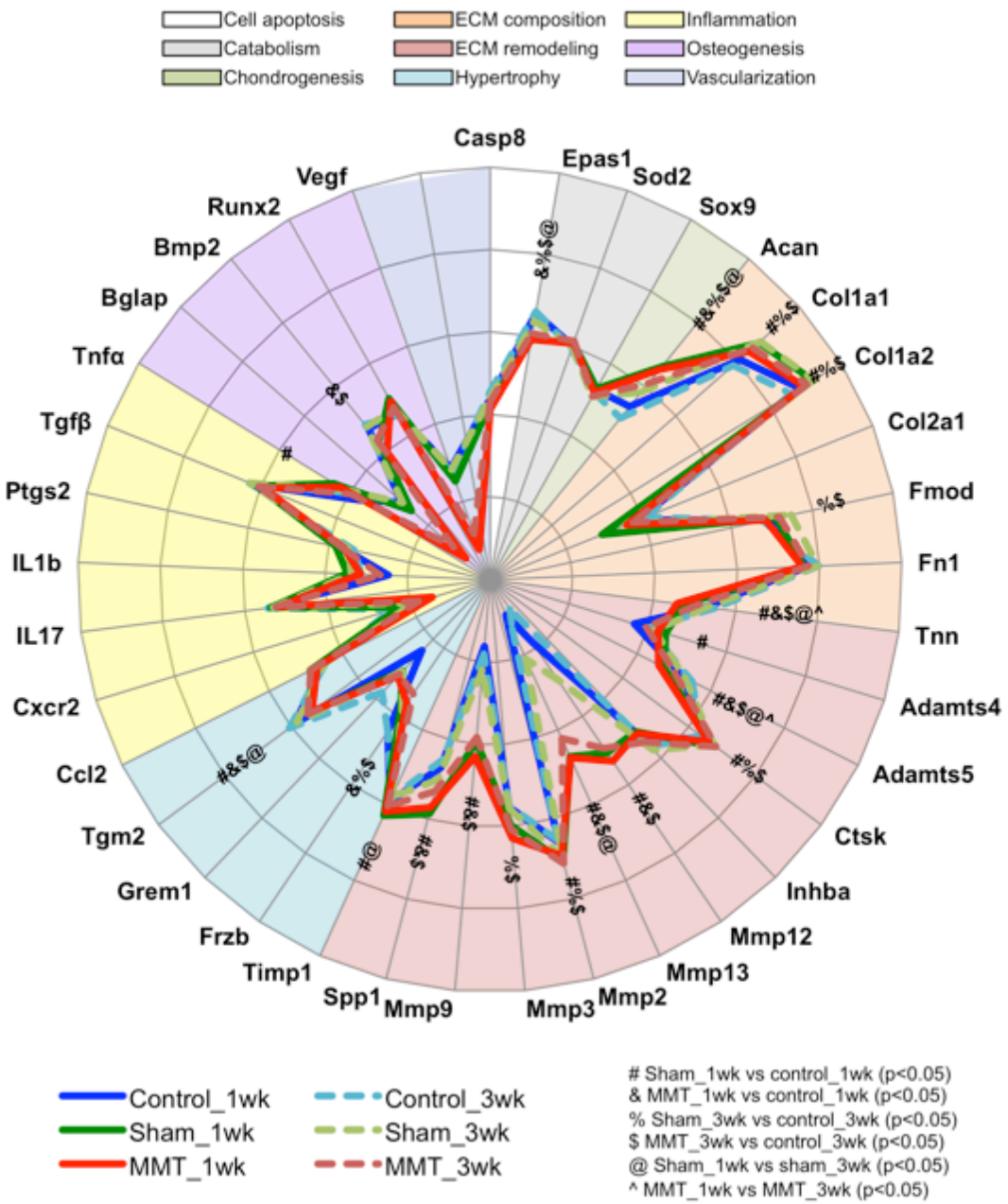

Figure 16. Radar plot of averaged (mean) ΔCt expression of individual genes in the unoperated, control medial synovial membrane (control), the sham medial synovial membrane (sham) and the MMT medial synovial membrane (MMT), at different timepoints. Statistical comparisons were carried out for each individual gene as described in the methods. # indicates significant (p<0.05) difference between sham and control at week 1; & between MMT and control at week 1; % between sham

and control at week 3; $ between MMT and control at week 3; @ between week 1 and 3 within sham group; and ^ between week 1 and 3 within MMT group.

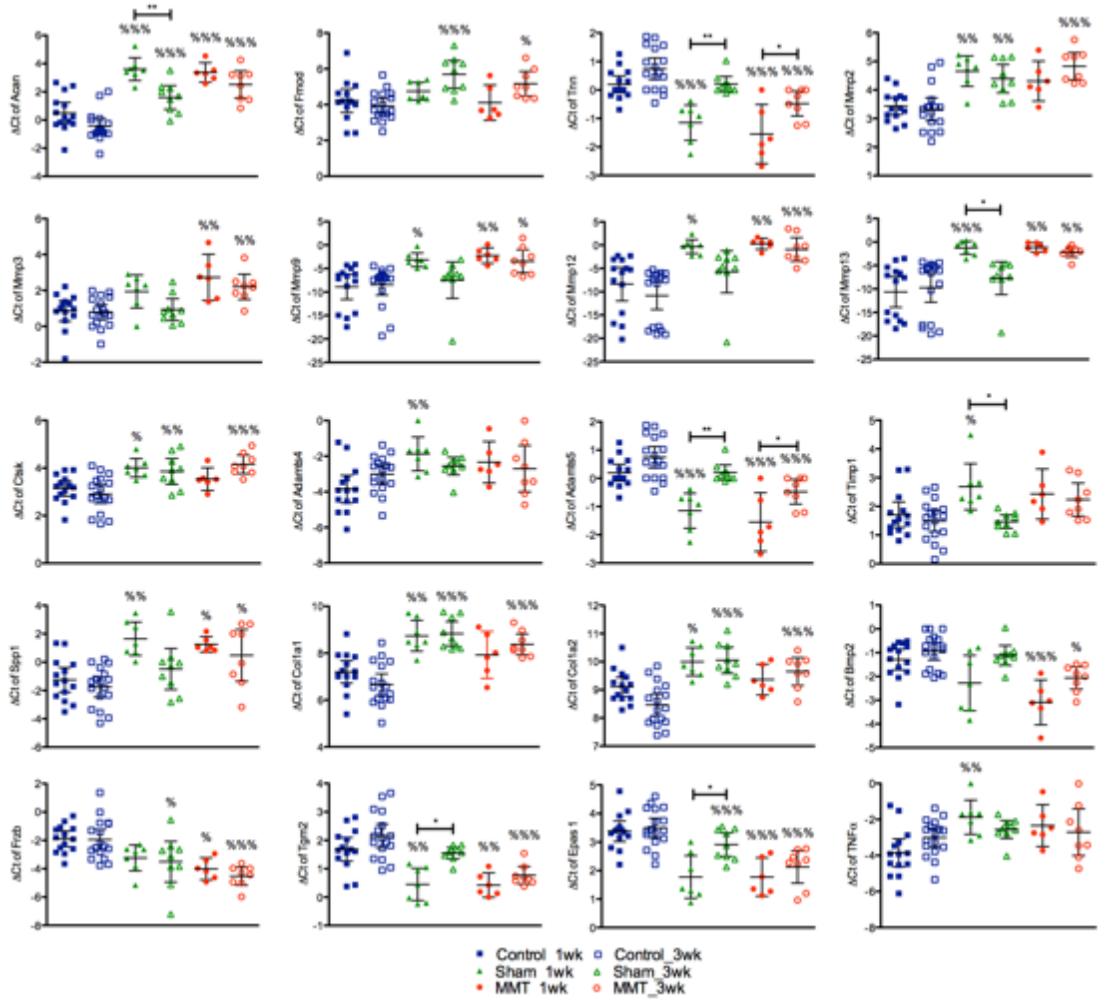

Figure 17. Significantly expressed genes in the distal medial synovial membrane for all groups, graphed as means ± 95% confidence interval. % indicates statistically significant group difference vs. control (p<0.05), %% = p<0.005, %%% = p<0.001; and * indicates timepoint difference (week 1 vs. 3) within a group (p<0.05), ** = p<0.005, *** = p<0.001.

In general, surgery had an effect on genes related to the ECM. ECM proteins *Acan* and *Fmod* (fibromodulin) were significantly upregulated, in both sham and MMT. *Acan* was overexpressed in the MMT and sham groups at week 1 and 3, compared to the control groups. *Fmod* was overexpressed in both surgery groups at week 3 only. While *Tnn* (tenascin) was significantly underexpressed at week 1 for the MMT and sham groups, it reached the level of the control group at week 3 for the sham group but remained significantly lower for the MMT group.

Comparing to the naïve control group, the synovium had a sustained significantly elevated expression of matrix degradation markers in the MMT group. In the sham surgery, these genes were also elevated at week 1 but most declined to the control level by week 3. *Mmp3*, *Mmp9*, *Mmp12*, and *Mmp13* were significantly higher in the MMT group at week 1 and remained so by week 3. *Mmp2* and *Ctsk* were significantly higher only at week 3 in the MMT group. In the sham group, *Mmp2*, *Mmp9*, *Mmp12*, *Mmp13* and *Ctsk* were significantly overexpressed at week 1. However, all, with the exception of *Mmp2* and *Ctsk*, declined to expression levels comparable to the control group by week 3. *Adamts4* was significantly higher in the sham group (vs. control) at week 1, but a similar trend could be observed; there seemed to be higher expression in the MMT groups at both timepoints and a lower level in the sham group at week 3 (vs. week 1). *Adamts5* was downregulated in the MMT group (vs. control) at week 1 and 3, while again in the sham group it was significantly lower at week 1 but recovered to the control group level by week 3. Matrix remodeling gene *Spp1* was overexpressed in both the sham and MMT at week 1 (vs. control), but only remainded overexpressed in the MMT at week 3. Metalloproteinase inhibitor *Timp1* was significantly higher in the sham group (vs.

control) at week 1, but followed the same pattern in that this expression significantly decreased by week 3 in the sham group, to a level comparable to the control. In the MMT, *Timp1* seemed to remain elevated, though this observation was not statistically significant.

Osteogenic markers were also dysregulated in the synovium. *Col1a1* and *Col1a2* were overexpressed in both the sham and MMT groups at week 1 (vs. control), but remained elevated in the MMT group at week 3. Although *Bmp2* (bone morphogenetic protein-2) showed significantly lower expression in the MMT group alone compared to the control at both timepoints, a similar trend was observed where the sham expression seemed lower at week 1 and closer to control levels by week 3.

Frzb was downregulated in both the sham and the MMT groups (vs. control) as early as week 1, but in this case, it remained low for the sham group as well as the MMT at week 3. *Epas1* had a similar profile, where both sham and MMT groups had significantly low expression even at week 3. *Tgm2* (transglutaminase-2) was underexpressed at week 1 for both groups (vs. control), yet recovered to the control level in the sham group by week 3. Tgm2 is modulated by inflammatory cytokines, and regulates chondrocyte hypertrophic differentiation and ECM mineralization [90, 91].

3.4.3 Confirmation of genes at the protein level

Immunostaining (Figure 18) of collagen type 2 protein (*col2a1* gene) showed morphological differences in the medial articular cartilage at week 3, confirming damage to this area due to MMT surgery. Mmp13 protein detection in the MMT group at week 3 was confined to the articular cartilage and synovium, confirming our gene expression

results. We hypothesize that it was not detected at week 1 (data not shown), as expected, due to the natural delay between translation and transduction, and the need for protein accumulation for immunolocalization. A similar case was observed with Osteopontin (*Spp1* gene). It was detected in the MMT group at week 3 only, in the articular cartilage and synovium.

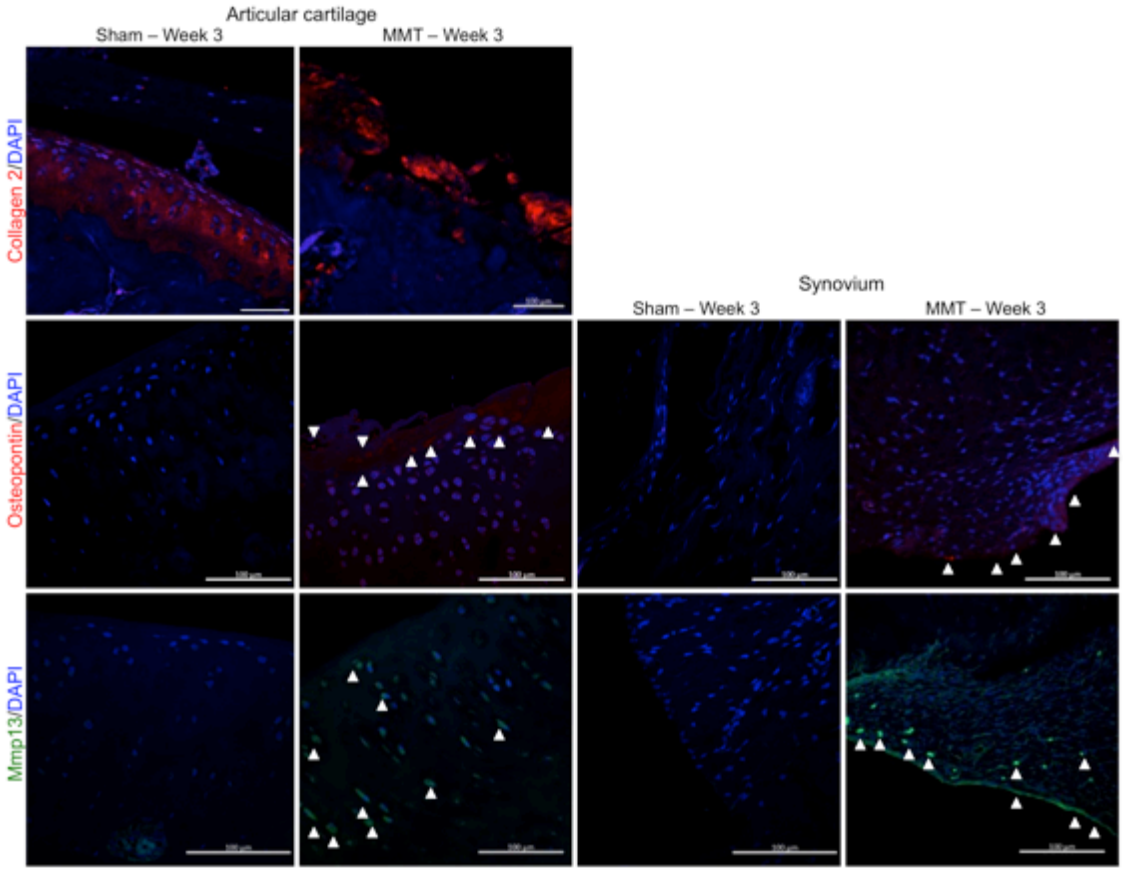

Figure 18. Fluorescent immunohistochemistry of collagen type 2, Mmp13, and osteopontin of the articular cartilage and the synovium at week 3. Collagen 2 staining was used to visualize the articular cartilage, in which fibrillation and lesion formation is apparent in the MMT group at 3 weeks post-surgery. White triangles point at positive staining of Mmp13 and Osteopontin. At 3 weeks post-surgery, Mmp13 and osteopontin were detected in the medial articular cartilage and synovium of the MMT group and absent in the sham group.

3.5 Discussion

3.5.1 Localized gene expression

Regional analysis of the tibial plateau shows that the lateral and medial sides have a significantly different gene expression profile, which is not surprising given the differences in anatomy between these two sides. MMT surgery creates localized damage in the medial tibial plateau [81], and analysis of this specific region allow us to pinpoint changes in tissue that might otherwise be lost by the pooling of tissue from both sides of the tibial plateaus and femoral condyles; a standard practice in gene expression studies [82-84].

Localized gene expression analysis is particularly important in the synovium. In this tissue type, there are differences in gene expression profiles among medial (unoperated) control, sham and MMT groups. In fact, we showed that there is a surgical effect that dominates at week 1 and which mostly subsides by week 3, though not entirely. This is not wholly surprising as the synovial membrane is cut to access and visualize the meniscus in both sham and MMT surgeries. Equally important, this study demonstrates that, unlike articular cartilage, both sides of the synovial membrane are affected by surgery and show significant differences in their gene expression profiles. The fact that changes in the lateral side cannot be pinpointed to the surgery type, microarray plate number (batch effect), or timepoint reemphasizes the importance of analyzing localized tissue (medial side, in this case) instead of pooling sample from the entire joint cavity.

3.5.2 Articular cartilage of the medial tibial plateau

This study is the first to report gene expression findings specifically for the medial tibial plateau of the MMT model. Here, we showed that the MMT model replicated several pathologies observed in human OA. Our findings also suggest that changes in chondrocyte phenotype may precede changes in ECM in this animal model, indicating that the response to destabilization may be firstly to readdress tissue composition and secondly to remodel.

Chondrocyte phenotype changes begin as early as week 1 in the MMT model. Previous studies have identified Wnt signaling to be involved in the response to mechanical injury to cartilage [87, 92, 93], since Wnt antagonists, Frzb and Grem1 function as natural brakes on hypertrophic differentiation of articular cartilage [94]. While Frzb inhibits Wnt directly, Bmp antagonist Grem1 functions indirectly [94]. Therefore, lower expression of Frzb and Grem1 in the MMT group points toward a de-differentiation of chondrocytes into the hypertrophic state in the medial tibial plateau.

Col10 expression was also significantly lower in the MMT model at week 1 and 3. Although col10 is a hypertrophic marker associated with endochondral ossification during growth and fracture healing and might, therefore, be expected to be expressed at higher levels, previous studies have also shown that its gene expression level is actually reduced in the OA disease state in animal models. In the anterior cruciate ligament (ACL) rabbit model of OA, Bluteau *et al.* (2001) observed reduced Col10 expression in the articular cartilage at 2 and 4 weeks post-surgery, whereas there was an increase in the meniscus at 9 weeks post-surgery [95]. Other studies have demonstrated the occurrence of col10 at the surface of normal human, porcine and rat articular cartilage, and have

suggested that the presence of this protein may be associated with the load bearing properties in different zones of the articular surface [96].

While chondrocyte phenotypic changes were discernible at week 1, changes in the articular cartilage ECM composition (elevated *Fn1* and *Col1a2*) were not significant until week 3. In OA, chondrocytes synthesize elevated levels of fibronectin, altering the cartilage ECM [97]. Although often considered an earlier sign of OA [97, 98], the MMT model did not show significant differences in *Fn1* expression until week 3. This suggests that, in the MMT model, changes in chondrocyte phenotype precede changes in the ECM of the articular cartilage. This is further supported by the fact that *Acan* and *Col2a1* were not expressed significantly different from the control group by week 3.

It is still unclear whether the increased synthesis of fibronectin in OA acts as an attempt by the chondrocytes to repair cartilage or whether it has a deleterious effect [97]. Its increased activity has been linked with a switch in synthesis of collagen type, an increased activity of locally secreted Mmps and induction of proteolytic activities against gelatin and fibronectin itself [97, 99]. In this study, we observed significantly higher expression of *Col1a2*, *Mmp2*, *Mmp13*, and *Ctsk* at week 3, the same timepoint as *Fn1*, paralleling the proposed mechanism for human OA [100, 101] and other rodent models [102].

The fact that metalloproteinase and aggrecanase inhibitors *Timp1* and *Inhba* (respectively) are overexpressed in the MMT group as early as week 1 suggests a protective mechanism in OA in the MMT model. This may be further corroborated by the downregulation of *Epas1* in the MMT group. A previous study has shown that

chondrocyte-specific knockout of *Epas1* in mice suppressed DMM (destabilization of the medial meniscus)-induced chondrocyte apoptosis and inhibited OA cartilage destruction [89]. We, therefore, propose that downregulation of *Epas1* in this case may be part of a protective mechanism in the MMT model.

Higher expression of the catabolism marker *Sod2* at weeks 1 and 3 indicates a homeostatic imbalance within the chondrocytes. Oxidative stress and dysregulated chondrocyte mitochondrial function contribute not only to impaired matrix synthetic function and viability, but also to molecular inflammatory processes and matrix catabolism in OA [103]. Ptgs2, which we have shown to be overexpressed in the MMT, is an inflammatory responsive gene and is regulated by nitric oxide [104].

Altogether, analysis of the medial tibial plateau articular cartilage shows that sham behaves similarly to the unoperated, control group and that MMT surgery replicates several human OA pathomechanisms. The pathomechanistic implications outlined in this study should be taken into account when using this model to test and/or explore therapeutic mechanisms. It is particularly important to understand the microenvironment which is encountered by the therapy of interest upon delivery, for which in depth molecular analysis and characterization of the MMT model as the disease progresses is needed.

3.5.3 Osteophyte tissue

At the joint margins in the interface between the cortical bone marrow and the periosteal lining, osteophytes form in human and experimental OA [105, 106]. While osteophytes have been reported and quantified at week 3 in the MMT model [81], they

are non-detectable via morphological analysis at week 1. In this study, we showed that we are able to detect gene expression differences between the sham and MMT groups at 3 weeks as well.

Osteophyte formation features vascularization of the tissue followed by endochondral ossification. It is well established that there are morphological differences in osteophyte formation between the MMT and sham groups at 3 weeks post-surgery, including increased mineralization and tissue formation [81]. However, we were not able to detect differences in these markers between the sham and MMT groups. Interestingly, we detected significant differences only in genes related to inflammation. Recent studies have reported evidence of the effects of inflammatory mediators on cellular differentiation [107]. In fact, Tnfα, IL1β, and NF-κB stimulate osteogenesis at low concentrations and inhibit it at high concentrations [107-112]. We, therefore, believe that the observed downregulation of inflammation genes in the MMT group is actually indicative of a pre-ossification phase of this region at week 3.

It is worthwhile mentioning that, while gene expression related to chondrogenic, chondrocyte hypertrophy and osteogenic markers is not different between the sham and MMT groups at any timepoint, there are signs of cell proliferation in the MMT group at week 3. The tissue from this region of the joint is fundamentally different than the tibial plateau, and so, we postulate that morphological differences between the sham and MMT at 3 weeks post-surgery are due to there simply being more tissue in the MMT model at this timepoint. To test this hypothesis, thorough profiling of markers related to proliferation in this area, perhaps by RNA sequencing, as well as extended timepoints of analyses, will be required.

3.5.4 Distal medial synovial membrane

To the best of our knowledge, this is the first study to report gene expression profiles of the synovial membrane in an experimental animal model, and specifically on the medial side of the synovial membrane. Surgical effect (sham and MMT) dominates the gene expression profile of the medial synovium at week 1, and it is not until week 3 that this surgical noise dissipates and meniscal instability starts to have a pronounced effect on the medial synovium. This MMT characteristic is of the upmost importance when considering experimental design of a new therapy, and it reemphasizes the importance of a sham group in an experiment.

Overall, we observed an increase in markers related to matrix degradation and remodeling in the synovium that remained elevated in the MMT at week 3. We also showed an overexpression of most osteogenic markers and underexpression of Wnt antagonists in the MMT. These findings suggest a feedback loop with the articular cartilage. As in human OA, the synovium is affected by the mechanical instability of the model and may exacerbate the changes to the articular cartilage. We, therefore, postulate that the joint space acts in concert in the MMT model.

3.5.5 Inflammation in the MMT model

Surprisingly, apart from *Ptgs2*, our genes related to inflammation (pro- or anti-) were not differentially regulated, except in the osteophyte region. We believe that this may have been due to our harvesting timepoint. Collecting tissues at earlier timepoints may have shown a detectable signal difference between unoperated and operated legs (control vs. sham and MMT). However, for the purpose of this study, we wanted to

minimize noise due to surgery (inflammation that is inevitable post-surgery) and so we decided to collect samples starting at week 1. It was, therefore, interesting that we still detected evidence of surgery in the synovium at this timepoint.

The MMT model is a mechanically induced model and it is generally not associated with substantial inflammation, unlike the MIA model [113]. Nevertheless, it is worth pointing out that even though we do not observe changes in genes generally associated with inflammation at our timepoints, we may be observing the consequences of their dysregulation in the sham and MMT surgical groups. In OA, *IL1* (pro-inflammatory) is synthesized by chondrocytes and capable of inducing the expression of *Mmps* and other catabolic genes [114]. A variety of inflammatory mediators and growth factors, including *IL1*, *Tnfα* and *Pdgf* (platelet-derived growth factor), stimulate *Spp1* transcription [88]. In fact, *Spp1* has both pro- and anti-inflammatory actions [88]. We have shown changes in the expression of several *Mmps* and *Spp1* in the articular cartilage and synovium in this study due to MMT surgery. Whether these changes are indeed downstream of inflammatory processes remains to be answered, and evaluating the model at earlier timepoints would be a useful start for future directions.

CHAPTER 4. LOCALIZED OSTEOARTHRITIS DISEASE-MODIFYING CHANGES DUE TO INTRA-ARTICULAR INJECTION OF MICRONIZED DEHYDRATED HUMAN AMNION/CHORION MEMBRANE

4.1 Abstract

Micronized dehydrated human amnion/chorion membrane (AmnioFix Injectable, MiMedx, Marietta, GA, USA) has anti-inflammatory, low immunogenic and anti-fibrotic properties, and its delivery intra-articular delivery into the joint space has been shown to have a chondro-protective effect on the articular cartilage in an *in vivo* model of post-traumatic OA. AmnioFix is an ECM-derived therapeutic, and its mechanisms of action on OA progression and potential modification remain largely undetermined. As AmnioFix is sequestered in the synovial membrane, we hypothesized that injection of AmnioFix attenuates catabolic and inflammatory signaling in the synovium, which in turn protects the articular cartilage from further degradation.

The objective of this study was to elucidate the molecular mechanisms of action of AmnioFix treatment with OA development and progression. Weight-matched Lewis rats underwent MMT surgery to induce OA-like clinical symptoms, and AmnioFix or saline was injected intra-articularly 1 day post-surgery. At 5, 7, and 21 days post-surgery, articular cartilage, synovial membrane, and osteophyte tissues from multiple regions were collected and analyzed by microarray RT-PCR.

Results demonstrated that there were no significant differences between groups for the articular cartilage or osteophyte tissue, suggesting that the AmnioFix treatment does not have a direct influence on these tissues. In the medial synovial membrane, pro- and anti-inflammatory markers were more highly expressed in the AmnioFix group than in the saline group. The gene expression profile of the AmnioFix group in the medial synovial membrane was markedly different from the saline group and the control group. These data suggest that AmnioFix treatment may modulate the microenvironment of the synovial membrane to a favorable chondro-protective profile. The upregulation of pro-inflammation-related cytokines could promote the recruitment of repair cells, and anti-inflammatory responses may act as a countermeasure to restore the shift in the pro-/anti-inflammation balance that occurs during disease progression and wound healing.

4.2 Introduction

An emerging focus of regenerative medicine is the development of ECM-based therapies that can stimulate tissue formation or repair by recreating the functional and structural properties of native ECM (scaffolds), or by acting as a source of growth factors. Decellularized ECM-derived treatments are prime candidates for potential DMOADs as they maintain many of the bioactive molecules specific to the native tissue, which are not present in synthetic materials, and do not produce an adverse immune response [115]. While another advantage of ECM-derived DMOADs is their high degree of translatability, a major disadvantage is the fact that these therapies are virtually black boxes, for which the mechanisms of effects are not well understood. ECMs are complex environments that house many interactions. Donor-to-donor variability of human tissue may also impact the biological properties of the resultant ECM-derived DMOADs.

Micronized dehydrated human amnion/chorion membrane (AmnioFix® Injectable, MiMedx, Marietta, GA, USA) has recently been granted the Regenerative Medicine Advanced Therapy (RMAT) designation for use in OA of the knee, and is currently undergoing Phase 2 clinical trials. While AmnioFix has shown promising pre-clinical and initial clinical data, its therapeutic mechanisms are still largely unknown. The composition and properties of AmnioFix have been largely characterized [116, 117], but its molecular interactions with tissues in the joint space as OA develops and progresses are not known.

Human amnion/chorion tissue is derived from the placenta and is rich in cytokines and growth factors known to promote wound healing [117]. The processing of AmnioFix Injectable permits retention of a large array of these factors – many of which may aid in cell proliferation, inflammation, metalloproteinase activity and recruitment of progenitor cells in a paracrine manner [116, 117]. Past studies have demonstrated efficacy, e.g. intra-articular injection of AmnioFix Injectable into the knee joint in the MMT model demonstrated a protective effect of this treatment on the articular cartilage [3]. At 3 weeks post-surgery, the articular cartilage showed little signs of degradation in terms of its proteoglycan content and morphology [3]. In this study, the AmnioFix microparticles were detected in the synovium up to 3 weeks post-surgery [3]. Therefore, a putative mechanism of action of AmnioFix would involve the synovial membrane.

In wound healing, human amniotic membrane allografts are known to decrease inflammation, reduce scar tissue formation, and support soft tissue regeneration [118, 119]. However, in OA, anti-inflammation drugs targeting the TNFα/IL1-driven cascades (inflammation) have not shown consistent evidence of chondro-protective mechanisms *in*

vivo and are not considered successful disease-modifiers [120-125]. Likewise, pharmacological upregulation of repair-promoting factors, e.g. TGFβ and/or IGF1, is not expected to contribute to disease modification in OA because anabolic repair pathways are already overexpressed in this disease [125].

Other studies have targeted different inflammatory pathways with initial success in clinical trials [125], and so reduced inflammation may be still be a contestant for the key therapeutic mechanism of AmnioFix treatment. It is worth noting, nevertheless, that the MMT model in which AmnioFix was shown to be effective is not regarded as an inflammation model. In fact, in our previous chapter, we did not find detectable levels of inflammatory markers as disease developed in the MMT model. Therefore, the question remains of which may be the key drivers of the chondro-protective effect observed in AmnioFix treatment.

The objective of this aim was to determine mechanisms of action of AmnioFix Injectable on localized regions of the articular cartilage, synovial membrane, and osteophyte-forming region within the knee joint of the MMT post-traumatic OA model. Our hypothesis was that AmnioFix targets and modulates the microenvironment of the synovial membrane as a means to alleviate catabolic mechanisms in the joint space and protect the articular cartilage.

4.3 Materials and methods

4.3.1 Animals: Surgery and treatment

The Georgia Institute of Technology Institutional Animal Care and Use Committee approved all experimental animal procedures (IACUC protocol #A14023). Weight-matched (275-300g) male Lewis rats were acclimated 1 week before receiving MMT surgery. Briefly, a small incision was made through the skin on the medial aspect of the femoro-tibial joint of the left limb. The medial collateral ligament was exposed by blunt dissection and transected to visualize the joint space and meniscus. The meniscus was then cut at its narrowest point. The naïve right limbs were used as contralateral baseline controls.

1-day post-surgery, animals were randomly divided into two groups to receive either 50µl of saline (saline group) or AmnioFix (AmnioFix group) intra-articular injections. AmnioFix injections were prepared from 5 pooled donors at a dose of 40 mg/ml, as previously described [3]. Animals were then taken down at 5 days, 7 days and 21 days post-surgery and tissues harvested for experiments. 36 animals were allocated for gene expression (n=9 per group per timepoint), 12 for histology (n=3 per group per timepoint), and 20 for protein extraction of the synovium tissue (n=4-5 per group per timepoint).

4.3.2 Microarray gene expression

Articular cartilage samples were harvested at 7 and 21 days post-surgery. From each leg, tissue was collected from 3 regions: the medial tibial plateau, the lateral tibial plateau, and the medial joint margin (osteophyte tissue). Osteophyte tissue was only collected from surgerized limbs (saline and AmnioFix groups) at 21 days post-surgery due to insufficient tissue in the unoperated limbs (control group) and at earlier timepoints.

Synovial membrane was harvested at 5, 7 and 21 days post-surgery. From each leg, 2 synovium samples were collected, from the medial and lateral sides of the joint, distal of the meniscus and directly adjacent to the tibial plateau. Each sample was stored separately in RNAlater (Ambion Inc.) at 4°C until processed.

Total RNA from cartilage and osteophyte tissues was extracted using the RNeasy MinElute Clean-up Kit with QIAzol Lysis Reagent. Total RNA from synovium was extracted using the RNeasy Lipid Tissue Mini Kit with QIAzol Lysis Reagent. RNA quality and concentration for all samples were determined using the Nanodrop ND-1000 Spectrophotometer (ThermoFisher). Normalized RNA was converted to cDNA via the RT^2 First Strand Kit. All reagents were from Qiagen unless otherwise stated.

RNA expression was quantified using the Taqman RT-PCR Fluidigm Dynamic Array Integrated Fluidic Circuits (BioMark, Fluidigm). Our cDNA samples were tested against 58 genes (TaqMan gene expression assays, ThermoFisher, Table 3), which were selected from literature detailing human OA pathomechanisms and about AmnioFix composition. AccuRef rat universal cDNA (Gene Scientific) and ultrapure water were used as positive and negative controls, respectively, to ensure run fidelity. The Ct values greater than 37 were treated as 37, namely as null (lower Ct values correspond to higher expression since they represent the PCR cycle at which a threshold level of product is observed).

Table 3. Taqman Gene Expression Assays for evaluation of the effects of AmnioFix in the MMT model. Assays were all purchased from Thermo Fisher Scientific. Where available, "best coverage" assays were used that are recommended by the company.

Category	Taqman Gene Expression Assays
ECM composition markers	*Col1a1* (Rn01463848_m1), *Col1a2* (Rn00670295_m1), *Col2a1* (Rn01637087_m1), *Acan* (Rn00573424_m1), *Fn1* (Rn00569575_m1), *Fmod* (Rn00589918_m1), *Tnn* (Rn01491027_m1)
ECM remodeling markers	*Mmp2* (Rn01538170_m1), *Mmp3* (Rn00591740_m1), *Mmp9* (Rn00579162_m1), *Mmp12* (Rn00588640_m1), *Mmp13* (Rn01448194_m1), *Adamts4* (Rn02103282_s1), *Adamts5* (Rn01458486_m1), *Ctsk* (Rn00580723_m1), *Spp1* (Rn00681031_m1), *Timp1* (Rn01430873_g1), *Timp2* (Rn00573232_m1), *Timp3* (Rn00441826_m1), *Inhba* (Rn01538592_m1)
Chondrogenesis marker	*Sox9* (Rn01751070_m1)
Chondrocyte hypertrophy markers	*Frzb* (Rn01746979_m1), *Grem1* (Rn01509832_m1), *Col10a1* (Rn01408030_m1), *Tgm2* (Rn00571440_m1)
Osteogenesis markers	*Bglap* (Rn00566386_g1), *Runx2* (Rn01512298_m1)
Vascularization marker	*Vegfa* (Rn01511602_m1)
Inflammation and tissue repair-related markers	*Tnfα* (Rn01525859_g1), *Tgfβ1* (Rn00572010_m1), *IL1a* (Rn00566700_m1), *IL1b* (Rn00580432_m1), *IL1rn* (Rn02586400_m1), *IL6* (Rn01410330_m1), *IL10* (Rn01483988_g1), *IL13* (Rn00587615_m1), *IL15* (Rn00689963_g1), *IL17ra* (Rn01757168_m1), *Infg* (Rn00594078_m1), *Ccl1* (Rn01752376_m1), *Ccl2* (Rn00580555_m1), *Ccl3* (Rn_01464736_g1), *Ccl7* (Rn01467286_m1), *Cxcl12* (Rn00573260_m1), *Ccr7* (Rn02758813_s1), *Csf1* (Rn01522726_m1), *Cxcr1* (Rn00570857_s1), *Cxcr2* (Rn02130551_s1), *Ptgs2* (Rn01483828_m1), *Fgf2* (Rn00570809_m1)
Catabolic factors	*Epas1 (Rn00576515_m1), Sod2 (Rn00690588_g1)*
Cell stress and apoptosis markers and inhibitors	*Casp8 (Rn00574069_m1), SIRT1 (Rn_01428096), Prkaa2 (Rn00576935_m1)*

Housekeeping genes	*Ppia (Rn00690933_m1), Rplp1 (Rn03467157_gH), Rpl13a (Rn00821946_g1), Gapdh ()*

4.3.3 Histological analysis

In order to confirm AmnioFix sequestration to the synovial membrane, full joints were fixed in 10% NBF, processed, and embedded in paraffin. 5 μm sections were stained with Hematoxylin and Eosin (H&E). Sections were also stained for CD68 (Bio-Rad MCA341R), a marker of macrophages. Briefly, antigen retrieval, permeabilization, and blocking were performed on the sections before overnight incubation in the primary antibody at 4°C. Secondary antibody (Cell signaling 4409S) was incubated for 1 hour at room temperature, followed by DAPI staining.

4.3.4 Statistical analyses

4.3.4.1 Gene expression

Ct values were subtracted from 37 in order to invert them. To calculate the relative gene expression (ΔCt values), Ct values were normalized by the geometric mean of four housekeeping genes: *Ppia*, *Rplp1*, *Rpl13a*, and *Gapdh* (Equation 1). In order to correct experimental differences observed between biological replicates and runs, the medians of each replicate experiment were median-centered. The QRO test was performed to remove any outliers. All statistical calculations were performed with JMP Genomic software (SAS Institute, Cary, NC, USA).

4.3.4.1.1 Principal component analysis (PCA) and unsupervised clustering analysis.

Scripts from JMP Genomic software were used to perform both analyses. In the weighted average proportions of the PCA models, a residual (unexplained) variance higher than 60% was considered as too noisy and to have too many potential confounding variables in the sources of variability (surgery, timepoint, batch effect) to draw conclusions.

4.3.4.1.1 Differential expression

Volcano plots were used to compare the gene expression profile of two groups. Significance was determined using Bonferroni correction (0.05 (p-value) divided by the number of observations).

For each individual gene expression, two-way ANOVA was used to compare differences among all groups (control, AmnioFix and saline). Tukey's *post hoc* comparison was performed to compare the means of parametric cases in which one-way ANOVA assumptions were fulfilled. Kruskal-Wallis *post hoc* test was used for non-parametric cases. P-values less than 0.05 were considered statistically significant.

Then, to calculate the difference in normalized expressions between the saline and AmnioFix groups, ΔΔCt values were calculated by subtracting the mean of the control group from the mean of the experimental group (saline or AmnioFix) for each individual gene expression (Equation 2). The SEM for ΔΔCt values was calculated using Gauβ error propagation equation (Equation 3). Two-way ANOVA was performed to determine the statistical significance of the differences between the means for each treatment and time

groups. Tukey's and Kruskal-Wallis were used as *post hoc* tests when appropriate. P-values less than 0.05 were considered statistically significant.

All graphs were plotted as means ± SEM. Analyses were carried out using JMP Genomic software and graphed in JMP, Excel, or GraphPad Prism, version 7 (San Diego, CA).

$$\Delta\Delta Ct = \Delta Ct_{experimental\ group} - \Delta Ct_{calibrator\ group}$$

Equation 2. Equation to calculate normalized relative expression ($\Delta\Delta Ct$) for each individual gene expression. In this chapter, samples from the unoperated contralateral control group were used as the calibrator.

$$SD' = \sqrt{SD^2_{experimental\ group} + SD^2_{calibrator\ group}}$$

Equation 3. Equation for SD of ΔΔCt, derived using Gauβ's error propagation.

4.4 Results

4.4.1 Articular cartilage

In agreement with the previous chapter, no significant differences in gene expression were observed in the lateral side of the articular cartilage from the tibial plateau between the (unoperated) control and the MMT surgery (regardless of treatment) (data not shown). This is expected, as it has been shown before that the MMT surgery creates a focal defect on the medial side of the tibial plateau, exclusively [81]. Therefore, we discuss only the medial side of the synovium forthwith.

4.4.1.1 Medial articular cartilage

The PCA showed that clustering was driven by surgery (unoperated vs. MMT) and then timepoint (Figure 19). Differences attributed due to treatment only accounted for 0.03%, which are considered negligible. There are only 2 significantly expressed genes that are different between the saline and AmnioFix groups in the medial articular cartilage. *Col1a1* and *Col1a2* (collagen type I isoforms) were overexpressed in the AmnioFix group comparing to the saline and control groups at 21 days post-surgery (Figure 20).

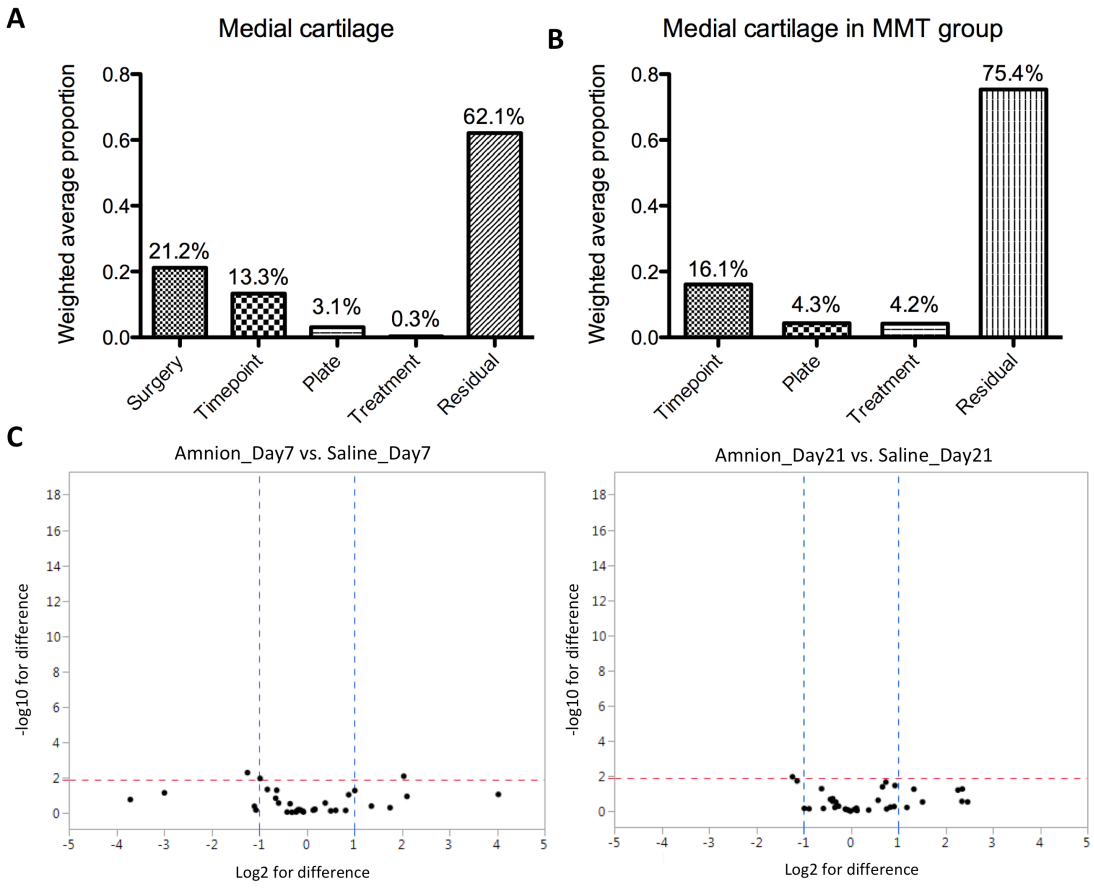

Figure 19. A. PCA of the medial articular cartilage tissues shows that difference in groups are driven by surgery first, then timepoint, plate (batch number) and lastly treatment. B. PCA of the medial articular cartilage of animals that underwent MMT surgery (saline and AmnioFix groups) shows that differences have a high

degree of noise (residual at 75%) and are driven by timepoint, plate and, last, treatment. Treatment does not appear to be an influential factor in molecular changes of the articular cartilage as OA progresses. C. Volcano plots of AmnioFix group versus saline group at day 7 and day 21 shows that there is no significant difference between the two groups due to gene expression. Only collagen type 1 (col1a1 and Col1a2) were higher expressed in the AmnioFix group.

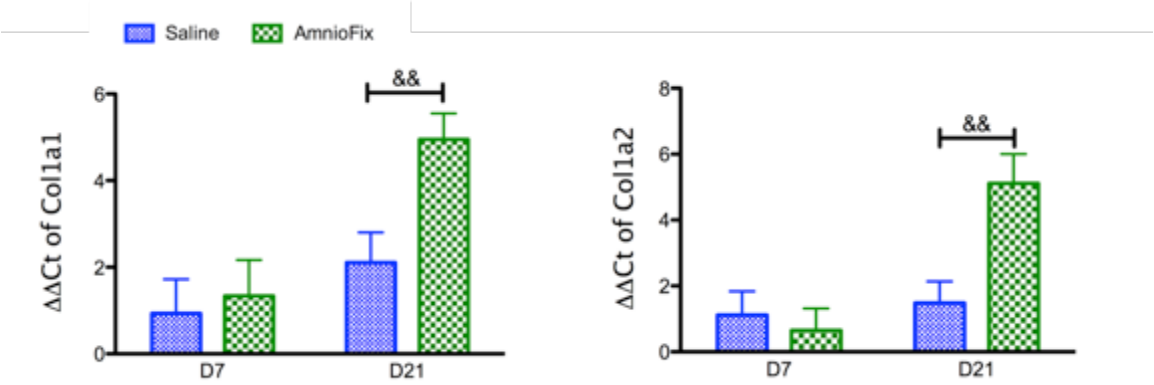

Figure 20. Col1a1 and Col1a2 were the only genes significantly different between the saline and AmnioFix groups in the medial articular cartilage of the tibial plateau of MMT animals, graphed as means ± SEM. && indicates significant difference between the two groups at the indicated timepoint at a p-value <0.01.

11 genes were differentially expressed between the unoperated animals (control group) and those which received MMT surgery (regardless of treatment, AmnioFix or saline groups), as shown in Figure 21. ECM gene *Fn1* (fibronectin) was significantly lower in the control group than in the saline and AmnioFix groups at day 21. ECM remodeling genes were also dysregulated due to MMT surgery. *Timp1* was significantly lower in the control than saline and AmnioFix at all timepoints. *Mmp13* and *Mmp2* were significantly lower in the control than the saline or AmnioFix at day 21. Ctsk was significantly lower in the control than the AmnioFix alone at day 21. *Spp1* was significantly lower in the control than saline at day 21 and AmnioFix at days 7 and 21. *Inhba* was significantly lower in the control than saline at days 7 and 21 and than AmnioFix at day 21 only. Chondrocyte hypertrophic markers *Frzb* were significantly higher in the control group than the saline and AmnioFix groups for all timepoints, while Grem1 was significantly higher than saline at day 7 and than AmnioFix at day 21. *Tgm2* was significantly lower in the control group than the other two at day 21 only. *Col10a1* was significantly higher in the control group than the AmnioFix group at all timepoints. Finally, *Sod2* was significantly lower in the control than in AmnioFix at day 21.

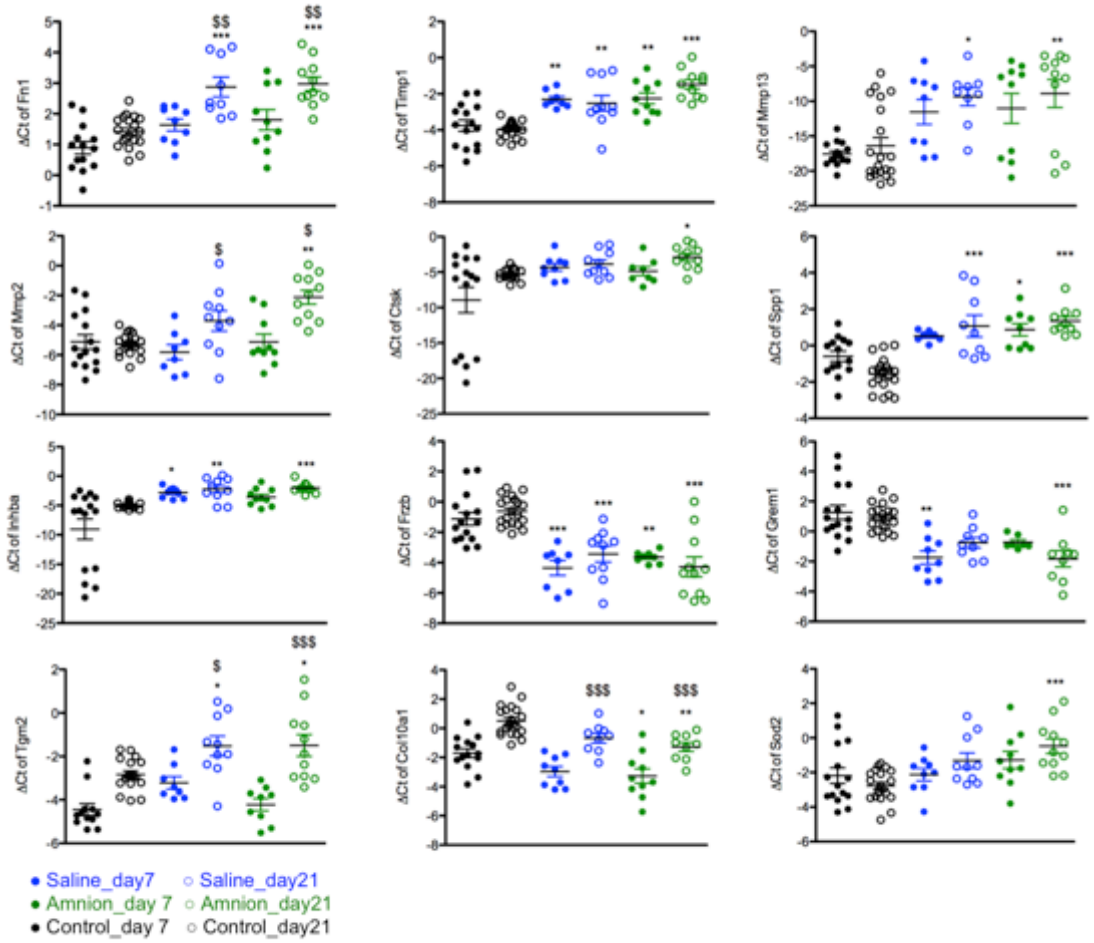

Figure 21. Significantly expressed genes in the medial articular cartilage of the tibial plateau, graphed as means ± SEM. * indicates significant difference between the group and the control at the indicated timepoints at p-value <0.05; ** at p-value<0.01; and * at p-value<0.001. $ indicated significant difference between the timepoints within the same group at p-value<0.05; $$ at p-value<0.01; and $$$ at p-value<0.001.**

4.4.2 Synovial membrane

According to PCA, the lateral side of the synovial membrane was largely affected by choice of treatment (data not shown). This is not surprising since AmnioFix is injected intra-articularly and therefore expected to not be specific to one side of the joint space. However, because we have shown in the previous chapter that the MMT surgery does not have clear effect on the lateral synovial membrane, but instead that differences are driven by a rather large percentage of unknown or confounded variables; we focused our analyses and interpretations on the medial side of the synovial membrane only.

4.4.2.1 Medial side of the synovial membrane

Surgery is the largest driver of separation among the groups, while treatment is second (Figure 22). It is worth noting that the AmnioFix treatment gives the medial synovial membrane of MMT rats a profile that is distinct from that of the unoperated, control (PCA plot, Figure 22. A. Unsupervised clustering of the distal medial synovial membrane tissue showed grouping based on surgery, followed by treatment. B. PCA confirms surgery as the largest factor of separation between groups, followed by treatment. It should be pointed out that all 3 groups have distinct profiles, which cluster in the PCA. The AmnioFix group is not the same as the unoperated control, but an entirely different profile.). There were 17 genes that showed significantly different expression between AmnioFix and saline groups (Figure 23).

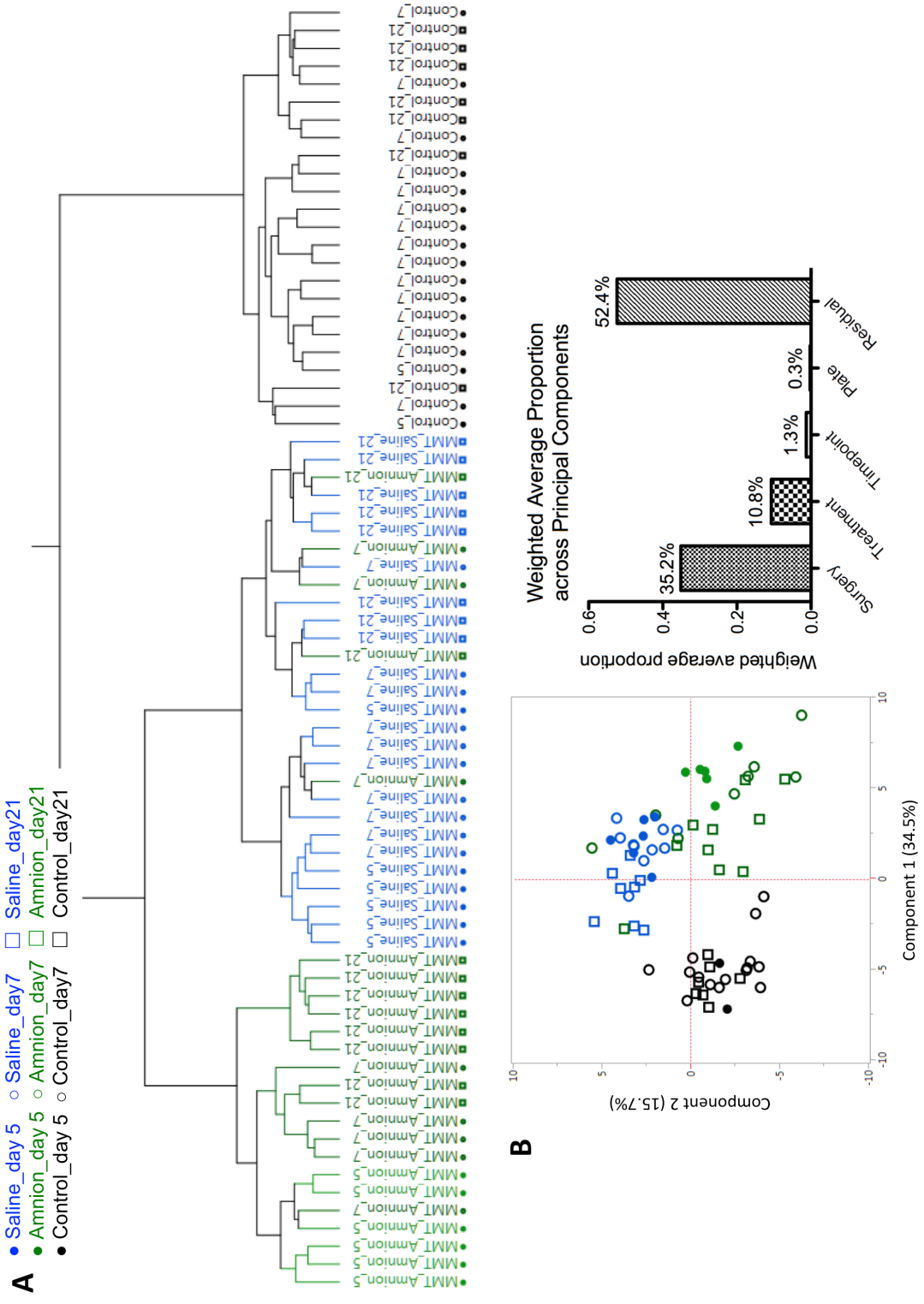

Figure 22. A. Unsupervised clustering of the distal medial synovial membrane tissue showed grouping based on surgery, followed by treatment. B. PCA confirms surgery

as the largest factor of separation between groups, followed by treatment. It should be pointed out that all 3 groups have distinct profiles, which cluster in the PCA. The AmnioFix group is not the same as the unoperated control, but an entirely different profile.

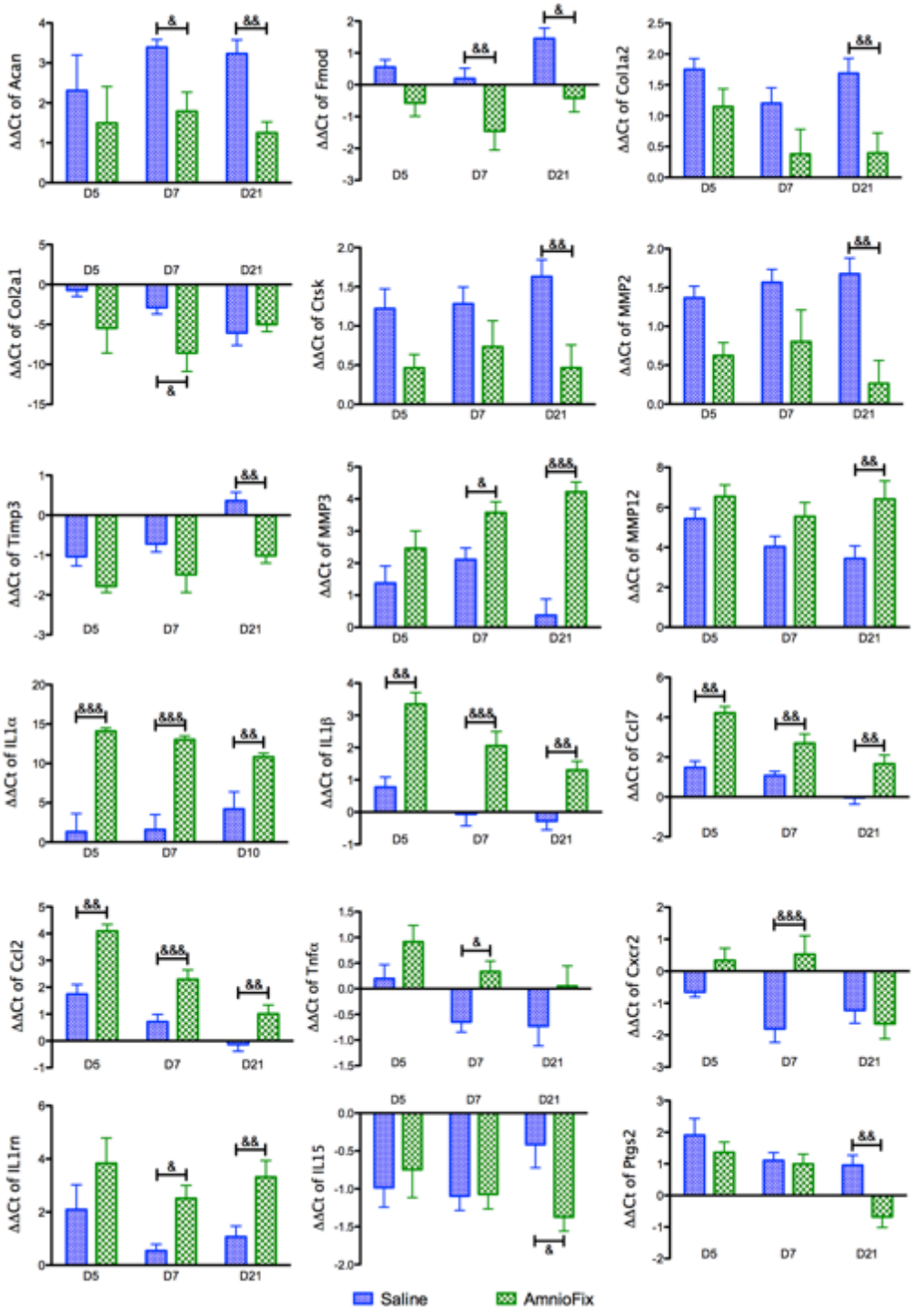

Figure 23. Significantly expressed genes between AmnioFix and saline groups of the medial synovial membrane, graphed as means ± SEM. & indicates significant difference between groups for the indicated timepoint at p-value<0.05; && at p-value<0.01; and $$ at p-value<0.001.

In general, genes related to the ECM structural composition were overexpressed in the saline group (vs. the AmnioFix group). The saline group had significantly higher expression of *Acan* and *Fmod* than the AmnioFix group at days 7 and 21. *Col1a2* was significantly higher in the saline group than the AmnioFix group at day 21. *Col2a1* was significantly higher in the saline group than in the AmnioFix group at day 7 only. Genes related to ECM remodeling had a variable response. *Ctsk*, *Mmp2* and *Timp3* were expressed significantly higher in the saline group than in the AmnioFix group at day 21. *Mmp3* and *Mmp12* were significantly higher in the AmnioFix group than in the saline group, at days 7 and 21 and at day 21 respectively.

10 genes related to immunomodulation were regulated when the MMT model was treated with AmnioFix. *IL-1a*, *IL1b*, *Ccl7*, *Ccl2*, and *Ifng* were higher expressed in the AmnioFix group than in the saline group at every timepoint. *Tnfa* and *Cxcr2* were significantly higher in the AmnioFix group than the saline group at day 7. *IL1rn* was significantly higher in the AmnioFix group than the saline group at days 7 and 21. *IL15* and *Ptgs2* were significantly lower in the AmnioFix group than the saline group at day 21.

8 genes were significantly different between unoperated animals (control group) and MMT animals, regardless of treatment; that is, differences were observed between control group vs. AmnioFix and vs. saline, but not between AmnioFix and saline (Figure 24). Several ECM remodeling markers were significantly different in the control group than the saline and AmnioFix groups. *Adamts4* was significantly lower in the control than the saline and AmnioFix at days 5 and 7. *Timp1* was significantly lower in the control group than in the other two groups for all timepoints. *Adamts5* and *Fgf2* were

significantly higher in the control group than in the saline and AmnioFix groups at all timepoints. *Spp1* was significantly lower in the control group than the saline at day 7 and the AmnioFix at all timepoints.

Tnn was significantly lower in the control group than saline and AmnioFix for all timepoints. *Csf1* was significantly lower in the saline at days 7 and 21 and in the AmnioFix at days 5, 7 and 21 than in the control group. *Epas1* was significantly lower in the saline and the AmnioFix at days 7 and 21 than the control group.

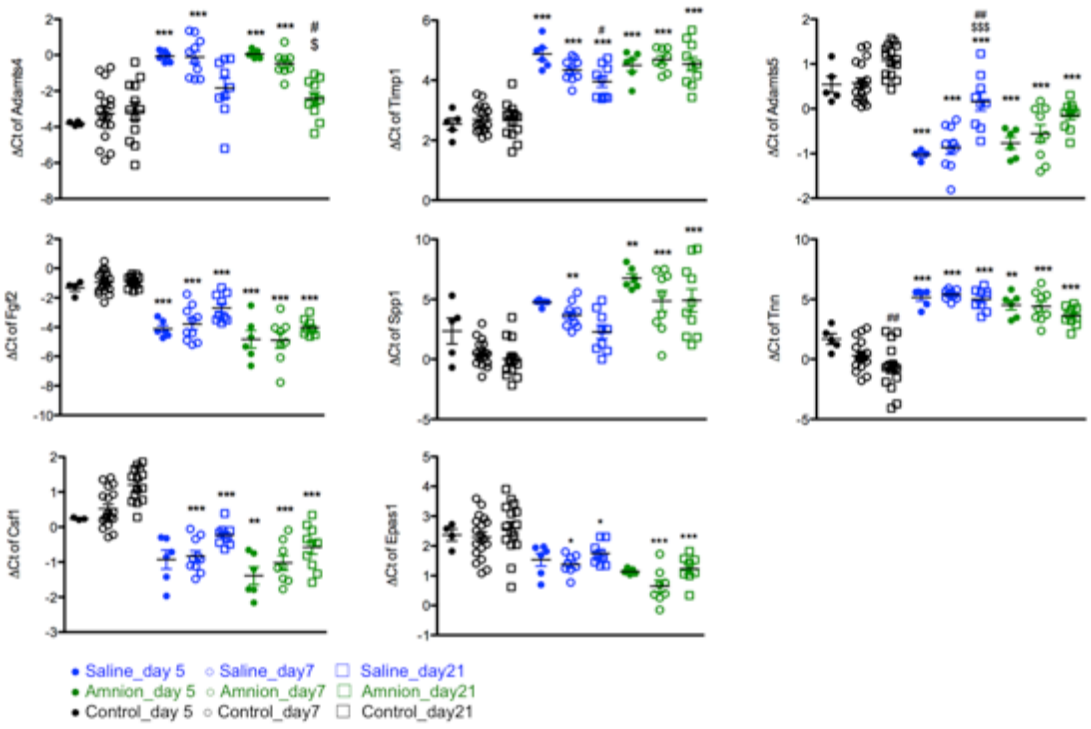

Figure 24. Significantly different genes in the medial synovial membrane, between the control group and the treatment groups, graphed as means ± SEM. * indicates significant difference between the group and the control at the indicated timepoint at p-value<0.05; ** at p-value<0.01; and * at p-value<0.001. # indicates significant difference between day 21 and day 5 for the indicated group at p-value<0.05; and ## at p-value<0.001. $ indicates significant difference between day 21 and day 7 for the indicated group at p-value<0.05; and $$$ at p-value<0.001.**

4.4.3 Osteophyte region

Gene expression results showed no significant differences between the saline and AmnioFix groups at day 21. There was no apparent organized clustering of the samples, according to the PCA (Figure 25).

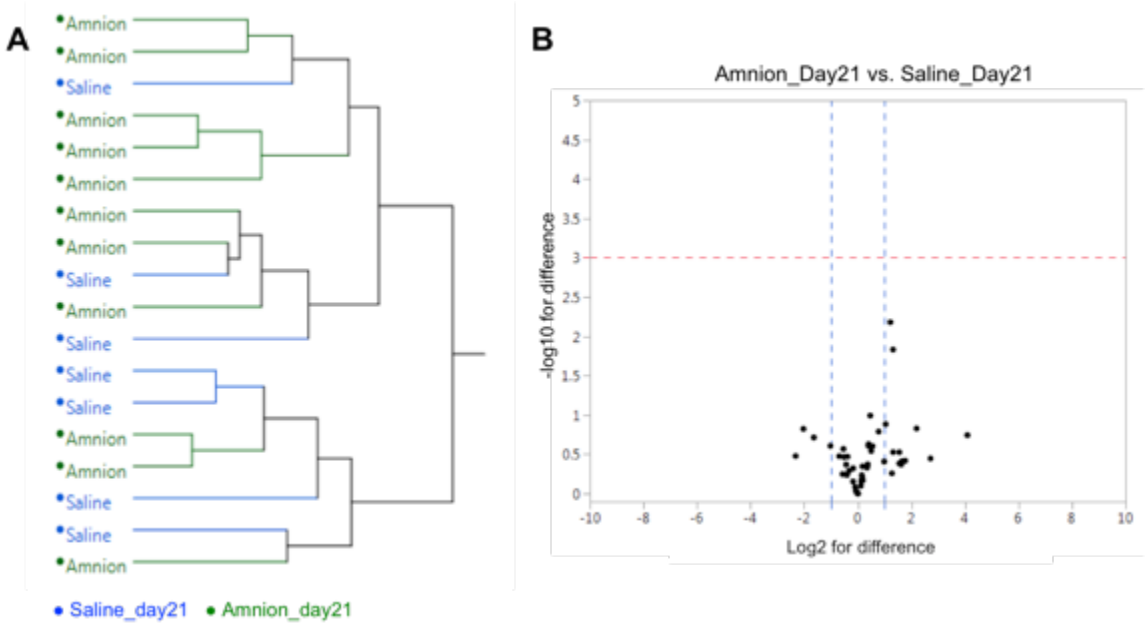

Figure 25. A. Unsupervised clustering shows no distinct grouping of samples harvested from the osteophyte region. B. Volcano plots show no significant difference between osteophyte tissue collected from saline and AmnioFix groups, suggesting that AmnioFix treatment did not directly affect molecular mechanisms in this region of the joint.

4.4.4 AmnioFix sequestration

At 7 days post-surgery, traces of AmnioFix Injectable were discernable only in the AmnioFix-treated group in the synovial membrane (Figure 26). AmnioFix was not discernable at 21 days post-surgery.

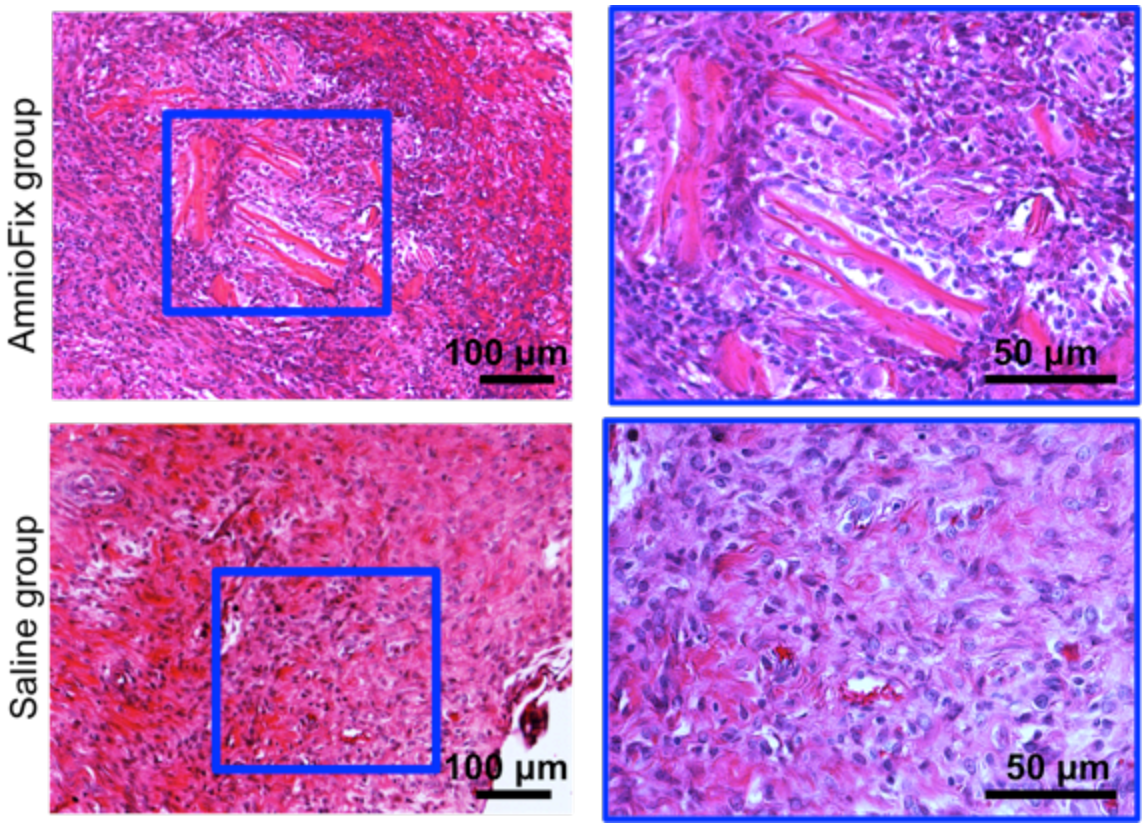

Figure 26. Hematoxylin & Eosin staining of the synovial membrane shows traces of AmnioFix Injectable in the AmnioFix treatment group and not in the saline group at 7 days post-surgery.

4.4.5 Recruitment of helper cells by AmnioFix

At 7 days post-surgery, cells in the AmnioFix treatment stained positive for CD68 marker of macrophages in the synovial membrane (Figure 27). No positive CD68 staining was observed in the saline group in the synovial membrane.

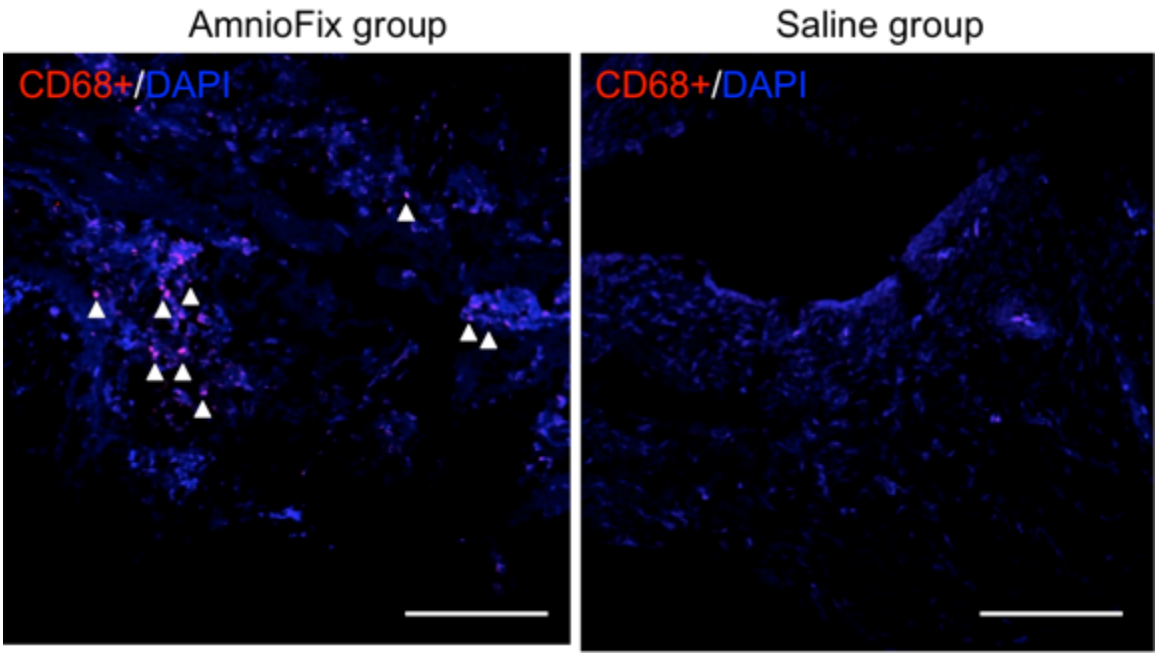

Figure 27. CD68+ staining of cells was observed at day 7 post-surgery in the AmnioFix group, but not in the saline group.

4.5 Discussion

Pre-clinical and clinical data have shown a protective effect on the articular cartilage after intra-articular injections of AmnioFix, yet the mechanisms of action of this potential disease-modifying OA drug cannot be inferred based on morphological endpoint readings or the composition of the material. By performing a localized gene expression study on multiple tissues of the MMT OA rat model, of different regions and at different timepoints, we were able to elucidate certain molecular events taking place with OA progression in this model and how AmnioFix may be modulate these pathological changes.

It was interesting to note that, apart from collagen type I, there were no significant differences in gene expression of the articular cartilage for the MMT animals between

treatments (saline vs. AmnioFix). In the previous chapter, we have shown that there are pathological changes at the molecular level which are identifiable using this gene analysis platform, and here also, we observed distinct changes in gene expression due to the MMT surgery (regardless of treatment). However, AmnioFix does not appear to act directly on the articular cartilage, or on the osteophyte-forming region of this post-traumatic OA model. The disease progressing mechanisms, including increased levels of ECM remodeling markers and activation of chondrocyte hypertrophic switches, are still taking place in the articular cartilage. *Mmp13*, *Mmp2*, *Ctsk*, *Inhba*, *Timp1*, *Timp3*, and *Spp1* were all upregulated as a consequence of MMT surgery, and AmnioFix treatment did not appear to influence these genes. Underexpression of *Grem1* and *Frzb* and overexpression of *Tgm2* may lift the block on chondrogenic differentiation and allows chondrocytes to become hypertrophic. These results suggest that, in spite of AmnioFix treatment, molecular pathomechanisms still continue in the articular cartilage. They also emphasize the role the synovial membrane plays in OA development in the MMT rat model. It is possible that by treating the synovial membrane, AmnioFix is able to delay morphological changes in the articular cartilage, even though changes have been initiated at the molecular level.

The influence of the synovial membrane in OA has been highlighted as a silent, yet pivotal contributor to disease progression in recent years [10, 11]. The joint acts as an organ, and it has been shown that OA-induced cartilage degradation triggers a Janus-like pro-inflammatory and anti-inflammatory response from the synovium [11]. It is believed that, due to the initial stimulus (cartilage injury) not being addressed, the immunogenic response becomes chronic and the synovium and the articular cartilage enter a positive

feedback loop, in which catabolic factors released by the synovium exacerbate the damage to the cartilage. The anti-inflammatory response from the synovium cannot offset the catabolic mechanisms at this point.

In the medial side of the synovial membrane, AmnioFix Injectable elevated the expression of pro-inflammatory cytokines and chemokines: IL-1a, IL1-b, IL15, Ccl2 and Ifng. AmnioFix Injectable itself is known to contain these factors [117], and results suggest that contact with the synovium may have stimulated further production by synovial cells. We suggest that this pro-inflammatory gene expression driven by AmnioFix may initiate remodeling/repair mechanisms akin to wound healing in the synovium, which may alleviate the microenvironment of the cells and prevent the synovium from entering the feedback loop with injured cartilage.

In wound healing, pro-inflammatory signals recruit helper cells, which in turn act to modulate the microenvironment of the wound by secretion of factors (including anti-inflammatory signals) and start the repair process. By promoting a pro-inflammatory state, AmnioFix may be recruiting repair cells to the synovial lining. Ccl2 and Ccl7 are CC-Chemokines that mediate inflammatory ($LY6C^{hi}$) monocyte recruitment [126]. Furthermore, high expression of Ccl2 suggests macrophage (MΦ) differentiation under the influence of macrophage colony-stimulating factor (M-CSF) [127, 128], indicating the specialization of recruited monocytes. Expression of Ifng and IL1 suggest a preference for M1 (proinflammatory, classically activated)-MΦ phenotype, which is involved with cytotoxicity and tissue injury [127]. Although studies have hypothesized that M-CSF-derived MΦ are pre-oriented to M2 (anti-inflammatory, alternatively activated) subtype [128-130], some studies have found that MC-CSF MΦ can polarize

toward a M1 phenotype after Ifng stimulation [129, 131]. If indeed MΦ infiltrate the synovium during OA development in the MMT model, our results suggest a bias toward polarization to the M1 phenotype. It is worth pointing out that MΦ polarization is not an analogy for a dial turning one direction or the other but, instead, for a spectrum in which cells can demonstrate traits of a phenotype along the x-axis and of another phenotype along the y-axis. In fact, Lacey *et al.* found the degree of anti-inflammatory phenotype of M1-MΦ to be the highest when derived from M-CSF origin [129, 132, 133].

Low expression of IL-15 and high expression of IL1rn (usually considered a M2-MΦ marker [129, 134, 135]) would also suggest an upregulation of an anti-inflammatory response in the AmnioFix group. Altogether, these results may suggest that intra-articular injection of AmnioFix enhances the recruitment of helper cells to the synovial membrane in the MMT model and that these cells may be differentiated along the pro-inflammatory/anti-inflammatory spectrum in such a way that their secretome is counteracting cartilage catabolism.

Moreover, IL-1 (alpha or beta) and IL-1ra can be produced by the same cells (early or late macrophages) [136, 137]. Cauli *et al.* found that in OA patients, there was a higher percentage of macrophages positively stained for IL-1ra detected than those for IL-1a, compared to RA in which there is no a statistical difference between the two [136]. This high IL-1ra/low IL1a ratio may be a driver for the observed chronic, low inflammation in the synovium as OA develops. Therefore the ratio between IL-1a and IL-1ra may help determine the disease process within the joint. Studies have indicated that in order to block IL-1-mediated effects, a 100-fold excess of IL-1ra is needed [136,

138, 139] Although probably not on this scale, AmnioFix Injectable may help neutralize the catabolic effects of IL-1 by influencing this ratio.

Synovial fibroblast-like cells make up the majority of cells in the synovium, yet a study has found that selective depletion of MΦ in the synovium during OA results in the downregulation of several fibroblast-produced cytokines and MMPs [140]. This would indicate that MΦ play a role not only by secreting factors themselves, but also by stimulating responses from synovial fibroblasts, possibly activating them. The synovium is part of the joint organ, and so its state and composition affects the articular cartilage and bone and vice versa. In a collagenase-induced OA mouse model, MΦ from the synovial lining played a pivotal role in mediating osteophyte formation and other OA-related pathology [30]. In the MMT model, we have not been able to detect inflammation-related responses due to injury (previous chapter), and so we are not able to postulate the baseline role of helper cells as OA-like characteristics develops in this model. We did, however, provide baseline molecular events as OA develops in this model, such as dysregulation of ECM composition markers and upregulation of ECM remodeling markers, especially elevated levels of MMPs. In this study, we have found that treatment with AmnioFix Injectable maintained ECM composition markers to levels comparable with the unoperated control group and that some ECM remodeling markers are downregulated. More interestingly, we observed a spike in the expression of immunomodulatory markers in response to AmnioFix treatment in the MMT model. We postulate that by targeting the synovium, AmnioFix is modulating its microenvironment in such a way that could lead to a bias in polarization of MΦ and their secretome. This would then influence the secretome to perhaps alleviate the catabolic factors produced by

the articular cartilage and thus slow down damage. In order to test this hypothesis, isolated cells from the medial synovial membrane of MMT rats with/without AmnioFix treatment would need to be further studied.

This study introduces a new perspective in the OA field, as conventional approaches have often focused on lowering inflammation by inhibiting inflammatory responses with agonists. Yet, to this date, these approaches have not shown a significant advantage as DMOADs, or consistent chondro-protective characteristics. We suggest to take a different perspective on inflammation, and instead of attempting to prevent it or remove it from the equation, that we leverage it to enhance tissue-repair responses such as the ones observed in response to AmnioFix treatment. Initial pro-inflammatory signaling is important in wound healing, yet if it extends into a chronic state, it would become a problem.

As an ECM-derived drug, AmnioFix is composed of many factors that may have several effects that cross-reference each other that we have not tested in this study. Moreover, the MMT model is a post-traumatic model, and it is not generally associated with the inflammatory OA subphenotype. Therefore, we suggest that the mechanisms of action of AmnioFix should continue to be studied, particularly in different models where inflammation is prominent. An *in vitro* study from this lab found that AmnioFix downregulated the pro-inflammatory response in cytokine-activated synovial fibroblasts. It could be entirely possible that, given its complex composition, AmnioFix has different effects in different models; that is, in different microenvironments. We propose that AmnioFix is further tested in OA models with an inflammatory component, such as the monoiodoacetate (MIA) model, and in models of rheumatoid arthritis (RA). RA occurs

when the immune system mistakenly attacks the synovial membrane, starting the pathological events that cause bone erosion and joint deformity. Since we have shown that AmnioFix directly targets the synovial membrane and that it is able to modulate its microenvironment, we think it would be a good candidate for RA treatment and it is worth investigating.

CHAPTER 5. DEVELOPMENT AND CHARACTERIZATION OF PATIENT-SPECIFIC INDUCED PLURIPOTENT STEM CELL-DERIVED IN VITRO MODELS OF JUVENILE OSTEOCHONDRITIS DISSECANS

5.1 Abstract

JOCD is a degenerative joint disorder in which an osteonecrotic lesion in the subchondral bone has secondary effects on the overlaying articular cartilage. Over time, a necrotic osteochondral fragment develops and detaches from the parent bone, permanently affecting the joint and altering its mechanics. These 5 to 19 year-olds develop early onset of OA and contribute to a larger burden to the healthcare system. JOCD treatments are mostly conservative, and in advanced stages, surgical intervention is used to fix the fragment in place or replace it with an allograft. Limited treatments are due to the lack of knowledge about the onset and development of JOCD. The objective of this study was to develop JOCD patient-specific iPSC-derived models of chondrogenic and endochondral ossification organoids in order to elucidate pathological mechanisms of this disorder.

JOCD-specific iPSCs from 3 donors were reprogrammed from skin fibroblasts and validated for pluripotency. Then, they were differentiated into MSCs (iMSCs) and validated according to the established minimal criteria. JOCD- and control-iMSCs underwent 3D chondrogenesis and endochondral ossification, and these organoids were

harvested at different timepoints for gene expression, GAG and calcium quantification, histology, and TEM.

Results from the chondrogenic model showed that cells derived from JOCD patients had a significantly lower chondrogenic capacity than those from control patients. In the endochondral ossification model, JOCD cells produced the same amount of calcium and stained equally well for collagen type I, yet their gene expression profile was significantly different than that of the control cells. This may suggest that although JOCD cells are able to undergo endochondral ossification, there are irregularities in this process, when compared to control cells. This study has utilized cutting-edge iPSC technology to study JOCD *in vitro* and it is the first to report on JOCD pathomechanisms during chondrogenesis and endochondral ossification.

5.2 Introduction

JOCD is an increasingly common degenerative joint disorder that predominantly affects adolescent and young adults, and progresses to early onset OA. JOCD is hypothesized to involve the formation of an avascular lesion in the subchondral bone with secondary effects in the overlaying articular cartilage. As this disease progresses, partial or complete fragmentation of the necrotic bone may occur, which jeopardizes the bone integrity and significantly alters the joint mechanisms [36]. Previous research has been limited to retrospective clinical studies, and the pathophysiological mechanisms associated with the onset and progression of JOCD have yet to be fully characterized.

Previous studies have shown that chondrocytes isolated from detached JOCD fragments maintain similar cell viability and proliferative activity to those from normal

healthy cartilage [41, 76, 77]. However, both JOCD loose body- and JOCD cartilage biopsy-derived primary chondrocytes showed intracellular accumulation of matrix proteins that affected their morphology [77]. This feature has also been observed in familial OCD (FOCD) [78] and in endoplasmic reticulum storage diseases (ERSD) [77]. Unlike JOCD, FOCD is associated with a mutation in the aggrecan gene. A previous study by Xu *et al.* showed that, because of this mutation, large amounts of the aggrecan protein accumulated within the ER of FOCD chondrocytes, which led to a marked absence of aggrecan in the ECM [78]. FOCD is, therefore, considered to be an ERSD. All ERSDs show critical accumulation of misfolded proteins that result in defective protein trafficking, which may cause defective ECM assembly [77].

However, JOCD is not known to be a genetic disease; there isn't a specific mutation associated with it, and a recent study has found that only 14% of patients have family history [69]. Furthermore, characteristic features of FOCD are systemic: people with FOCD have multiple lesions that affect several joints, have short stature and develop OA at an early age. In contrast, JOCD is not systemic. There may be lesions in one than one joint, but developmental abnormalities are not associated with JOCD, as they are in the case of FOCD. Therefore, it is unclear whether JOCD may also be a disease of the ER. Previous studies have focused on isolated primary chondrocytes and the cartilage aspect of JOCD, yet this disorder is hypothesized to initiate in the subchondral bone, in the secondary ossification center. Because JOCD patients are still developing, the endochondral epiphyseal ossification is still undergoing. This differentiation process is prominent in JOCD patients, yet it has never been studied.

The objective of this study is to establish JOCD patient-specific iPSC-derived *in vitro* models of chondrogenesis and endochondral ossification in order to investigate pathological mechanisms in this disorder. Because these are pediatric patients and their lesions are usually treated without the excision of the fragment, stem cells were not a viable source. Instead, with as little as a $2mm^2$ skin biopsy, we were able to generate patient-specific iPSCs, which provided us with an unlimited supply of disease-specific stem cells and the ability to differentiate them into different tissues to study different aspects of the same disease. We chose to study endochondral ossification processes as they are highly relevant to the site where JOCD lesions develop (epiphyseal ossification), and chondrogenesis processes because cartilaginous templates are a key step in endochondral ossification. We hypothesized that cells from JOCD patients produce a suboptimal matrix during endochondral ossification and that this is a result of protein accumulation in the ER.

5.3 Materials and methods

5.3.1 Tissue and cell samples

Sin biopsies (2mm in diameter) from 3 JOCD patients were obtained in collaboration with Children's Healthcare of Atlanta, Orthopeadics department (IRB study #13-098). Dermal fibroblasts from these biopsies were sent to Washington University's iPSC core facility (St. Louis, MI) for reprogramming with sendai virus. 3 clones from each JOCD iPSC line were chosen in order to have (3) biological copies of each JOCD patient. In order to study a disease, it is important to work with multiple clones per

patient as previous studies have found that clone-to-clone variability exists, similar to donor-to-donor variability observed in human cells [141].

Control (non-disease) iPSC lines were purchased from ATCC and kindly gifted by the Shen lab (National University of Ireland Galway, Galway, Ireland). Known characteristics of the donors are detailed in Table 4 and Table 5.

Table 4. Detailed characteristics of JOCD iPSC lines.

Group	Line	Characteristics	
JOCD	JOCD1	Age	16
		Sex	Male
		Race	Caucasian
		Involved in competitive sports?	Yes (basketball, soccer)
		Affected joint	Right knee
		Surgery	Osteochondral allograft
		Number of iPSC clones used in this study	3
		iPSC source	Skin fibroblasts
		Reprogramming method	Sendai
	JOCD2	Age	12
		Sex	Male
		Race	African-American
		Involved in competitive sports?	Yes (basketball)
		Affected joint	Right & left knee
		Surgery	Drilling for intact OCD + BMAC
		Number of iPSC clones used in this study	3
		iPSC source	Skin fibroblasts
		Reprogramming method	Sendai
	JOCD3	Age	19
		Sex	Female
		Race	African-American
		Involved in competitive sports?	No
		Affected joint	Right knee
		Surgery	Autologous graft to lesion
		Number of iPSC clones used in this study	3
		iPSC source	Skin fibroblasts
		Reprogramming method	Sendai

Table 5. Detailed characteristics of control iPSC lines.

Group	Line	Characteristics	
Normal	Control 1	Age	9
		Sex	Male
		Race	Caucasian
		Involved in competitive sports?	No
		Affected joint	--
		Surgery	--
		Number of iPSC clones used in this study	2
		iPSC source	Skin fibroblasts
		Reprogramming method	Lentiviral
	Control 2	Age	20
		Sex	Female
		Race	Caucasian
		Involved in competitive sports?	No
		Affected joint	--
		Surgery	--
		Number of iPSC clones used in this study	1
		iPSC source	Skin fibroblasts
		Reprogramming method	Lentiviral
	Control 3	Age	33
		Sex	Male
		Race	African-American
		Involved in competitive sports?	Unknown
		Affected joint	--
		Surgery	--
		Number of iPSC clones used in this study	1
		iPSC source	Bone marrow CD34+ cells
		Reprogramming method	Sendai
	Control 4	Age	31
		Sex	Male
		Race	Non-Hispanic Caucasian
		Involved in competitive sports?	Unknown
		Affected joint	--
		Surgery	--
		Number of iPSC clones used in this study	1
		iPSC source	Bone marrow CD34+ cells
		Reprogramming method	Sendai

For the purpose of this study, we grouped the iPSC lines (and their derivatives) into two groups, as described in Table 6. Every experiment described within this study (e.g. cell line characterization and validation, differentiation models, etc.) were performed using every one of the cell lines in Table 6.

Table 6. Control group was composed of 2 iPSC lines gifted from REMEDI (one of which had 2 clones) and 2 iPSC lines purchased from ATCC, described in Table 5. JOCD group consisted of 3 JOCD-specific iPSC lines, with 3 clones each (described in Table 4). Cell line identifying number is denoted by the number after the group (i.e. cntrl#2, or control cell line #2) and clone number, within the cell line) is denoted by the number after the dash (i.e. cntrl#1-1, or control cell line #1-clone#1).

Control group	Cntrl 1-1	Cntrl 1-2	Cntrl2	Cntrl3	Cntrl4				
JOCD group	JOCD 1-1	JOCD 1-2	JOCD 1-3	JOCD 2-1	JOCD 2-2	JOCD 2-3	JOCD 3-1	JOCD 3-2	JOCD 3-3

5.3.2 iPSC culture, characterization and validation

iPSCs were cultured in 6-well plates, coated with Geltrex (Thermo Fisher Scientific A1413302), with E8 Flex media (Gibco, Thermo Fisher Scientific). In order to determine whether reprogramming had an adverse effect on the chromosome of a cell line, Karyotyping analyses were performed by Cell Guidance Systems (Cambridge, UK), for which samples were prepared following the company's guidelines. To validate the pluripotency of iPSCs, RT-PCR and IHC of the pluripotent markers were performed. Embryonic body (EB) and teratoma formation were also carried out in order to show the lines' ability to differentiation into the 3 germ layers.

To form EBs, iPSC colonies were dissociated with Dispase (Stemcell Technologies 07923) for 10 min at 37 °C and cultured in ultra-low attachment well plates (Corning CLS3471). Two days after, medium was changed to 50:50 E8 Flex medium (iPSC medium) : EB medium. Then, two days after, medium was changed to 100% EB medium, which contains knock-out DMEN, 20% FBS, 1% L-glutamine, 1% non-essential amino acid (NEAA), and 0.014mM β-mercaptoethanol. EB medium was changed every other day, and EBs were fixed in 10% NFB (overnight, at 4°C) at the 5 week timepoint.

To form teratomas, iPSCs were dissociated with Dispase and injected subcutaneously (Georgia Institute of Technology IACUC protocol A16043) in 60% Geltrex. Teratomas were allowed to grow for 8 to 12 weeks.

5.3.3 iMSC differentiation

iPSCs were differentiated into iMSCs (iPSC-derived mesenchymal stem cells) via an EB intermediate step, as previously described [142, 143]. EBs were formed as previously described. After 9 days, EBs were plated on gelatin (0.1%)-coated flasks with EB medium. After 5 days, the outgrowth cells were typsinized and passaged into gelatin-coated T-75 flasks with MSC differentiation medium, which contains knock-out DMEN, 10% FBS, 1% Penicillin streptomycin (PS), 1% L-glutamine, and 1% NEAA. Cells were cultured and passaged until a homogeneous (>70%) fibroblastic morphology appeared. Then, differentiating cells were passaged to non-coated, standard tissue culture flasks, and cultured with MSC maintenance media (αMEM, 10% FBS and 1% PS) with 2 ng/ml FGF2.

5.3.4 iMSC characterization and validation

To confirm MSC status, the International Society for Cellular Therapy's minimal criteria was tested [144] (Table 7). iMSCs automatically fulfill the first criterion as part of the differentiation protocol. The second criterion, phenotype, was tested by conducting fluorescence-activated cell sorting (FACS) of the indicated MSC surface markers. The Human MSC Analysis Kit (BD Biosciences, #562245) was used for this purpose.

Table 7. Summary of criteria to identify MSC, as set by the International Society for Cellular Therapy [144].

1. Adherence to plastic in standard culture conditions		
2. Phenotype	Positive (≥95%)	Negative (≤2%)
	CD105	CD45
	CD73	CD34
	CD90	CD14 or CD11b
		CD79α or CD19
		HLA-DR
3. In vitro differentiation: osteogenesis, adipogenesis, and chondrogenesis (demonstrated by staining of *in vitro* cell culture)		

5.3.4.1 Multipotency test

5.3.4.1.1 Osteogenesis

iMSCs were cultured at a seeding density of 10,000 cells/cm^2 and in MSC Maintenance Medium. Once cells reached confluency, they were induced and fed with osteogenic medium (DMEN low glucose, 10% FBS, 1% PS, 10mM β-glycerol, 100 μM L-ascorbic acid, and 100nM dexamethasone) every other day.

After 4 weeks, cultures were taken down for Alizarin Red and Von Kossa stainings. For Alizarin Red, cells were washed with PBS and fixed with 10% NBF at RT for 15 minutes. Cells were then rinsed with dH_2O and stained with Alizarin Red (pH 4.1) for 5 minutes. For Von Kossa, cells were washed with PBS and fixed with 70% Et-OH for 30 minutes at RT. Cells were rinsed with dH_2O and incubated with silver nitrate under UV. The reaction was stopped with sodium thiosulfate.

5.3.4.1.1 Adipogenesis

iMSCs were cultured at a seeding density of 20,000 cells/ cm^2 and in MSC Maintenance Medium. Once cells reached confluency, they were induced with adipogenic induction medium (DMEN high glucose, 10% FBS, 1µM dexamethasone, 10µg/ml insulin, 200µM indomethacin, 500µM MIX, and 1%PS). Adipogenic induction medium was changed every 3-4 days, 3 times; then, medium was switched to adipogenic maintenance medium (DMEN high glucose, 10% FBS, 10µg/ml insulin, and 1% PS) for 3 days before fixing. Cells were fixed with 10% NBF for 10 minutes at RT and stained with oil red-o solution.

5.3.4.1.1 Chondrogenesis

2×10^5 iMSCs in 10 µl of MSC maintenance media were incubated at 37°C for 2 hours in low-adherence tubes. Then, 200 µl of MSC maintenance medium was added to each tube, followed by overnight incubation. The next day, medium was replaced by chondrogenic medium (DMEN high glucose, 100nM dexamethasone, 50µg/ml Ascorbic acid, 40 µg/ml L-proline, 1% ITS + supplement, 1mM sodium pyruviate, and 1% PS) with 10ng/ml of TGF-β3 and changed every second day for 21 days. Cell pellets were

fixed with 10% NBF overnight at 4°C, routinely processed, embedded in paraffin, and sectioned at 5 μm thickness. Sections were stained with 0.01% toluidine blue (pH 4.0) and counterstained with nuclear fast red.

5.3.5 Chondrogenic and endochondral ossification differentiation models

5.3.5.1 3D chondrogenesis

3D chondrogenesis model of iMSCs was performed using the high cell-density micromass culture model as previously described [78]. Briefly, 2×10^5 iMSCs in 10 μl of MSC maintenance media were incubated at 37°C for 2 hours in low-adherence round-bottom 96-well plates (Sigma-Aldrich). Then, 200 μl of MSC maintenance medium was added to each well, followed by overnight incubation. Medium was replaced by chondrogenic medium with 10ng/ml TGF-β3 (Peprotech) the following day and was changed every second day for 49 days. Micromass cultures were harvested at different timepoints.

5.3.5.2 3D Endochondral ossification

The 3D endochondral ossification differentiation model was carried out as shown in Figure X. The micromass cultures for endochondral ossification were started like in the chondrogenesis model and cultured with chondrogenic media for the first 21 days. At day 21, medium was replaced by osteogenic medium and changed every second day for an additional 28 days. Micromass cultures were harvested at different timepoints.

5.3.6 Quantitative analyses of differentiation

5.3.6.1 DNA

Samples were harvested at day 21 and day 49 (n=5 per cell line). Pellets were digested overnight in papain (Sigma Aldrich) at 60°C. DNA was measured by Picogreen dsDNA assay kit (Thermo Fisher Scientific), according to the manufacturer's protocol.

5.3.6.2 Sulfated glycosaminoglycan (GAG)

Dimethylmethylene blue (DMMB) quantification was performed as previously described [78], with the same papain-digested samples that were used for DNA quantification. To assess the chondrogenic capability of control- and JOCD-iMSCs, the ratio of GAG to DNA per sample was calculated.

5.3.6.3 Calcium

Samples designated for calcium (n=5 per cell line, per timepoint) were vortexed overnight at 4°C in 1 N acetic acid to solubilize calcium. Calcium deposition was determined by the colorimetric Arsenazo III readent assay (Diagnostic Chemicals Ltd., Oxford, CT, USA). To assess the osteogenic capability of iMSCs, the ratio of calcium to DNA was calculated. Because these two assays were not quantified from the same pellets, the mean and SD of each assay was calculated separately. Then, the ratio was computed by dividing the mean of the calcium content by the mean of the DNA concentration, for each group. To calculate the SD of the ratio (averaged calcium : averaged DNA content), Taylor's expansion formula was used with the assumption of independent variables (Equation 4 and Equation 5).

$$V(A/B) = \left(\frac{A}{B}\right)^2 \times \left(\frac{V_A}{A^2} + \frac{V_B}{B^2} - \frac{2 \times C(A,B)}{A \times B}\right)$$

Equation 4. Approximation formula [145, 146] for the variance of the quotient of two random variables; where A and B are the mean values and V_A and V_B are their corresponding variances. The covariance (C(A,B)) is zero and drops out of the equation when variables are assumed to be independent.

$$\boldsymbol{SD(A/B) = \sqrt{V(A/B)}}$$

Equation 5. The variance is squared-rooted in order to calculate the sampled standard deviation.

5.3.7 Gene expression

5.3.7.1 iPSCs and iMSCs

Total RNA was extracted by RNeasy Mini Kit (Qiagen). Normalized RNA was then synthesized to cDNA using SuperScript VIlo cDNA synthesis kit (Invitrogen). RT-PCR was run following Taqman's Gene Expression Assays Protocol, using the Taqman gene expression assays specified in Table 8. AccuRef human universal cDNA (Gene Scientific) and ultrapure water were used as positive and negative controls, respectively, to ensure run fidelity.

Ct values greater than 37 were treated as 37, namely as null. Gene expression analysis was carried out using the ΔΔCt method, outlined in Equation 1 and Equation 2. Briefly, the Ct value of each gene was normalized by the expression of the housekeeping gene GAPDH to get the relative expression (ΔCt). Then, the ΔCt of each target was normalized by the ΔCt of the calibrator (in this case, a control BM-MSC line), to get the

ΔΔCt for each gene. In order to get the fold change, ΔΔCt values were transformed using Equation 6. Results were graphed in log10 format.

$$Fold\ change = 2^{-\Delta\Delta Ct}$$

Equation 6. Equation to calculate fold change from the normalized relative expression (ΔΔCt).

5.3.7.2 Differentiation models

Total RNA from micromass cultures was extracted using the RNeasy MinElute Clean-up Kit with QIAzol Lysis Reagent (Qiagen). Then, normalized RNA was synthesized to cDNA using RT^2 First Strand Kit (Qiagen).

RNA expression was quantified using the Taqman real-time PCR Fluidigm Dynamic Array Integrated Fluidic Circuits (BioMark, Fluidigm), for the Taqman gene expression assays specified in Table 8. AccuRef human universal cDNA (Gene Scientific) and ultrapure water were used as positive and negative controls, respectively, to ensure run fidelity.

Ct values greater than 37 were treated as 37 (null). Gene expression analysis was carried out using the ΔΔCt method, outlined in Equation 1 and Equation 2. The Ct value of each gene was normalized by the geometric mean of the expressions of the housekeeping genes to get the relative expression (ΔCt). Then, the ΔCt of each target was normalized by the ΔCt of the calibrator to get the ΔΔCt for each gene. For the differentiation experiments, the calibrators were the micromass cultures at 2 hours post-seeding, of the respective cell line. SD was derived using Gauβ's error propagation (Equation 3).

Then, in order to calculate the averaged control or JOCD expression for a specific gene, the weighted averaged was computed. The pooled SD formula (Equation 7) was used to calculate the SD of averaged control or JOCD expression results.

$$SD_{pooled} = \sqrt{\frac{(n_1 - 1)SD_1^2 + (n_2 - 1)SD_2^2 + \cdots + (n_k - 1)SD_k^2}{n_1 + n_2 + \cdots + n_k - k}}$$

Equation 7. Equation for calculating the pooled SD for three or more groups [145, 147, 148].

Results were graphed in the log2 form (ΔΔCt) because this is the linear form of the values and allow for representation of values with descriptive statistics (mean, SD, SEM). Converting ΔΔCt into fold change would change the distribution to not longer symmetric and would not allow these descriptive statistics, which are essential for comparison of statistical significance.

Table 8. List of Taqman Gene Expression Assays used for each experiment. Where available, assays were of "the best coverage", recommended by the company. Some assays may be listed more than once as they belong to multiple categories and/or were used for different experiments.

Experiment	Category	Taqman Gene Expression Assays
iPSC characterization and validation	Pluripotency	Sox2 (Hs01053049_s1), Oct4 (Hs04260367_gH), Nanog (Hs02387400_g1)
	Housekeeping gene	GAPDH (Hs02786624_g1)
iMSC characterization and validation	Pluripotency	Sox2 (Hs01053049_s1), Oct4 (Hs04260367_gH), Nanog (Hs02387400_g1)
	Housekeeping gene	GAPDH (Hs02786624_g1)
Differentiation models	Chondrogenesis	Acan (Hs00153936_m1), Col2a1 (Hs00264051_m1), Col1a1 (Hs00164004_m1), Comp (Hs00164359_m1), Runx2 (Hs01047973_m1), Sox9 (Hs00165814_m1), Fmod (Hs05632658_s1)
	Endochondral ossification	Col1a1 (Hs00164004_m1), Sp7 (Hs01866874_s1), Bglap (Hs01587814_g1), Col10a1 (Hs00166657_m1), Mmp13 (Hs00942584_m1), Runx2 (Hs01047973_m1), Fmod (Hs05632658_s1)
	Housekeeping genes	Gapdh (Hs02786624_g1), Rps18 (Hs01375212_g1), Actb (Hs0106665_g1)

5.3.8 Histology

5.3.8.1 iPSCs

iPSC colonies were fixed with 4% PFA at RT for 10 minutes. iPSCs were permeabilized with 0.5% saponin, blocked with 1% BSA in 0.05% saponin for 1 hour at RT, and incubated in primary antibody (Table 9) at 4°C overnight. The next day, they

were incubated in secondary antibody (Cell Signaling 4409 and/or 4412, depending on the primary) for 1 hour at RT and in Hoecht for 5 minutes at RT.

5.3.8.2 EBs and differentiation models

Samples were fixed in 10% NBF overnight at 4°C. Only endochondral ossification pellets were decalcified with ImmunoCal (StatLab) overnight at 4°C. Samples were routinely processed, embedded in paraffin, and sectioned at 5 um. Antigen retrieval (sodium citrate buffer), permeabilization (0.1% Triton-X) and blocking were performed on the sections, before incubation overnight in primary antibody at 4°C. Table 9 lists the antibodies used for the corresponding experiment. Secondary antibody (Cell Signaling 4409 and/or 4412, depending on the primary) was incubated for 1 hour at RT, followed by counterstaining with DAPI (ThermoFisher S36938).

Table 9. List of primary antibodies used in immunohistochemistry for each experiment.

Experiment	Category	Primary antibody
iPSC characterization and validation	Pluripotency	Cell signaling technology (#9656): 1:100 Sox2, 1:100 Oct4, 1:100 Nanog, 1:100 SEEA4
Embryonic body validation	Mesoderm	1:500 α-smooth muscle actin (Sigma #A2547)
	Endoderm	1:50 α-Fetoprotein (Sigma #A8452)
	Ectoderm	1:500 Nestin (Millipore #MAB5326)
Differentiation models	Chondrogenesis	1:200 Collagen type 2 (Santa Cruz #52658), 1:200 Aggrecan (ab36861)
	Osteogenesis	1:200 Collagen type 1 (ab34710)

5.3.9 Transmission electron microscopy (TEM)

Micromass cultures were harvested at day 49 for each differentiation model (n=5 per cell line), fixed in 25% glutaraldehyde in 0.2M cacodylate buffer, and sent to Emory's Robert P. Apkarian Integrated Electron Microscopy Core (Atlanta, GA) for analyses. Day 49 was chosen as the only timepoint to allow a longer period of time for possible protein accumulation in the ER.

5.3.10 Statistical analyses

Data were graphed as means ± SEM. Group comparisons were made with Two-way ANOVA analysis. Tukey's and Kruskal-Wallis were used as *post hoc* tests where appropriately. P-values less than 0.05 were considered statistically significant.

5.4 Results

5.4.1 iPSC reprogramming, characterization and validation

JOCD-iPSC lines (and their clones) did not have any abnormal chromosome changes due to reprogramming (data not shown). They stained positive for intracellular pluripotent stem cell markers Sox2, Oct4 and Nanog, and one of the cell surface pluripotency markers, SEEA4, as shown in Figure 28. RT-PCR confirmed expression of the pluripotent stem cell markers. Control-iPSC lines also tested positive for staining and gene expression of pluripotent markers.

JOCD-iPSC lines (and their clones) were able to form EBs, and these EBs stained positive for all 3 germ layers: endoderm, ectoderm, and mesoderm. Control-iPSCs lines

from the Shem lab also tested positive for the 3 germ layers. EB pluripotency test was not performed for Control-iPSC lines from ATCC as they were certified by ATCC itself.

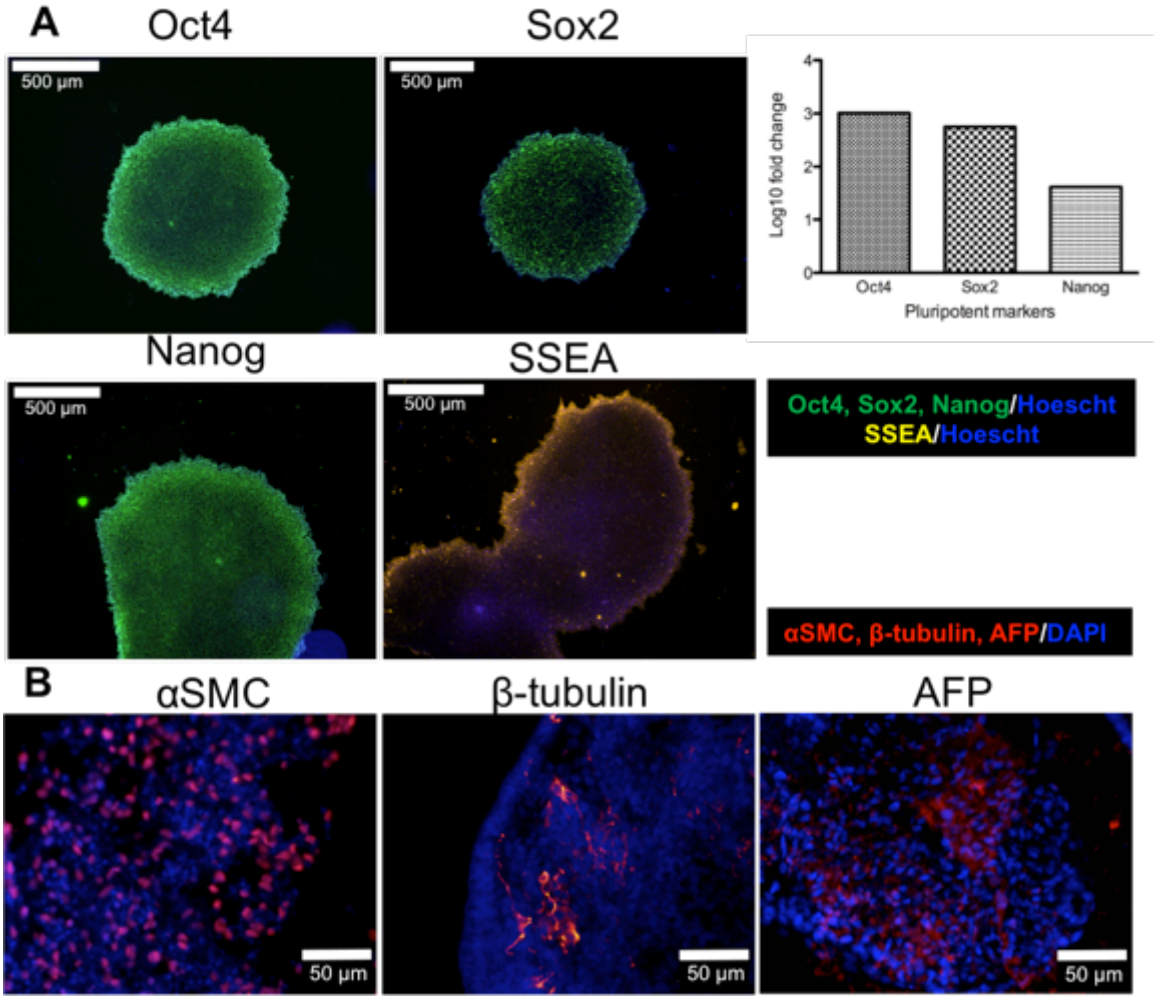

Figure 28. iPSC characterization and validation. Representative images from JOCD1-1 (JOCD-iPSC donor #1, clone #1) showed A. positive staining for pluripotent stem cells markers, B. gene expression of pluripotent stem cell markers, and C. positive staining for the 3 germ layers once differentiated into EBs: αSMC (mesoderm), β-tubulin (ectoderm), and AFP (endoderm).

5.4.2 iMSC characterization and validation

Control- and JOCD-iMSCs passed the International Society for Cellular Therapy's minimum criteria. As Figure 29 shows, chosen iMSCs passed the approved

MSC surface marker panel. They were also shown to be multipotent and that the expression of pluripotent stem cell markers were now downregulated (comparing to their iPSC state).

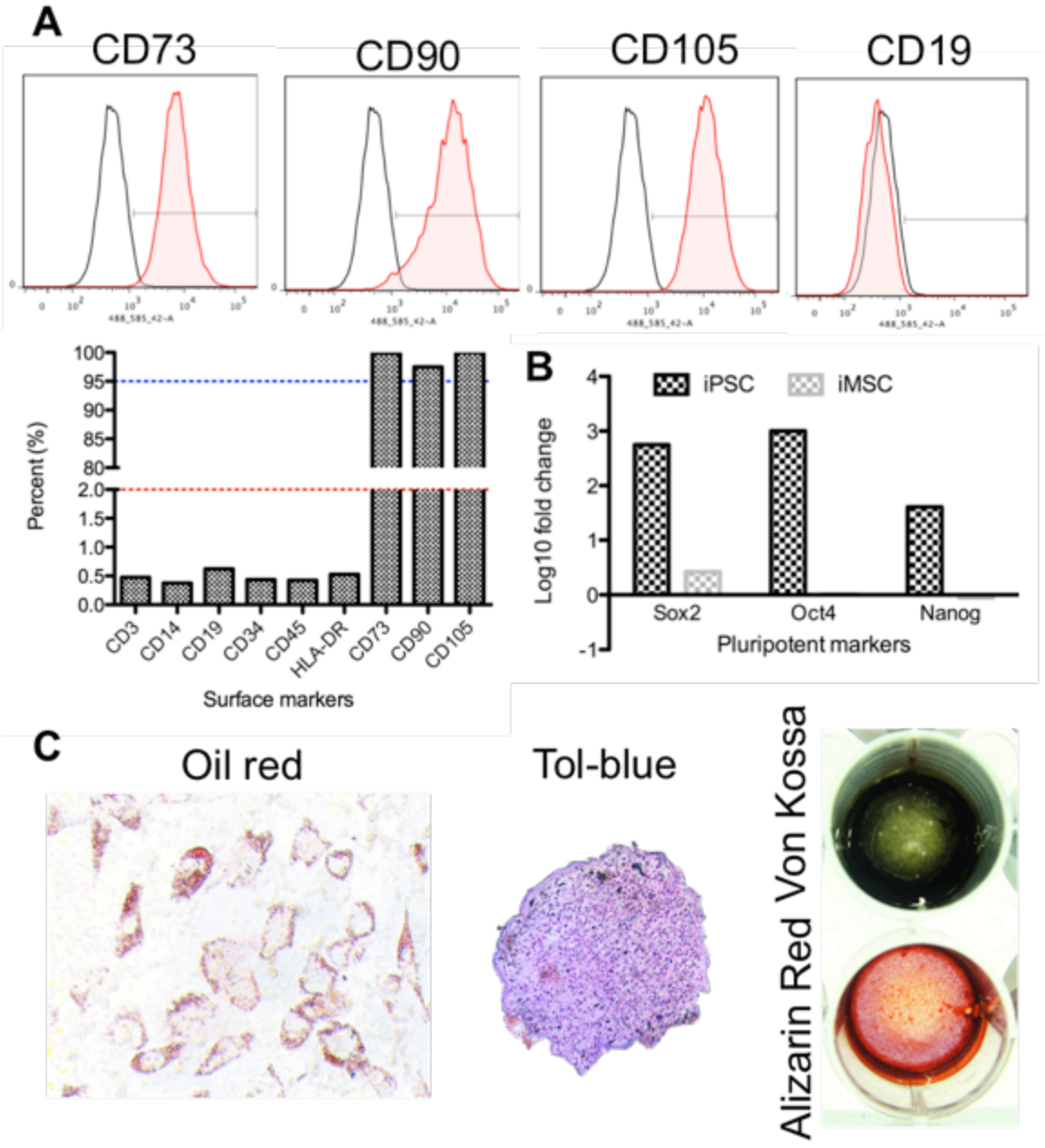

Figure 29. Characterization and validation of iMSCs. Representative images for iMSC line JOCD1-1 (derived from JOCD-iPSC donor #1, clone #1) shows A. the appropriate cell surface markers, B. lower expression of plutipotent stem cell

markers, and C. positive staining for adipogenesis (oil red), chondrogenesis (tol-blue), and osteogenesis (Von Kossa and Alizarin Red).

5.4.3 Chondrogenesis model

JOCD- and control-iMSC-derived chondrogenic pellets showed significant differences in gene expression as they differentiated, as shown in Figure 30. JOCD-chondrogenic pellets had significantly lower expression of Acan, Col2a1, Comp, Runx2 and Sox9—all of which are markers of chondrogenesis. JOCD pellets had significantly lower expression of Acan (aggrecan gene) than control pellets at days 14, 21 and 49. Col2a1 (collagen type II) expression was significantly lower in JOCD- than control-pellets only at day 28. Comp (cartilage oligomeric matrix protein) and Sox9 (SRY-Box 9) expression were significantly lower in JOCD than control-pellets for every time point. Runx2 (runt-related transcription factor-2) expression was significantly lower in JOCD- than control-pellets at days 7 and 21.

JOCD-chondrogenic pellets had significantly higher expression of Fmod (fibromodulin) and Col1a1 (collagen type I), considered a marker of fibrous cartilage during differentiation. Fmod expression was significantly higher in JOCD- than control-pellets at days 7, 21, and 49. Col1a1 expression was significantly higher in JOCD- than control-pellets at every single timepoint.

Because Col2a1 is a typical marker of differentiated chondrocytes in hyaline cartilage, as opposed to Col1a1, the ratio of RNA expression levels of Col2a1 to Col1a1 can be utilized as a differentiation index related to the expression of collagens during chondrogenic differentiation to better assess the efficiency of chondrogenic differentiation [149]. Figure 30 shows that JOCD-chondrogenic pellets had a

significantly lower ratio of Col2a1 to Col1a1 than control-chondrogenic pellets at days 7, 21, 28, 35, and 49.

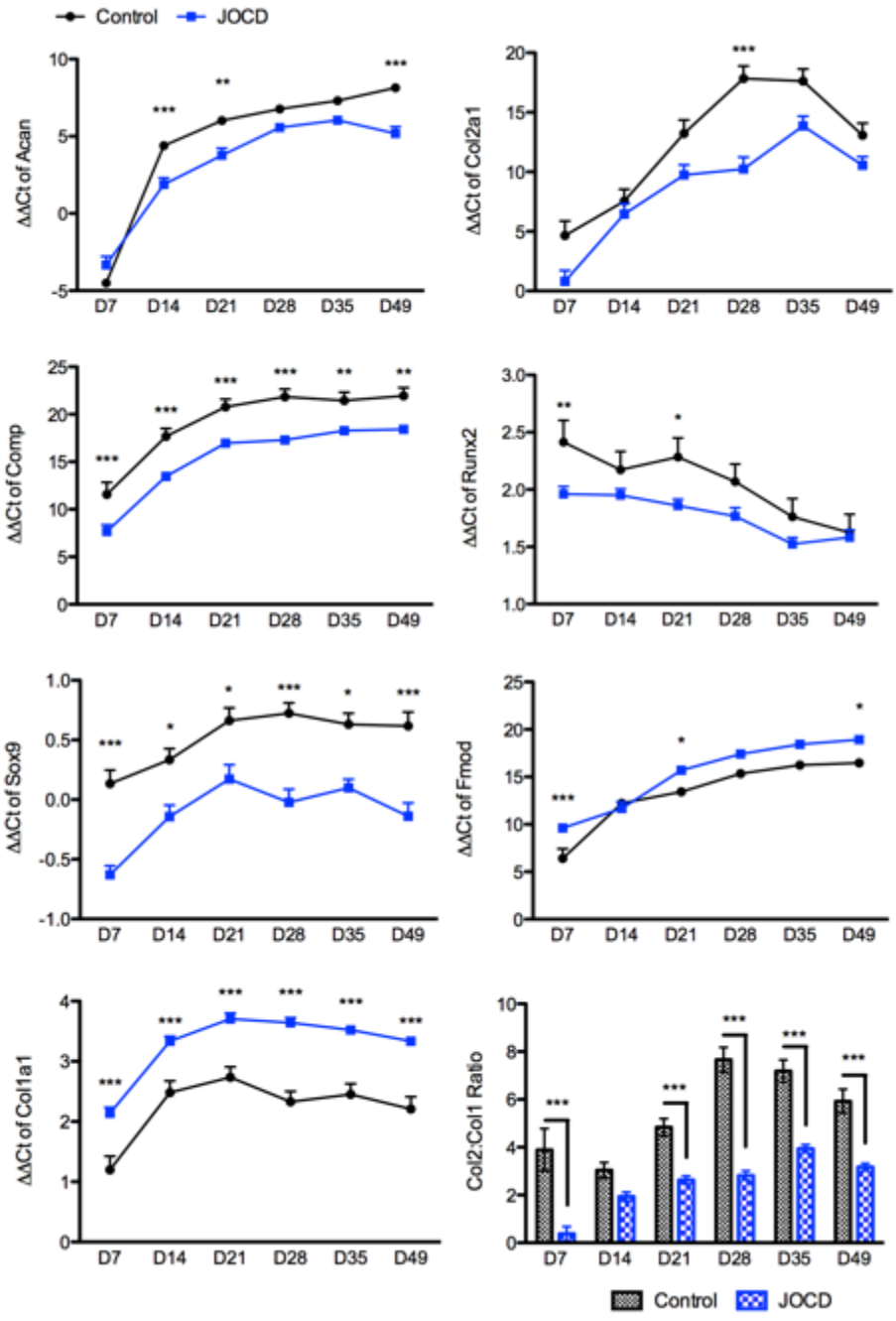

Figure 30. A. Significantly expressed genes in the chondrogenic pellets, graphed as mean ± SEM. B. Col2a1 to Col1a1 ratio is used as an index of chondrogenic differentiation. *

indicates statistically significant difference between JOCD-chondrogenic pellets and control-chondrogenic pellets at p-value<0.05, ** at p-value<0.01, * at p-value <0.001**

There were no significant differences between GAG content in the control-chondrogenic pellets versus the JOCD-chondrogenic pellets (Figure 31).

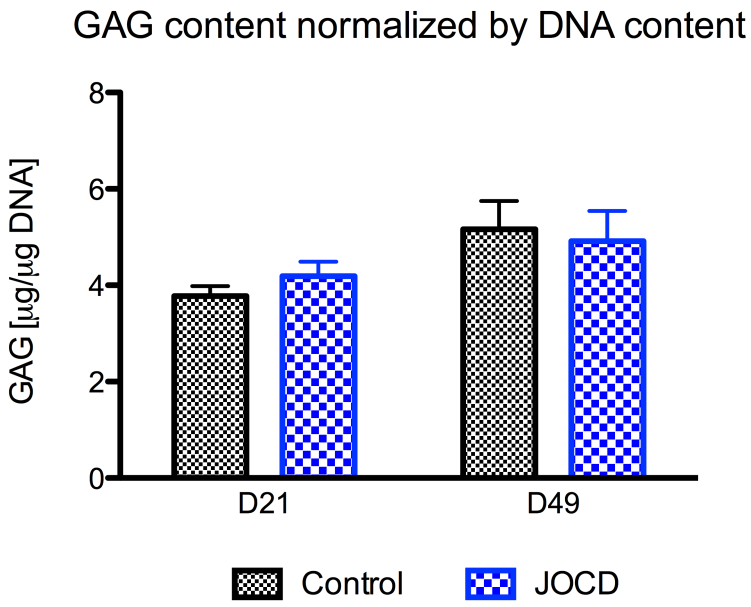

Figure 31. GAG deposition by chondrogenic pellets, normalized to DNA content; graphed as means ± SEM.

Col2/Col1 IHC staining showed positive staining at both day 21 and day 49 of both markers (Figure 32). At day 21, control-iMSC-derived chondrogenic pellets had seemingly less Col1 staining than JOCD-iMSC-derived chondrogenic pellets. At day 49, both groups showed an overall increase in Col1-postive staining, and JOCD-chondrogenic pellets had more Col1-positive staining than control-chondrogenic pellets. JOCD-chondrogenic pellets were more likely to form a fibrous shell (2/3 of the time vs. ½ of the time). Col1 and Col2 stained throughout the pellets, with no apparent signs of

intracellular protein retention. Aggrecan IHC also did not show apparent differences in protein location within the chondrogenic pellets at day 21.

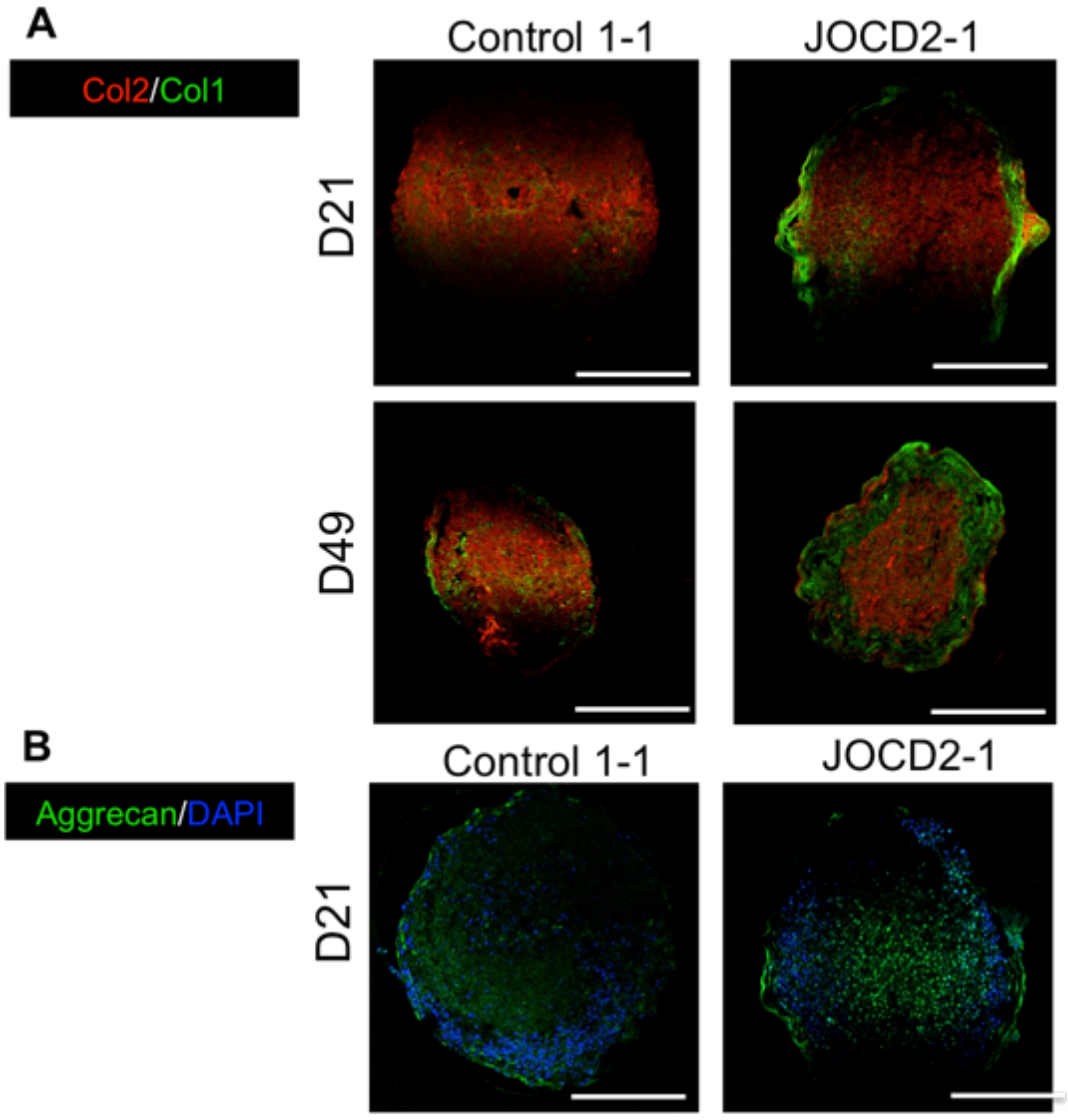

Figure 32. Immunohistochemistry staining of A. Collagen 2 and Collagen 1 and B. Aggrecan of chondrogenic pellets. Representative pictures from Control1-1 (Control-iPSC donor #1, clone #1) and from JOCD2-1 (JOCD-iPSC donor #2, clone #1).

5.4.4 Endochondral ossification model

JOCD-osteogenic pellets had significantly higher expression of Col1a1 than control-osteogenic pellets at every single timepoint. However, JOCD pellets had significantly lower expression of endochondral ossification markers than control pellets. Col10a1 and Mmp13 are markers of chondrocyte hypertrophic, which is a key step in endochondral ossification. JOCD-osteogenic pellets had significantly lower col10a1 than control-osteogenic pellets at every time point. Mmp13 expression was significantly lower in the JOCD-ostegenic pellets at day 49 only. Runx2 plays an essential role during commitment and differentiation of mineralized cell types, and its deletion results in complete loss of skeletal mineralization [150]. Here, we observed a lower expression of Runx2 during endochondral ossification of our pellets for the JOCD group at days 7, 21, 28, 35, and 49. Runx2 plays a role in the regulation of Sp7 (osterix), and we observed a lower expression of Sp7 in the JOCD-osteogenic pellets at days 21 and 35. Finally, Fmod was only significantly higher in the JOCD group at day 7.

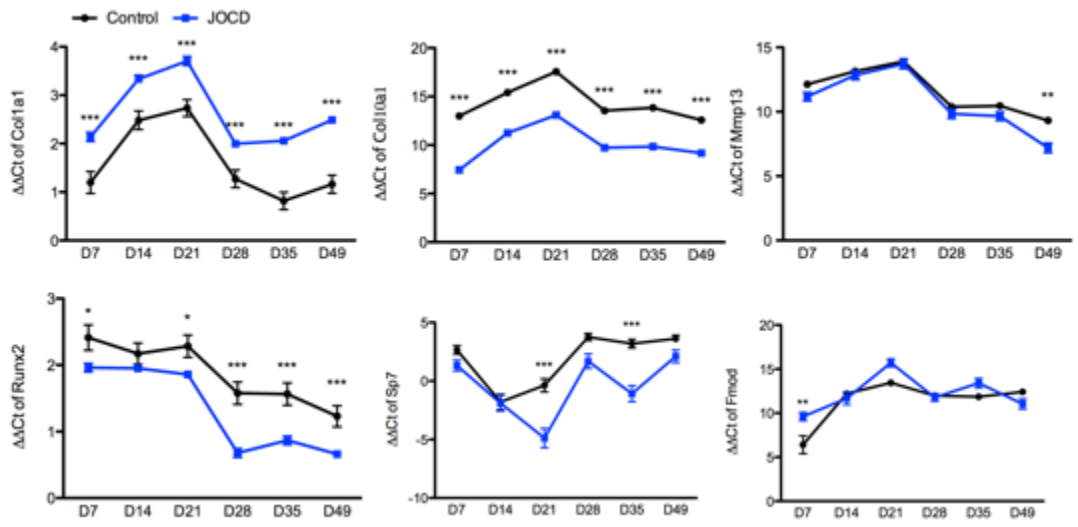

Figure 33. Significantly expressed genes in the osteogenic pellets, graphed as means ± SEM. * indicates statistically significant difference between JOCD-chondrogenic pellets and control-chondrogenic pellets at p-value<0.05), ** at p-value<0.01, * at p-value<0.001.**

The osteogenic pellets did not show significant differences in calcium deposition for any timepoint, but each group did significantly increase its deposition over time as the pellets differentiated (**Error! Reference source not found.**).

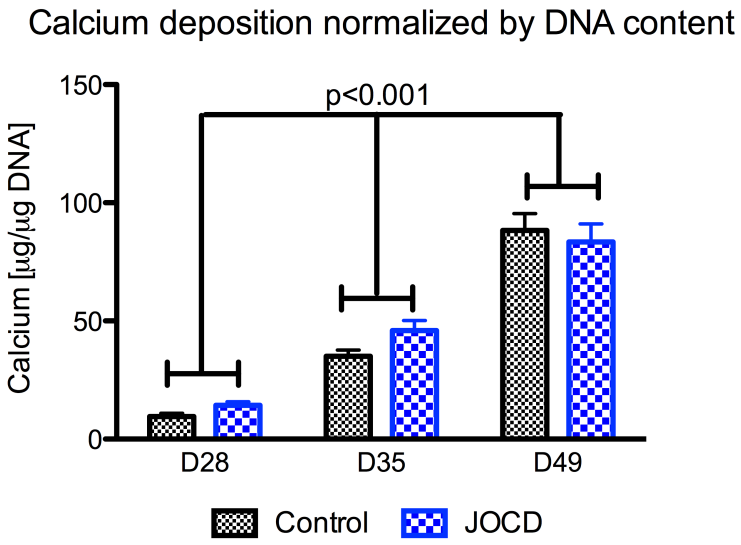

Figure 34. Calcium deposition by osteogenic pellets, normalized by DNA content; graphed as means ± SEM.

Col2/Col1 IHC showed positive staining for both markers in both groups. At day 49, both groups had substantially more col1-postive staining and there were no apparent differences in the amount of protein stained or location within the osteogenic pellets (Figure 35).

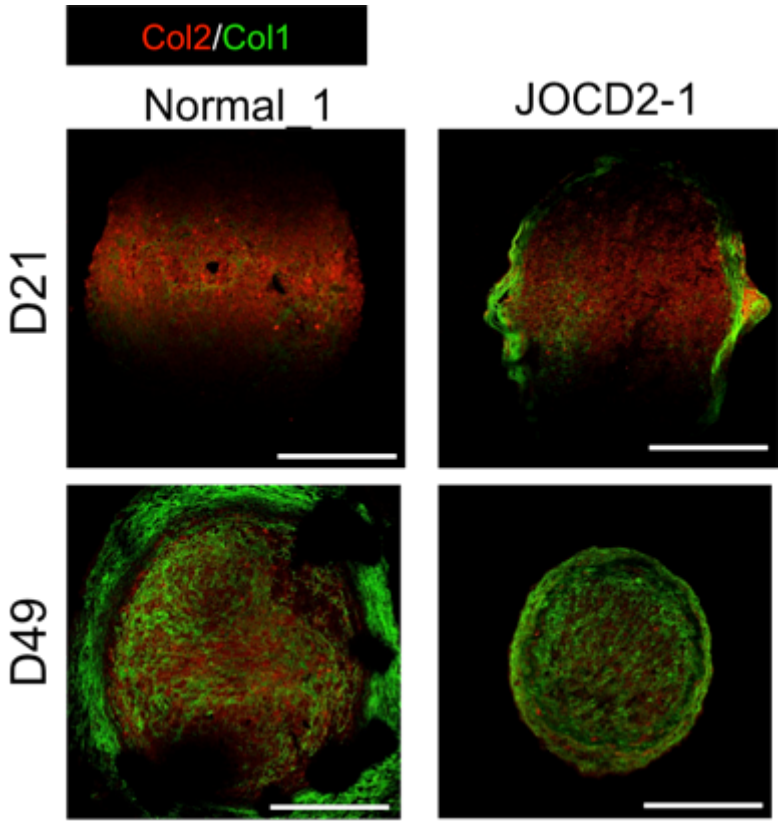

Figure 35. Immunohistochemistry staining of Collagen 2 and Collagen 1 of osteogenic pellets. Representative pictures from Control1-1 (Control-iPSC donor #1, clone #1) and from JOCD2-1 (JOCD-iPSC donor #2, clone #1).

5.4.5 Protein accumulation in the ER during differentiation

TEM did not show differences in ER volume between JOCD and control groups, as shown in Figure 36.

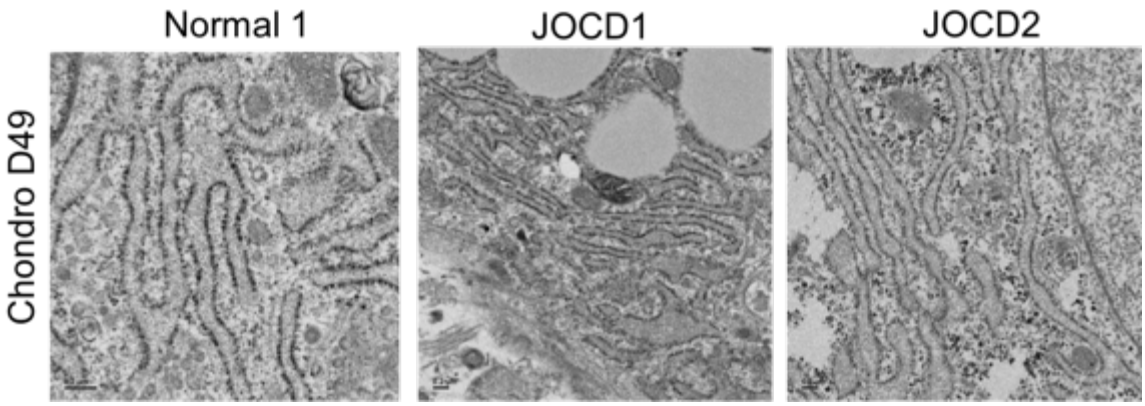

Figure 36. TEM representative images of chondrogenic pellets of Control-1 and JOCD1-1 and JOCD2-1 at day 49.

5.5 Discussion

Microtrauma, ischemia, genetic predisposition, and abnormal ossification have all been hypothesized as plausible causes of JOCD. Research limited to retrospective clinical studies and histological findings has translated into limited knowledge about the pathological mechanisms underlying JOCD, which has, in turn, hampered innovation in treatment strategies. In this study, we sought to elucidate possible pathological mechanisms of JOCD during chondrogenesis and endochondral ossification. JOCD occurs in patients with open epiphysis; therefore, endochondral ossification is an important physiological process occurring at the injury site. Endochondral ossification initiates from a cartilaginous template, and so studying chondrogenesis of JOCD patients may also elucidate pathological events in this disorder.

In this study, we observed that JOCD patient-specific chondrogenic pellets had significantly lower expression of chondrogenic markers than the control chondrogenic pellets. This result may have two explanations. First, JOCD-specific iMSCs have a lower

chondrogenic potential than control-iMSCs. This result is supported by the significant differences in col2a1 to col1a1 ratio, for which JOCD-chondrogenic pellets show a lower index of chondrogenic differentiation for most timepoints. IHC confirmed this lower chondrogenic potential hypothesis. The GAG assay, however, did not show significant differences between the control and JOCD chondrogenic pellets, but the DMMB assay may not be sensitive enough. Another possibility for the lower expression of chondrogenic markers may be that there is a small amount of protein accumulation in the ER, and although not enough to visibly engorge the ER (TEM), it is having an effect on protein production. When proteins get accumulated in the ER, response mechanisms include the downregulation of those proteins until the cell is able to reduce stress in the ER. In order to test this second explanation, we would have to test for ER stress-related genes in the differentiation models over time.

JOCD endochondral ossification model showed decreased expression of chondrocyte hypertrophic markers as well endochondral ossification orchestrators Runx2 and Sp7. Because col1a1 expression, a key protein in bone, was significantly higher in JOCD-osteogenic pellets, it is unclear whether the endochondral ossification process is impaired. We suggest that cells from JOCD patients may have an irregular endochondral ossification, as demonstrated by significantly lower expressions of Runx2 and Sp7, but additional markers would have to be assessed to elucidate pathological pathways.

During skeletogenesis, Runx2 is expressed in both chondrocytes and osteoblasts, and its global deletion results in disrupted chondrocyte and osteoblast differentiation [150]. Runx2 expression is required to promote chondrocyte hypertrophy, and conditional ablation of Runx2 gene in chondrocytes leads to failed endochondral ossification [150].

In both the chondrogenic and endochondral ossification models, we observed significantly lower expression of Runx2 in JOCD organoids. This result may suggest lower ability to undergo endochondral ossification for JOCD cells. Runx2 also regulates Sp7, which regulates MSC-mediated endochondral ossification.

With respect to the endochondral ossification model, it was surprising to see that once medium was changed at day 21 to induce osteogenesis on the chondrogenic pellets, the expression of most markers decreased. It is unclear why expression of Col1a1 decreased from day 21 to day 28. A possible explanation may be that the snapshots in time that we chose (timepoints) missed a spiked expression of the markers earlier. Another explanation may be that these findings in gene expression are specific to the *in vitro* model we have developed. *In vitro* models often diverge in differentiation pathways due to a number of factors (e.g. cell source variability, difference in FBS and other materials, etc) when compared to *in vivo*.

Additionally, it is worth pointing out that, despite successfully fulfilling all the MSC criteria, iMSCs are not MSCs. iPSCs are thought to be reprogrammed cells that replicate embryonic state. Differentiation of MSCs derived from embryonic, fetal and adult sources varies. One studied showed that human embryonic and fetal MSCs were able to differentiate towards 3 different cardiac lineages, in contract with adult MSCs, and the key difference was cellular response to stimuli [151]. Furthermore, the scientific community is often revising its definition of MSCs, as much uncertainty still remains regarding the defining characteristics of these cells, including their potency and self-renewal [152]. For example, the majority of the surface markers in the International Society for Cellular Therapy's minimal criteria are exclusion markers for other cell types.

Only 3 markers in the panel are specific to MSCs, and CD105 has been shown to be expressed in other cell types [153, 154] and to be absent in some MSCs [155] .

Despite these potential shortcomings of iPSC-based *in vitro* models, iPSCs provide a limitless source of stem cells and are already launching forward the stem cell field. In disease modeling, iPSCs allow for patient-specific models, which may revolutionize precision and personalized medicine. In this study, JOCD-specific chondrogenic and osteogenic organoid models were developed and studied. Results suggest that JOCD cells may have a lower chondrogenic potential than control cells. Furthermore, while they are able to undergo calcification to a level comparable to the control cell lines (as shown by histology and calcium deposition), the gene expression profile of JOCD cell lines during endochondral ossification may suggest irregularities in this process. Altogether, we postulate that JOCD pathological mechanisms are tied in with chondrogenesis and endochondral ossification processes. Mechanistic studies should be done in the future to dissect possible aberrant pathways during differentiation. Lastly, because we did not see protein accumulation in the ER at day 49 in either differentiation model, we can conclude that protein accumulation was not a key driver of JOCD pathology. However, ER stress may still be implicated in the development and progression of JOCD.

CHAPTER 6. ENDOPLASMIC RETICULUM STRESS RESPONSE SIGNALING IN JUVENILE OSTEOCHONDRITIS DISSECANS IN VITRO MODELS

6.1 Abstract

FOCD and equine OCD have been linked to ER dysfunction, and JOCD has been hypothesized to involve the ER as well, by evidence of protein accumulation in primary chondrocytes. However, no study to date has investigated the role of the ER in JOCD. Unlike FOCD, JOCD is not associated with a gene mutation and is not present at the systemic level. Therefore, the following question arises: if protein accumulation is a pathological event in JOCD, why is clinical JOCD not seen in all joint, similar to FOCD? The objective of this study was to isolate the ER mechanism in JOCD-specific cells by studying the response signaling to induce ER-stress. We hypothesized that JOCD is indeed an ER stress-related disease but its pathomechanisms are not in response to protein accumulation, but instead, that an impaired UPR is responsible and may cause cell death, and thus ultimately the initial necrotic lesion in the epiphyseal.

In the JOCD-specific chondrogenic and endochondral ossification differentiation models, we observed a heightened ER-stress response, which may indicate that JOCD cells experienced higher levels of ER stress during differentiation. When the ER stress was equated (using our ER-stress induction models), results demonstrated a significantly lower expression of all ER-stress-response markers in JOCD than in control cell lines, with the exception of those associated with protein degradation. Altogether, these

findings suggest that JOCD cells do respond differently to ER stress (during physiological and pathological processes). We propose that the impaired ER-stress response of JOCD cells may lead to cell death in this disorder, which may initiate the necrotic lesion in JOCD patients under pathological processes, such as microtrauma or interruption of the microvasculature.

6.2 Introduction

ER stress has been hypothesized to be a key player in the disease development of the OCD umbrella (FOCD, equine OCD, and potentially JOCD). A study by Skagen et al found abundant accumulation of matrix proteins within dilated rER in chondrocytes from JOCD-loose fragments and cartilage biopsies [77]. However, it remains unclear what could have trigged this protein accumulation and whether this is a pathological feature of JOCD. In our previous chapter, we did not observed protein accumulation in our JOCD-specific *in vitro* models of chondrogenesis or endochondral ossification. In FOCD, however, a similar model of FOCD-specific *in vitro* chondrogenesis showed protein accumulation, marked by dilated ERs [78]. Unlike JOCD, FOCD is associated with a mutation in the aggrecan gene that prevents its released into the ECM, and this initial protein accumulation leads to secondary accumulation of other matrix proteins, resulting in a compromised ECM. While FOCD is systemic, JOCD occurs as a single incident. Therefore, the following questions remain to be answered: does protein accumulation occur in JOCD as well? If it does, what may cause a localized protein accumulation versus the systemic event observed in FOCD? Is protein accumulation primary or secondary feature of JOCD?

Protein accumulation leads to ER stress, but the opposite is also true. Cells can accumulate protein in response to ER stress, which can be induced due to change in the internal and external microenvironment of the cells and due to both physiological [156] and pathological insults [77, 157]. Chondrocytes and osteoblasts undergo physiological ER stress-related response signaling in the course of normal maturation [158]. Endochondral ossification is regulated by several genes that also regulate stress responses to the ER [159]. Moreover, conditions such as ischemia, obesity (nutrition in pathological excess), diabetes mellitus, under-nourishment (glucose starvation), infection and chemically induced tissue injury might also give rise to ER stress and therefore accumulation of proteins in cells [77].

The ER stress-related response signaling is called the unfolded protein response (UPR). 4 processes may be activated with the UPR: increased expression of ER resident protein chaperones and protein foldases; increased rate of ER-associated degradation (ERAD) to eliminate irreparably misfolded proteins; decreased protein production; and when the prosurvival efforts are exhausted, ER-stress related apoptosis [160]. In mammals, the UPR is signaled through three ER transmembrane protein sensors: inositol-requiring kinase 1 (IRE1), pancreatic ER eIF2 kinase (PERK), and activating transcription factor 6 (ATF6) [161]. Table 10 shows the three major ER-stress sensors and their role to the UPR activated processes.

Table 10. Unfolded protein response (UPR) has three major ER-stress sensors: PERK, ATF6 and IRE1, which play particular roles in the ER-stress related activated response [162].

	ER sensor	Downstream effector	Role
ER stress	PERK	Phopholiration of eIF2α	Translation inhibition
			Redox response apoptosis
	ATF6	ATF6F	Chaperone synthesis
	IRE1	Splicing of XBP1	Unfolded protein degradation

The typical chemicals that induce ER stress include thapsigargin, which disturbs the calcium (Ca2+) homeostasis; tinucamycin, which suppresses glycosylation; and brefeldin A, which inhibits protein transportation to the Golgi complex [163]. Thapsigargin is a specific inhibitor of sarcoplasmic/ER Ca2+-ATPase (SERCA), and thus treatment with Thapsigargin results in a decrease in ER calcium levels [164]. When calcium levels are lowered in the ER, calcium-dependent chaperones lose their chaperone activity, leading to the accumulation of unfolded proteins [164]. Tunicamycin is an inhibitor that blocks the initial step of glycoprotein biosynthesis in the ER, thus causes accumulation of unfolded glycoproteins in the ER [164]. Brefeldin A inhibits transportation of proteins from the ER to the Golgi and induces retrograde protein transport from the Golgi apparatus to the ER [164]. Accumulation of unfolded/misfolded proteins due to these chemicals induce ER stress.

The objective of this study was to evaluate the UPR in JOCD-specific models in order to assess their response to ER stress. To this end, we utilized our differentiation in vitro models (chondrogenesis and endochondral ossification) in order to assess responses to physiological ER stress during differentiation, and established ER-stress induction models to study the ER-stress related responses to well-controlled, pathological settings. We hypothesized that JOCD is indeed an ER stress-related disease but its pathomechanisms are not in response to protein accumulation, but instead, that an impaired UPR is responsible and may cause cell death, and thus ultimately the initial necrotic lesion in the epiphyseal. Therefore, we expect to observe lower levels of most of the UPR-related genes tested in our ER-stress induction models, except for those which are also related to ER-stress associated apoptosis.

6.3 Materials and methods

6.3.1 Cell lines

Skin biopsies from 3 JOCD patients were used to derive JOCD-specific iPSC lines. In order to establish the disease phenotype per patient, 3 clones (analogous to biological copies) were used per cell line as indicated in Table 11. Control (non-disease) patients were gifted by REMEDI and purchased from ATCC.

iMSCs from JOCD and control groups were differentiated from iPSCs via an EB intermediate step, as previously described [142, 143]. iMSCs were characterized and validated according to the International Society of Cell Therapy's minimum criteria [144]. iMSCs were cultures in MSC maintenance medium with 2 ng/ml FGF2 (Peprotech), until experiments.

Table 11. Control group was composed of 2 iPSC lines gifted from REMEDI (one of which had 2 clones) and 2 iPSC lines purchased from ATCC, described in Table 5. JOCD group consisted of 3 JOCD-specific iPSC lines, with 3 clones each (described in Table 4). Cell line identifying number is denoted by the number after the group (i.e. cntrl#2, or control cell line #2) and clone number, within the cell line) is denoted by the number after the dash (i.e. cntrl#1-1, or control cell line #1-clone#1).

Control group	Cntrl 1-1	Cntrl 1-2	Cntrl2	Cntrl3	Cntrl4				
JOCD group	JOCD 1-1	JOCD 1-2	JOCD 1-3	JOCD 2-1	JOCD 2-2	JOCD 2-3	JOCD 3-1	JOCD 3-2	JOCD 3-3

6.3.2 Chondrogenic and endochondral ossification models (organoids)

3D chondrogenesis of iMSCs was performed using the high cell-density micromass culture model as previously described [78]. Briefly, 2×10^5 iMSCs in 10 µl of MSC maintenance media were incubated at 37°C for 2 hours in low-adherence round-bottom 96-well plates (Sigma-Aldrich). Then, 200 µl of MSC maintenance medium was added to each well, followed by overnight incubation. Medium was replaced by chondrogenic medium with 10ng/ml TGF-β3 (Peprotech) the following day and was changed every second day for 49 days.

For the model of 3D endochondral ossification, micromass cultures were started the same as in the 3D chondrogenesis model and cultured for the first 21 days in chondrogenic medium. At day 21, medium was replaced by osteogenic medium, and the pellets were cultured for an additional 28 days.

6.3.3 ER stress-induction model

iMSCs were seeded at a 5,000/cm^2 cell density in 35mm petri dishes and cultured with MSC Maintenance Medium. Once cells reached 60-70% confluency, the medium was replaced by MSC Maintenance Medium + ER-stress drug (5ng/ml Tunicamycin (Sigma Aldrich) or Protein Transport Inhibitor Cocktail (eBioscience)). It was important to expose cells to the ER-stressor at subconfluency in order to prevent cell-contact inhibition. Furthermore, we chose 3 different drugs in order to observe cell responses across different ER-stress stimuli and confirm potential mechanistic results.

6.3.4 Gene expression

6.3.4.1 RNA extraction

Total RNA from organoid cultures was extracted using the RNeasy MinElute Clean-up Kit with QIAzol Lysis Reagent (Qiagen). Total RNA from the ER-stress-induction cultures was extracted using the RNeasy MinElute Clean-up Kit (Qiagen). Normalized RNA was synthesized to cDNA using the RT^2 First Strand Kit (Qiagen).

6.3.4.2 Microarray RT-PCR

RNA expression was quantified using the Taqman real-time PCR Fluidigm Dynamic Array Integrated Fluidic Circuits (BioMark, Fluidigm). Differentiation models were tested again the array indicated in Table 12, and ER-stress induction models were tested again the array specified in Table 13. AccuRef human universal cDNA (Gene Scientific) and ultrapure water were used as positive and negative controls, respectively, to ensure run fidelity.

Ct values greater than 37 were treated as 37 (null). Gene expression analysis was carried out using the ΔΔCt method, outlined in Equation 1 and Equation 2. The Ct value of each gene was normalized by the geometric mean of the expressions of the housekeeping genes to get the relative expression (ΔCt). Then, the ΔCt of each target was normalized by the ΔCt of the calibrator to get the ΔΔCt for each gene. For the differentiation experiments, the calibrators were the micromass cultures at 2 hours post-seeding of the respective cell line. For the ER-stress induction cultures, the calibrators were the respective cell line at the 0 hr timepoint, before the induction of stress with drugs. SEM was derived using Gauβ's error propagation (Equation 3).

Table 12. List of Taqman gene expression assays used to evaluate the expression of ER-stress genes in the chondrogenesis and endochondral ossification *in vitro* models. Where available, the assays with the best coverage (recommended by the company) were selected. Some assays may be listed more than once as they fall in more than one category.

Category	Taqman Gene Expression Assays
Sensors which trigger UPR	Eif2ak3 (common name PERK, Hs00984003_m1), Atf6 (Hs00232586_m1), Ern1 (common name IRE1, Hs00980095_m1)
Translation inhibition	Eif2ak3 (common name PERK, Hs00984003_m1)
Redox response apoptosis	Atf4 (Hs00909569_g1), Ddit3 (common name CHOP, Hs00358796_g1)
Chaperones & chaperone-synthesis promoter	Hspa5 (common names BIP and GRP78, Hs00607129_gH), Hsp90b1 (common name GPR94, Hs00427665_g1), Xbp1 (Hs00231936_m1)
Protein degradation	Edem1 (Hs00976004_m1), Ern1 (Hs00980095_m1)
Stimulators of osteogenesis	Atf4 (Hs00909569_g1), Atf3 (Hs00231069_m1), Serpinh1 (Hs01060397_g1), Creb3l1 (Hs00369340_m1), Gadd45b (Hs00169587_m1)
Housekeeping genes	Gapdh (Hs02786624_g1), Rps18 (Hs01375212_g1), Actb (Hs0106665_g1)

Table 13. List of Taqman gene expression assays used to evaluate the molecular response of JOCD and control cell lines to ER-stress induction models. When available, the assays with the best coverage (recommended by the company) were selected. Some assays may be listed more than once as they fall in more than one category.

Category	Taqman Gene Expression Assays
Sensors which trigger UPR	Eif2ak3 (common name PERK, Hs00984003_m1), Atf6 (Hs00232586_m1), Ern1 (common name IRE1, Hs00980095_m1)
Translation inhibition	Eif2ak3 (common name PERK, Hs00984003_m1)
Redox response apoptosis	Atf4 (Hs00909569_g1), Ddit3 (common name CHOP, Hs00358796_g1), Asns (Hs04186194_m1)
Chaperones & chaperone-synthesis promoter	Hspa5 (common names BiP and GRP78, Hs00607129_gH), Hsp90b1 (common name GPR94, Hs00427665_g1), Xbp1 (Hs00231936_m1)
Protein degradation	Edem1 (Hs00976004_m1), Dnajb9 (Hs01052402_m1), Dnajc10 (Hs00405977_m1), Ern1 (Hs00980095_m1)
Housekeeping genes	Gapdh (Hs02786624_g1), Rps18 (Hs01375212_g1), Actb (Hs0106665_g1)

6.3.5 Statistical analyses

Data were graphed as means ± SEM. Group comparisons were made with Two-way ANOVA analysis. Tukey's and Kruskal-Wallis were used as *post hoc* tests where appropriately. P-values less than 0.05 were considered statistically significant.

6.4 Results

6.4.1 Differentiation models

6.4.1.1 Chondrogenesis

ER-stress genes related to chondrogenic maturation and osteogenic differentiation were upregulated in the JOCD group (Figure 37). Atf3 was significantly higher in JOCD than control at days 14, 21, 35 and 49. Atf4 was significantly higher in JOCD than control at days 14, 21, 28, 35 and 49. Creb3l1, Gadd45b and Serpinh1 were significantly higher in the JOCD group than control at all timepoints.

Expression of the sensors which trigger UPR were also upregulated in the JOCD group (Figure 37). Atf6 was significantly higher in JOCD at days 14, 35 and 49. Eif2ak3 (common name PERK) was significantly higher in the JOCD group than the control group at days 7, 14, 28, 35, and 49. Ern1 (common name IRE1) was significantly higher at days 14, 21, 28, 35 and 49. Eif2ak3 is directly involved in inhibition of protein inhibition and Ern1 in degradation of unfolded protein. Edem1 is also a marker of ER-associated degradation, and it was significantly higher in JOCD at days 14, 21, 28, 35 and 49.

Total Xbp1 expression is related to an increased in protein chaperone synthesis, and this gene was unregulated in the JOCD group at all timepoints. Consistently, chaperone Hspa5 (commonly known as BIP or GPR78) was significantly higher in the JOCD group than the control group at days 7, 14, 28, 35, and 49. Chaperone Hsp90b1 (known as GRP94) was significantly higher in JOCD at day 14 only.

Genes associated with ER-stress-induced apoptosis had a variable response (Figure 37). Atf4 was significantly higher in JOCD at days 14, 21, 28, 35 and 49. Ddit3 (commonly known as CHOP) was higher in the control group at day 7, but higher in the JOCD group at the later timepoints days 35 and 49.

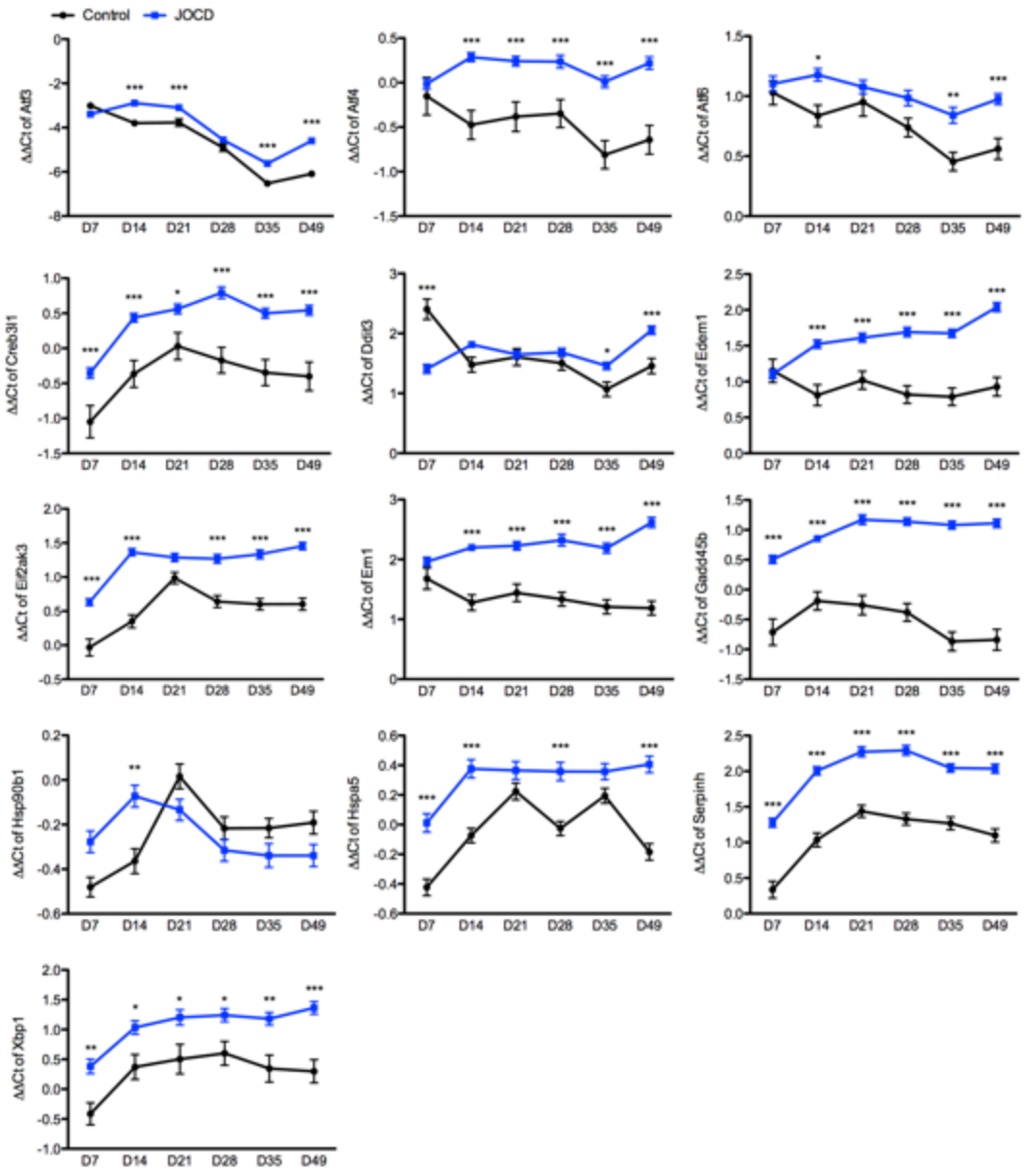

Figure 37. Normalized relative expression of ER-stress related genes during chondrogenesis of JOCD- and control-specific iPSC-based organoids, graphed as means ± SEM. * indicated difference between JOCD and control cell lines for the indicated timepoint at p-value <0.05, ** p-value <0.01, and *** p-value <0.001.

6.4.1.2 Endochondral ossification

In general, the JOCD group expressed higher levels of all ER-stress related genes during endochondral ossification (Figure 38). Genes specifically related to ER stress during chondrocyte maturation and osteogenesis (Atf4, Creb3l1 and Gadd45b) were significantly higher in JOCD at all timepoints. Atf3 was significantly higher at days 28 and 49.

Expression of the three sensors which trigger UPR (Eif2ak3, Atf6 and Ern1) were upregulated in the JOCD group. Eif2ak3 and Ern1 were significantly higher in JOCD at all timepoints, while Atf6 was only significantly higher at days 14, 35 and 49. Edem1, like Ern1, is a marker of ER-associated degradation, and it was significantly higher in the JOCD group than control group at days 14, 21, 48, 35 and 49.

Xbp1 and Hspa5, markers of increased chaperone activity, were also significantly higher in JOCD. Xbp1 was significantly higher at days 35 and 49, and Hspa5 at every timepoint. Chaperone Hsp9b1, however, was not significantly different between the JOCD and control groups, for any timepoint. Atf4 is also an indicator of redox balance apoptosis and so is Ddit3. Ddit3 was significantly higher in JOCD at days 28 and 35.

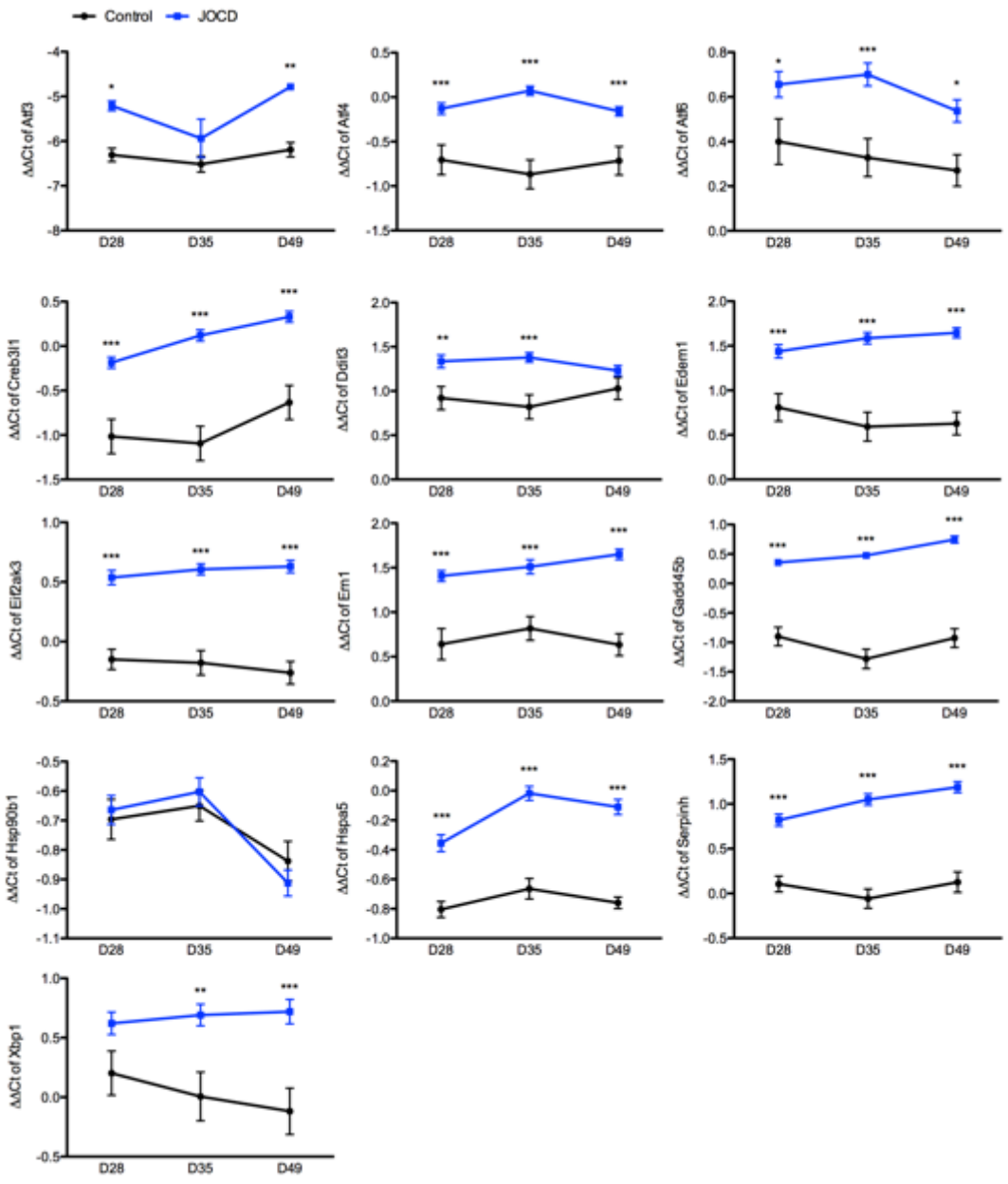

Figure 38. Normalized relative expression of ER-stress related genes in response to 3D endochondral ossification differentiation, graphed as means ± SEM. * indicated difference between JOCD and control cell lines for the indicated timepoint at p-value <0.05, ** p-value <0.01, and *** p-value <0.001.

6.4.2 ER-stress models

6.4.2.1 Protein Transport Inhibitor Cocktail

The normalized relative expression of all genes tested is shown in Figure 39. The gene markers for the three sensors that are triggered by ER stress and thus initiate UPR had variable expression. Eif2ak3 and Atf6 had similar expression in the control group as the JOCD group, for all timepoints. Ern1 was significantly higher in JOCD at 2, 6 and 12 hours than control. Ern1 is also a marker of ER-stress-associated protein degradation, as well as Dnjab9, Dnajc10 and Edem1. Dnajb9 and Edem1 were significantly higher in the JOCD group than the control group at 6 hours, while Dnajc10 had similar expression in both groups.

Expression of genes related to ER-stress induced redox balance apoptosis were upregulated in the control group. Ddit3 was significantly higher in the control group than JOCD at 12 hours, and Asns at 12 and 24 hours. Expression of genes related to protein chaperones were generally upregulated in the JOCD group. Xbp1 was significantly higher in the JOCD group at 6 hours, and chaperone Hspa5 was significantly higher in the JOCD group at all timepoints. There were no significant differences between JOCD and control for chaperone Hsp90b1.

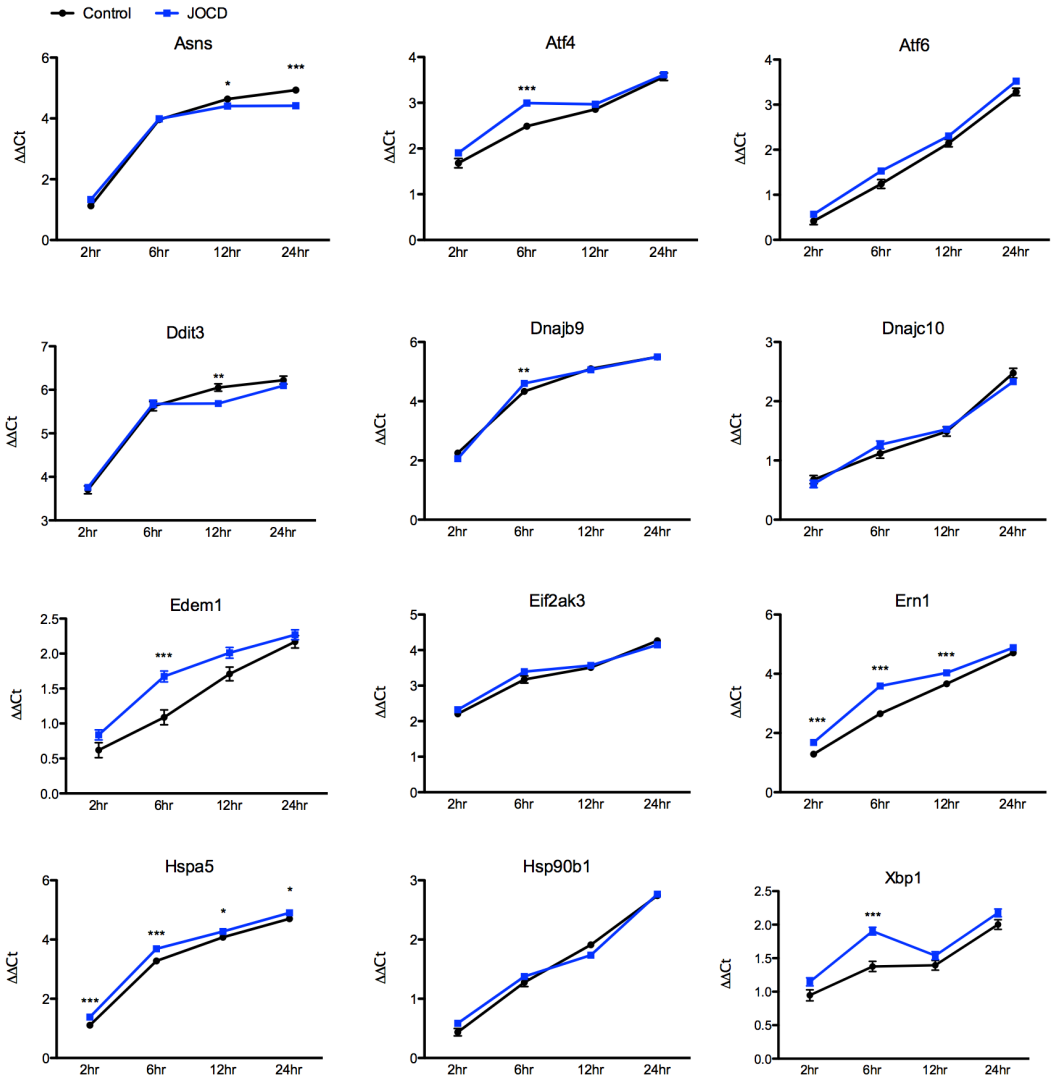

Figure 39. Normalized relative expression (ΔΔCt) of ER-stress related genes in response to PTIC drug, graphed as means ± SEM. * indicated difference between JOCD and control cell lines for the indicated timepoint at p-value <0.05, ** p-value <0.01, and *** p-value <0.001.

6.4.2.2 Tunicamycin

Figure 40 shows the normalized relative gene expression in response to tunicamycin treatment. UPR activation transmembrane sensor Eif2ak3 was significantly

higher in the control at 6 and 24 hours, while Ern1 and Atf6 had similar expressionin both groups for all timepoints.

The expression of other markers of protein degradation were upregulated in the control group: Dnjab9 was significantly higher in the control group than the JOCD group at 2 and 24 hours, while Dnajc10 was significantly higher in the control group at 2, 6 and 24 hours. Dnjac10 was significantly lower in the control group than the JOCD group at 12 hours. Finally, Edem1 was also significantly lower in the control group than JOCD group at 12 hours. Increased chaperone activity and synthesis were also observed in the JOCD group. Hspb901 was significantly higher in the control group at 2 hours and lower in the control group than the JOCD group at 12 hours. Hspa5 was also significantly lower in the control group than the JOCD group at 12 hours. Xbp1 showed a similar trend, but differences between groups were not significant.

Markers related to ER-stress-induced apoptosis were also upregulated in the control group. Asns was significantly higher in the control group than JOCD at 2, 6 and 24 hours, while Ddit3 was significantly higher at 24 hours. Atf4 was significantly higher in the JOCD group than the control group at 12 hours.

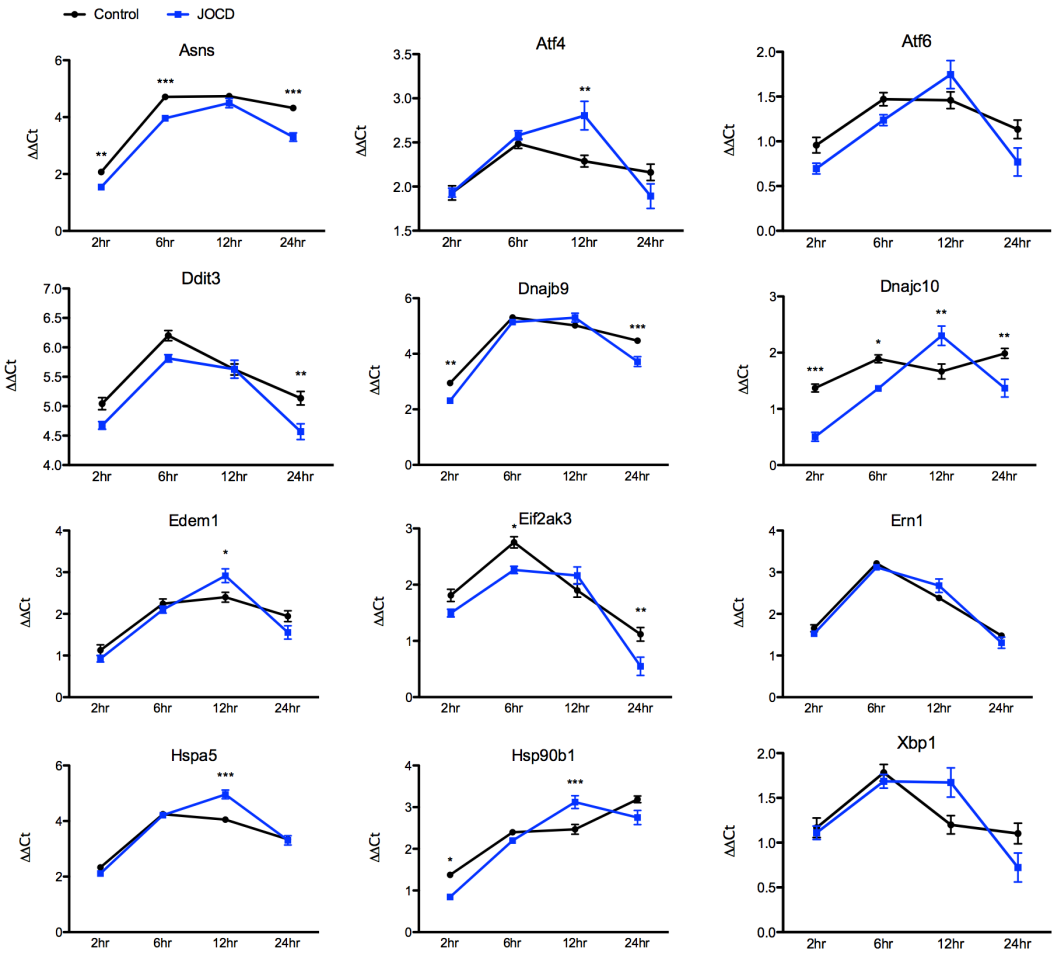

Figure 40. Normalized relative expression (ΔΔCt) of ER-stress related genes in response to tunicamycin drug, graphed as means ± SEM. * indicated difference between JOCD and control cell lines for the indicated timepoint at p-value <0.05, ** p-value <0.01, and *** p-value <0.001.

6.5 Discussion

ER stress is an important physiological response to normal processes, such as osteogenic differentiation, and pathological conditions. Although FOCD and equine OCD have been linked with ER-stress related pathogenesis, to this date, no study had explored the molecular mechanisms of JOCD related to ER stress. The objective of this work was to investigate ER-stress mechanisms during chondrogenic and endochondral ossification of JOCD cell lines and in a controlled environment in response to ER-stress inducers.

Our chondrogenic and endochondral ossification differentiation models showed increased expression of UPR-related genes in the JOCD group. This result may suggest that JOCD cell lines may be experiencing a higher ER stress during differentiation than control cell lines. Higher expression of Eif2ak3, Atf6, and Ern1 particularly suggest the activation of the three transmembrane sensors, which act in response to protein accumulation and ER stress. Chaperone Hsp90b1 was the only marker that did not have a significantly different expression in JOCD versus control cell lines. Previous studies have pointed at distinct functions between the chaperones Hsp90b1 and Hspa5 [165]. Compared to Hsp5, the client proteins of Hsp90b1 are more selective with critical roles in immunity, growth signaling and cell adhesion [166], which may discard these types of proteins from being the culprit of heightened ER stress in JOCD cell lines during differentiation.

Higher expression of ER-related genes that are also involved in chondrocyte maturation and osteogenesis may indicate a premature differentiation of our model to chondrocyte hypertrophy in the JOCD group. This suggestion agrees with the previous

chapter, in which we observed a higher gene expression of col1a1 and deposition of collagen type I protein in JOCD chondro-organoids. Expression of Gadd45b is essential for chondrocytes during terminal differentiation. In fact, its expression has been shown to increase from the proliferative phase to the hypertrophic phase, and to stimulate Mmp13 (a marker of terminal differentiation of hypertrophic chondrocytes) [167]. Atf4 stimulates osteoblast-specific genes and Atf3, whose upregulation has been also reported during chondrocyte differentiation and shown to activate a Runx2-dependent promoter [159]. Creb3l1 is a transcription factor expressed in osteoblasts, which activates Atf6 of the UPR pathway [168]. Atf6 is related to the increased synthesis of protein chaperones, and we observed this feature in our differentiation models, including Serpinh1. Serpinh1 is a collagen-specific molecular chaperone that, unlike other chaperones, specifically recognizes the folded conformation of its client [169], and it is, therefore, directly involved in collagen biosynthesis.

Differentiation of cells is a highly variable process, and even under the same differentiation-promoting conditions, there is known donor-to-donor variability and also clone-to-clone variability within the same iPSC donor [170-173]. In other words, cell lines respond differently to the same stimuli during differentiation. Therefore, in order to investigate the cells' response to ER stress in a controlled environment, ER stress was induced with PTIC and tunicamycin.

PTIC is a cocktail of Brefeldin A and Monensin, and thus prevents protein transport to the extracellular space, retaining proteins in the ER and inducing ER stress. In PTIC-treated cells, results indicated an increased ER-stress response in JOCD-specific

cells comparing to control cells. This heightened response was particularly observed at earlier timepoints and confirmed by tunicamycin treatment.

In PTIC and tunicamycin treatments, the only genes for which JOCD cells lines had a significantly lower expression than control cells were related to ER-stress-induced apoptosis: Asns and Ddit3 (CHOP). The increased expression of the other genes related to the UPR mechanisms in JOCD cells may lead to higher survival and thus lower activation of these apoptotic markers.

Altogether, these observations point to two overarching conclusions. The first, the results from the differentiation models and ER-stress induction models may suggest that JOCD cell lines are more susceptible to stress (i.e. physiological and pathological stresses). This may indicate that upon encounter with physiological and pathological stresses, JOCD cells may respond differently and this characteristic may be linked to its pathology. Dysregulated UPR activity may lead to failure to cope with ER stress over prolonged periods of time, which may eventually lead to cell death and may be responsible for the initial necrotic lesion observed in clinical JOCD.

Ischemia is a pathological stresses and a hypothesized etiology for JOCD. It may be that upon trauma, which can cause interruption of the microvasculature, JOCD cells are not able to cope with the temporary ischemia as well as non-JOCD cells and thus they undergo ER-stress-induced cell death, causing initial necrotic lesion observed in JOCD patients. This hypothesis may be tested by studying our chondro- or osteo-organoids under ischemic conditions (low glucose or a glucose-blocker, and low oxygen).

Secondly, we may conclude that chondrogenic and endochondral ossification differentiations trigger a higher ER stress in JOCD cell lines, which may suggest that there is a difference in differentiation processes between the two groups. This suggestion also partially agrees with the previous chapter, in which we saw that although the end result of endochondral ossification was similar between the two groups (calcium content and collagen type I staining), gene expression during differentiation was significantly different. This second point is not in conflict with our first, but an entirely different observation. A study by Vellanki *et al.* showed that knock-down of Creb3l1 in human glioma cell lines resulted in an attenuated UPR to ER stress, but induction of the col1a1 was unaffected [174]. JOCD cells may have a different UPR activation compared to control cell lines, but this does not necessarily affect their osteogenic ability.

CHAPTER 7. SUMMARY AND FUTURE DIRECTIONS

7.1 Overall summary

In order to improve therapeutic interventions of joint disorders, the knowledge gap concerning their pathological mechanisms need to be bridged. The overall objective of this thesis was to elucidate pathomechanisms of OA and JOCD in order to provide insights about their development and how they may be addressed therapeutically. Both OA and JOCD are complex joint diseases that lack appropriate disease-modifying treatments.

In the case of OA, the lack of well-characterized models may be partially responsible for failed clinical trials with promising pre-clinical data. In accordance with our overall objective, we developed a microarray gene expression tool and established a baseline of molecular events for multiple tissues, in different regions, and at different timepoints, for the MMT model of post-traumatic OA (Specific Aim I, Chapter 3). By characterizing OA development in this model, we were also able to provide insights about possible tissue interactions in OA. Utilizing this microarray gene expression tool, we then investigated the mechanisms of action of micronized dehydrated human amnion/chorion membrane (AmnioFix Injectable, MiMedx, USA) with the goal to understand its chondro-protective effect to leverage it in the future development of more specific therapeutic (Specific Aim II, Chapter 4). Results showed that AmnioFix does not have a direct influence on the gene expression of articular cartilage or tissue from the osteophyte-forming region of the joint. Instead, AmnioFix acted through the synovial membrane, modulating its microenvironment. These results further supported the

importance of tissue interactions in the MMT model and in OA, and also provided a new viewpoint concerning disease-modifying approaches for OA.

Lastly, we sought to elucidate pathological mechanisms of JOCD by establishing novel disease-specific iPSC-derived *in vitro* models (Specific Aim III, Chapter 5 and 6). This groundbreaking technology allowed us to study different aspects of JOCD. JOCD-specific chondrogenic organoids demonstrated a lower chondrogenic ability than control (non-diseased)-specific organoids. Even though JOCD-specific endochondral ossification model was able to calcify and produce an ECM similar to that of the controls, we suspect from the gene expression results that there are irregularities in this differentiation process for JOCD. Through ER-stress induction models, we were able to further dissect pathological mechanisms of JOCD and demonstrated that JOCD cells possess a significantly different UPR signaling (compared to control). We ultimately hypothesized that when physiological or pathological events that induce ER stress in the epiphyseal occur, JOCD patient cells may not respond properly, which may lead to the eventual death of these cells, which turns into the initial necrotic lesion observed in JOCD patients. Microtauma and ischemic injury may be possible initiators of the demonstrated JOCD pathological events.

Overall, this thesis presents original research regarding joint degenerative models for OA and JOCD, and it provides the scientific field with well-characterized platforms for future therapeutic development and testing.

7.2 Future directions

There a number of exciting directions that the work presented in this thesis may take. Firstly, AmnioFix Injectable should be further explored in an inflammatory *in vivo* model in order to validate the results observed in this work, or perhaps elucidate the variable effect of AmnioFix in environments with different degrees of inflammation. Effects of AmnioFix in RA would be particularly interesting, since the primary pathomechanisms in RA affect both the synovial membrane and the immune system. With respect to OA, the suggested mechanistic effects of AmnioFix in the MMT model may point to a benefit from increased pro-inflammatory signaling. Pro-inflammation is, after all, important in wound healing at early timepoints. Future work should attempt to regulate the inflammatory response in the synovial membrane of the MMT model in order to see if similar results are obtained. It will also be worth assessing the response of the MMT model due to prolonged modulation, possibly by multiple treatments of AmnioFix Injectable with temporal proximity.

The differentiation processes of JOCD-specific cell lines should also be further assessed. We observed potential dysregulation in endochondral ossification processes in JOCD, yet similar end-point results between JOCD and control. We propose large-scale array analyses, such as RNA-seq, in order to further dissect differences in cell differentiation in JOCD patients. From our ER-stress induction models, we hypothesized that a different UPR activation in JOCD cells may ultimately lead to ER-stress-associated cell death in the epiphyseal due to changes to the extracellular environment, such as ischemia. This hypothesis should be tested by studying our JOCD-specific *in vitro* models under ischemic-like conditions (low to no glucose, low oxygen).

APPENDIX A. TOWARDS AN EARLY-STAGE SMALL ANIMAL MODEL OF OSTEOCHONDRITIS DISSECANS

A.1 Introduction

Currently, there are no disease models which recapitulate the development and progression of JOCD. A mechanically-induced lapine model is currently available; however, this model only replicates the severe late stage in which the osteochondral fragment is completely separated from the native bone (stage IV) [175]. In skeletally immature female New Zealand White rabbits, a 4-mm diameter plug is taken from the weight-bearing osteochondral surface on the medial femoral condyle, as shown in Figure 5A [175]. Then, a piece of acellular collagen-glycosaminoglycan matrix is placed into the cavity and the plug is replaced (Figure 5B) [175]. The matrix prevents healing and reattachment of the osteochondral plug, thus creating an osteochondral defect and replicating the last stage of JOCD.

The Mauck group has developed a similar technique in a swine model. An osteochondral defect was created using a curved osteotome, removed, and later replaced following interposition of a slowly degrading nanofibrous poly(ε-caprolactone) (PCL) barrier membrane [176]. Unlike in the lapine model, sutures were used to secure the progeny fragment to the defect site. This swine OCD model attempts to replicate ICRS OCD grade III, in which there is a partially detached lesion; essentially, a dissecan *in situ*. However, thanks to advanced imaging modalities and improved guidelines, JOCD is now

typically detected in patients at ICRS OCD grade I or II (stable lesion). Therefore, although these preclinical animal models may be relevant for late stages of JOCD, their utility in the field is limited. Furthermore, it is the failure to treat JOCD at early stages what results in the progression of this disorder into partial or complete separation of the fragment, which jeopardizes the integrity of the joint and significantly alters the normal joint mechanics [35, 36, 177]. At this point, patients will develop OA at an early age. Therefore, a new pre-clinical model of early-stage JOCD is needed. Introducing a small animal model of JOCD with the ability to emulate early stages of this disorder will allow exploration of novel treatment options, as well as tailoring of current clinical approaches. The objective of this work was to explore multiple techniques in an effort to develop a small animal model of early-stage JOCD, marked by a necrotic lesion around the subchondral area and with intact articular cartilage.

A.2 Success criteria

The success criteria for this animal was determined in consultation with the surgeons specialized in JOCD from Children's Healthcare of Atlanta, Orthopaedics and was as follows:

A.2.1 Bone

There should be a localized (emphasis on the localization aspect) osteonecrosis near the subchondral bone area. There should be the least amount of fibrosis possible; none is ideal. Because the model is meant to be used for early-stage OCD testing, continuous bone tissue is essential (e.g. no partial detachment or holes).

A.2.2 Articular cartilage

The articular cartilage overlaying the bone insult should be have intact surface and bottom (interface with subchondral bone). This means no fibrillation or remodeling; however, thickening of the articular cartilage is acceptable and even desired. When measure by uCT methods, there should be only low signal changes in the articular cartilage.

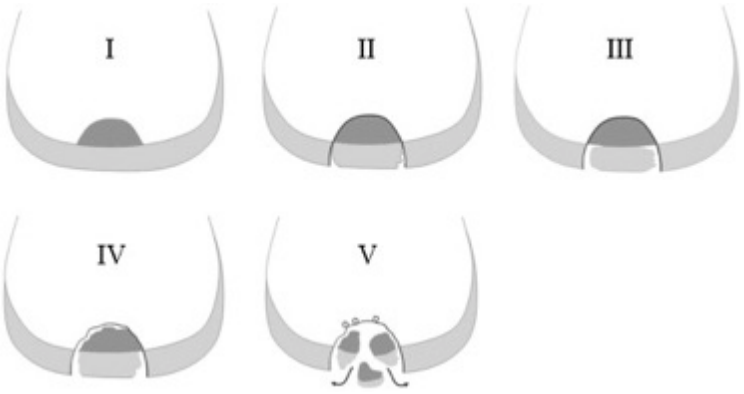

Figure 41. OCD grading system. Early-stage OCD includes grades I and II. Our goal was to develop an animal model that emulated OCD grade I.

A.3 Chemical insult

A.3.1 Surgical procedure

The Georgia Institute of Technology IACUC approved all animal procedures (#A15023). In male Lewis rats (270-300 mg), the MCL was transected to access the lateral aspect of the left medial femoral condyle. Using a customized setting of the stereotaxic frame, a drill hole was made, 0.5 mm in diameter and 1 mm in depth, in the region just above the subchondral bone layer. After cauterizing, bonewax was placed over the drill hole. In OCD animals, 5 µl of 2ml/50ul of monosodium iodo-acetate (MIA)

was injected through the bone wax to chemically induce the initial necrotic lesion. In sham animals, saline was injected. All animals were sacrificed at 3 weeks post-surgery.

The stereotaxic frame allowed for consistent location and depth of the drill hole (Figure 42). The MIA was injected through the bonewax because previous preliminary studies have shown a problem with liquid retention at the drill hole site. Even though we cauterized after drilling, blood backflow reinitiates after a few seconds.

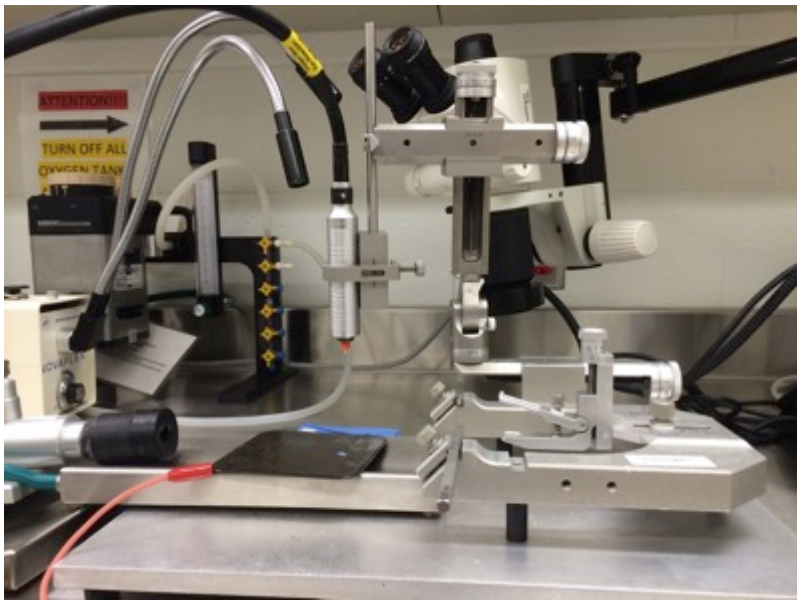

Figure 42. Set-up of stereotaxic frame and cauterizer for OCD surgeries.

MIA was chosen to induce bone cell death because preliminary work (Figure 43) showed confirmed MIA-dependent cell death of pre-osteoblasts. The concentration used for initial experiments was 5uM of MIA; however, we did not observed cell death at the drill hole site and thus increased the dose to a level comparable to high-dose MIA model of OA.

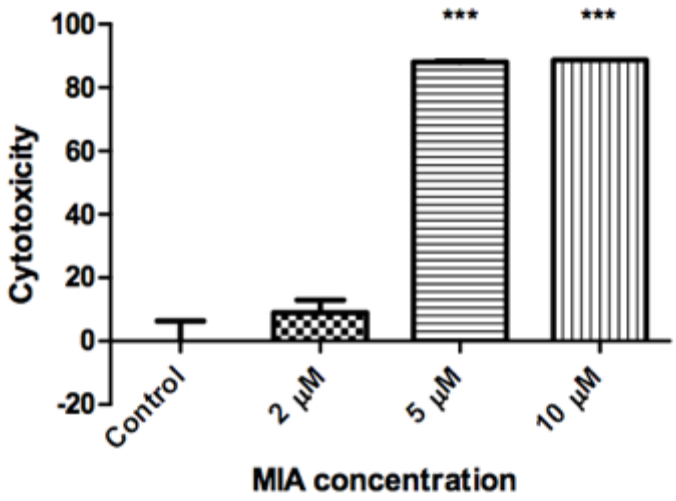

Figure 43. MC3T3 pre-osteoblast cells after 24 hours of MIA treatment at the various concentrations. MTT assay was used to read cell survival after treatment. * indicates p-value <0.001.**

A.3.2 Results and discussion

We observed a reproducible technique in terms of drill hole location and depth thanks to the use of the stereotaxic frame. However, MIA injections did not show significant differences from saline injections (sham animals), indicating that the MIA injections were not having an effect (Figure 44). This is mostly due to the limited space allowed for injections (0.5 mm drill hole). We hypothesize that MIA in simply not retained at the drill hole site.

Moreover, histological analysis of the bone showed signs of remodeling (Figure 44). It appeared that fibrous tissue had formed around the drill hole site. For the purpose of this model, we want zero to very minimal fibrous tissue in the bone and we need the

bone tissue to be continuous (i.e. not have a hole). Therefore, this chemically-induced model failed to pass the success criteria for the desired OCD pre-clinical model.

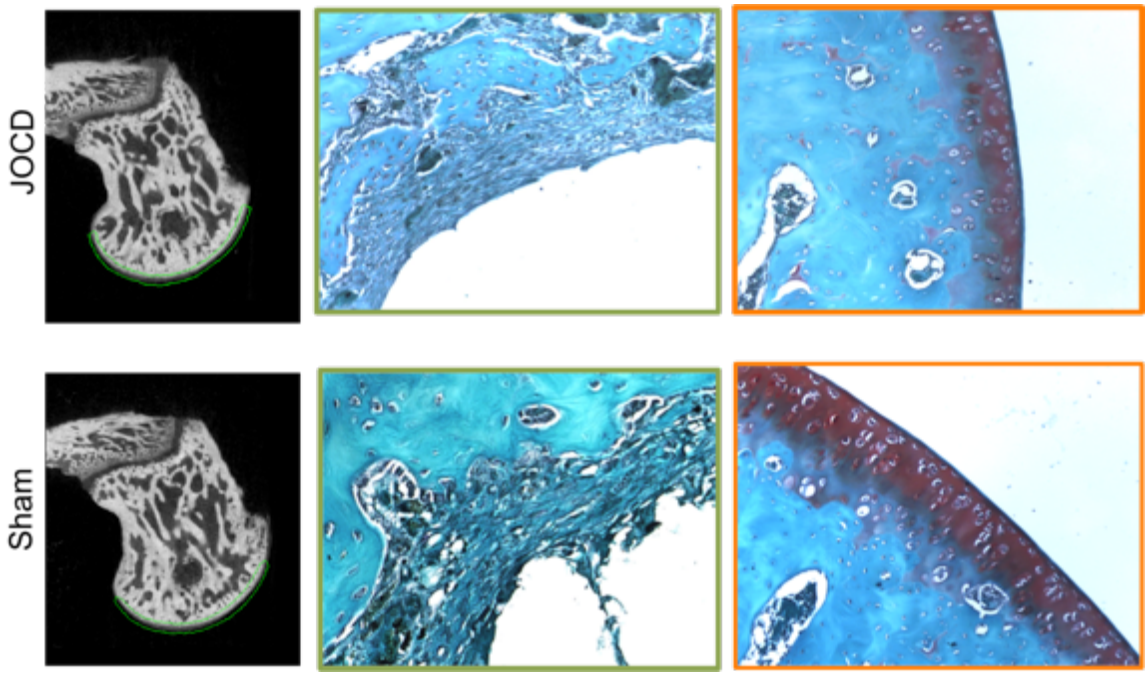

Figure 44. uCT scans showed consistent drill hole site. Saf-o (red)/Fast green (blue/green) staining showed remodeling of the bone at the drill hole site, marked by fibrous tissue. Additonatly, there were no signs of articular cartilage degradation, as shown by intact staining of Saf-o (red).

A.3 Thermal insult

A.3.1 Surgical procedure

The Georgia Institute of Technology IACUC approved all animal procedures (#A15023). Cryogenic insults, coupled with vascular ligation, have been increasingly adopted to induce osteonecrosis [178-180]. In cryosurgery, the freezing process causes direct cellular and vascular injury [180]. For the purpose of this work, we

sought to create localized necrosis near the subchondral bone with the help of a cryogenic insult in combination with vascular ligation. The left leg of weight-matched Lewis rats (300-325 mg) were surgerized; the right leg was used as contralateral control. We tested 3 groups (n=2): (A) cryogenic insult only, (B) ligation only, and (C) cryogenic insult coupled with ligation. For the cryogenic insult, a drill hole was made near the subchondral bone, cauterized, and a direct stream of liquid nitrogen was delivered continuously for 10 seconds into the hole followed by warm saline (10 s). The thermal insult was repeated 5 times, then the hole was sealed with bonewax. The medial superior genicular artery was chosen for ligation because it branches close to the femoral condyles, supplying them and the knee-joint. Figure 45 shows a diagram of the surgical procedure to induce OCD. Animals were sacrificed 3 weeks post-surgery.

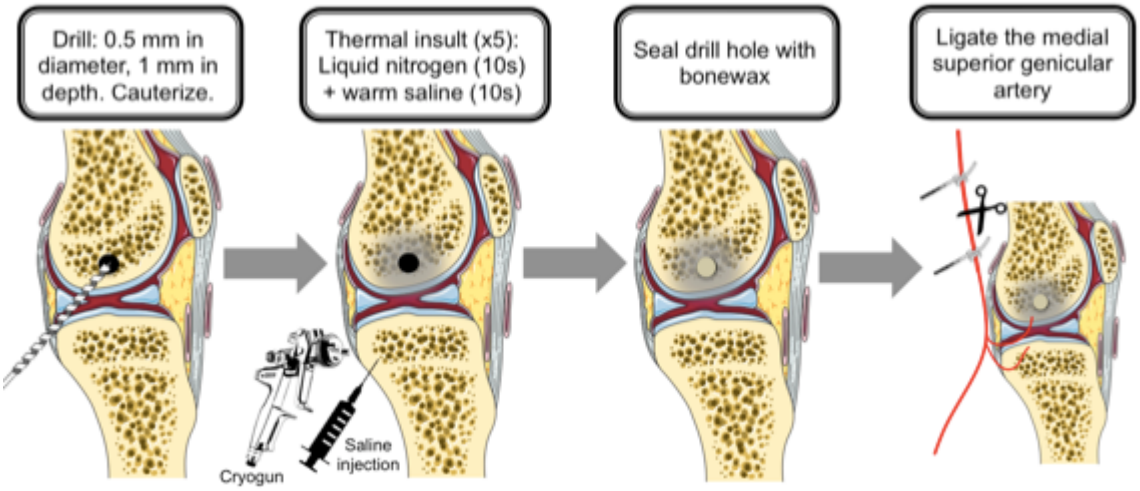

Figure 45. Diagram of surgical procedure for thermally-induced OCD animal model.

A.3.2 Results and discussion

Figure 43. shows representative pictures of the gross morphology of each group. Group C was the most severely damaged, having the entire medial femoral condyle completely or partially fragmented (Figure 46). The region around the lesion site showed cell death in all groups, as indicated by patches in the trabecular bone devoid of osteocyte nuclei (Figure 47). However, only groups B and C had signs of potential osteoclasts (further staining would need to be done to confirm this claim) at the edges of the dead bone as well as woven bone on the surface of the dead traberculae. These characteristics match previously reported morphologic modifications associated with osteonecrosis [181]. Also, it is noteworthy to mention that there appeared to be a higher level of remodeling in the Group C.

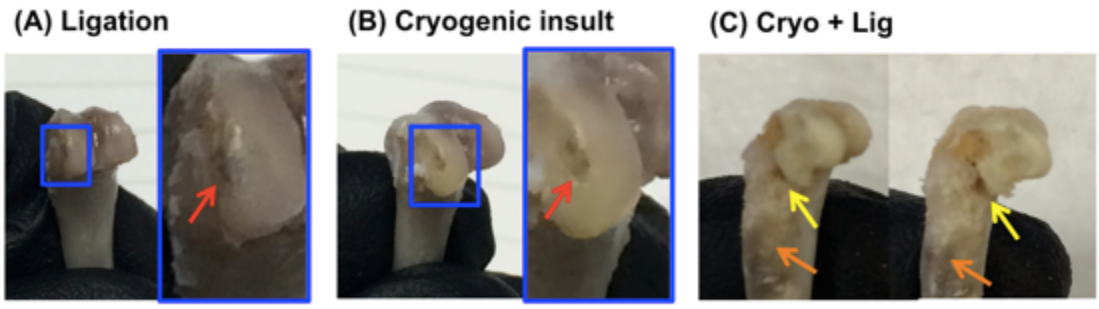

Figure 46. Representative pictures of the gross morphology of each group: (a) ligation only, (b) cryogenic insult only, and (c) cryogenic insult in combination with ligation. Blue boxes show magnification of the medial femoral condyle. Red arrows point at the drill hole site. Yellow arrow points at the partial fragmentation of the medial femoral condyle observed in the cryogenic insult plus ligation group, while orange arrow points at the damage throughout the shaft of the femur.

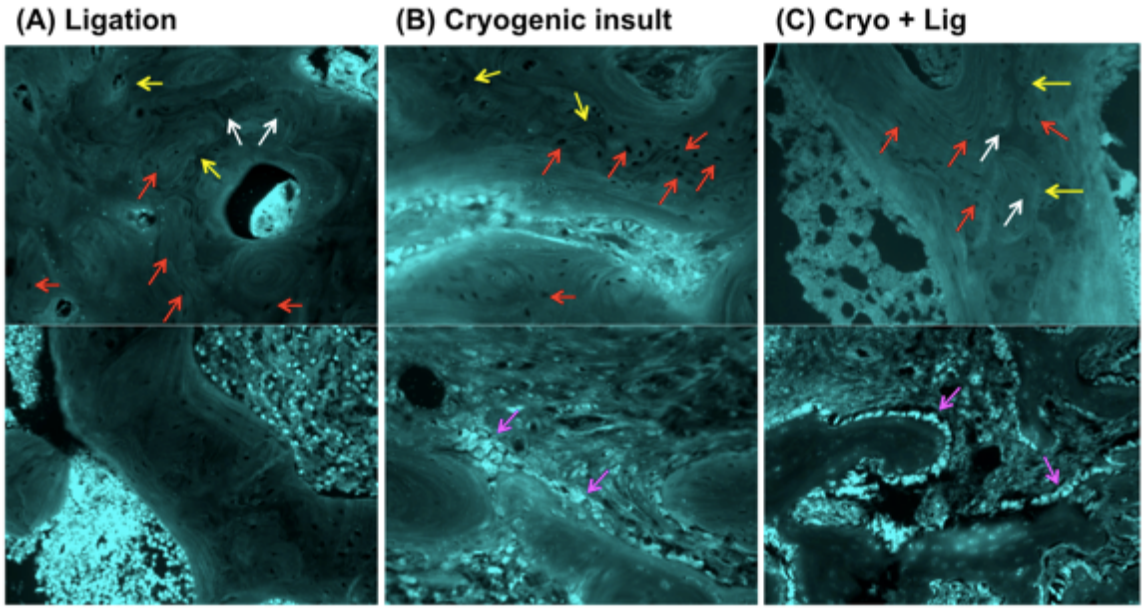

Figure 47. DAPI staining (cyan) of group A) ligation, group B) cryogenic insult and group C) cryogenic insult plus ligation in the region of the drill hole/lesion site. Red arrows point at empty while white arrows point at filled osteocytic lacunae. Yellow arrows point at signs of woven bone. Magenta arrows point at possible osteoclasts at the edges of the traberculae.

The articular cartilage was also affected, as shown in Figure 48. Histological analysis showed significantly less proteoglycans in the articular cartilage, in groups B and C. In group C, however, there was evident modification of the structure and integrity of the cartilage.

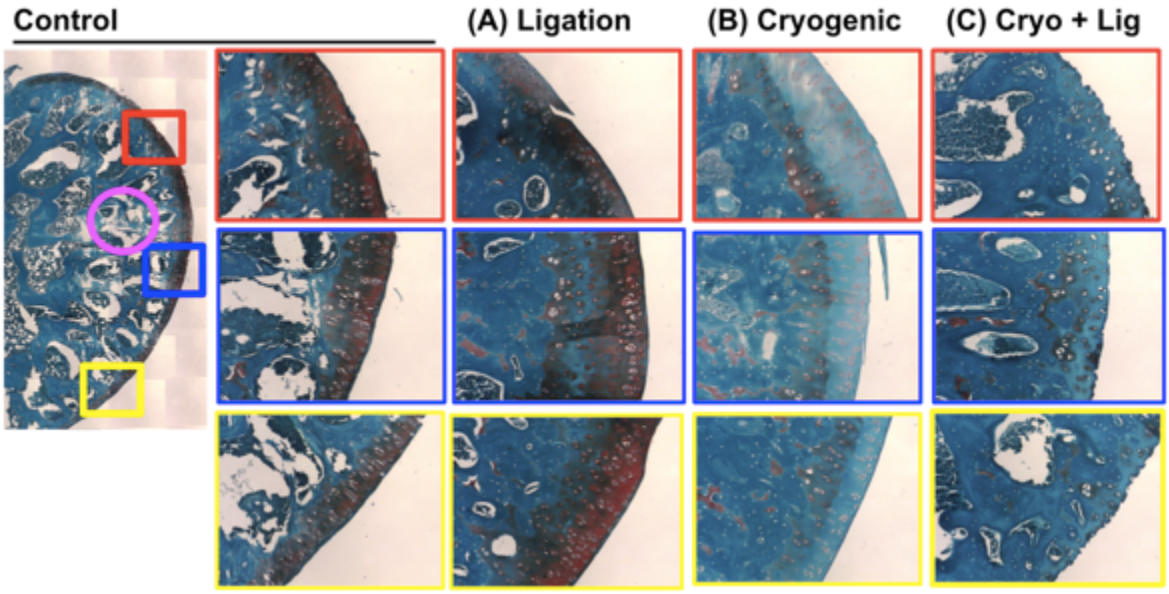

Figure 48. Saf-O/fast green staining of the medial femoral condyle of the contralateral control, group A) ligation, group B) cryogenic insult, and group C) cryogenic insult in combination with ligation. Magenta circle selects the drill hole/lesion site location. The red box shows 20x magnification of the top section of the cartilage; blue, of the middle section; and yellow, of the bottom section.

In this preliminary study, we observed an effect in the region of the initial lesion site as well as an effect on the articular cartilage in groups B and C. However, group C showed severe damage to the shaft of the femur, which might suggest that the insult created in this group is too drastic for what our goal was. We, therefore, concluded that cryogenic insult alone may be sufficient to accomplish our objective. We followed this study with three other ones, in which we sought to optimize the different parameters of the thermal insult (duration and frequency).

At the end, we concluded that it was the liquid nitrogen that was affecting the articular cartilage, thus this effect was not secondary to the osteonecrotic lesion. More specifically, spraying of the liquid nitrogen was having a direct effect on the cartilage regardless of duration and frequency of the treatment. We tried to control for this variable

with a different nozzle for the liquid nitrogen sprayer, which was the same diameter size as the drill hole (Figure 46). We hoped that this precaution would limited the uncontrolled spraying, and we did see an improve articular cartilage composition in studies to follow.

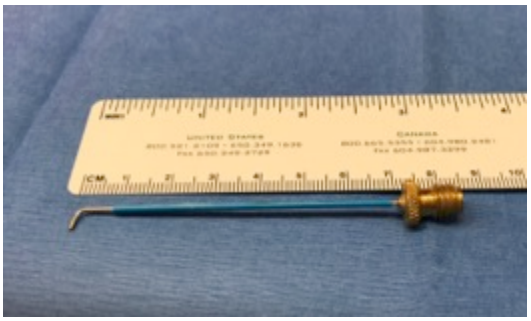

Figure 49. Attachment for the liquid nitrogen sprayer/gun, of the same diameter as the drill hole (0.5 mm).

Moreover, on the bone side, we concluded that this technique could not be localized because of the nature of the thermal insult. By decreasing the duration and frequency, we would fall below the minimum threshold and not longer see osteonecrosis in this model. In other words, this model had two settings: osteonecrotic death throughout the condyle and no detectable cell death. Because of our inability to localize the lesion in this model and the damage observed to the cartilage, this surgical procedure was abandoned.

A.4 Mechanical-barrier insult

A.4.1 Surgical procedure

The Georgia Institute of Technology IACUC approved all animal procedures (#A17023). The mechanical-barrier approach consisted of inserting a hollow

tube in the bone of the femoral condyle with the expectation that the bone in contact with this surface would undergo osteonecrosis. It was hypothesized that, after a period of time, when the hollow tube was pulled out, there will be an osteonecrotic lesion akin to OCD.

The lateral aspect of the femoral condyles of male Lewis rats (~400mg) was assessed through blunt dissection. Then, a 2mm biopsy punch was used to core out spacing in the lateral femoral condyle for the microtube. The lateral femoral condyle was chosen as the lesion site because it was anatomically more resistant to this process. We found that medial femoral condyles would collapse more easily under the force of the biopsy punch. Furthermore, a biopsy punch was chosen as our tool to make spacing for inserting the microtube because companies do not manufacture holesaws (or trephine) of the size we needed. In accordance with our success criteria, we did not want to compromise the entire condyle, thus 2 mm diameter was the largest size we could core in the femoral condyle.

The microtube was polyamide-made, 1.98 mm in diameter and 1.5 mm in depth (courtesy of MicroLumen, FL). Before surgeries, it was washed in detergent and subsequent water washes in the sonicator, and then autoclaved sterilized. The microtubes were fit-pressed into the spacing made by the biopsy punch, in the lateral condyle. One week after surgery, a second surgery took place to remove the microtubes. Animals were taken down 2 weeks after the second surgery.

In sham animals, the biopsy punch was used to make the spacing for the microtube, but no microtube was inserted. The right, contralateral legs were used as naïve controls.

A.4.2 Results and discussion

In this pilot study, we observed morphological differences in the bone at the site of the insult, for both OCD and sham groups (Figure 50). Remodeling is typical a sign of active repair, and thus does not suggest necrosis at the lesion site. Histology would have to be performed in order to truly assess whether there is osteonecrosis at the site (DAPI staining).

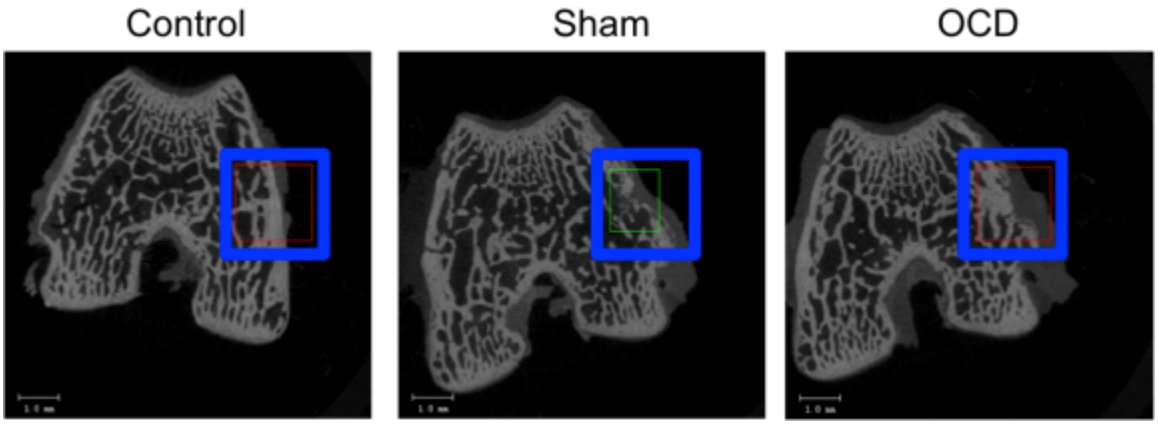

Figure 50. uCT scans showed signs of bone remodeling at the lesion sites (blue square) in both sham and OCD groups.

REFERENCES

1. Kotlarz, H., et al., *Insurer and out-of-pocket costs of osteoarthritis in the US.* Arthritis & Rheumatism, 2009. **60**(12): p. 3546-3553.

2. Amoako, A.O. and G.G.A. Pujalte, *Osteoarthritis in Young, Active, and Athletic Individuals.* Clin Med Insights Arthritis Musculoskelet Disord, 2014. **7**: p. 27-32.

3. Willett, N.J., et al., *Intra-articular injection of micronized dehydrated human amnion/chorion membrane attenuates osteoarthritis development.* Arthritis Res Ther, 2014. **16**(1).

4. Krause, M., et al., *Healing predictors of stable juvenile osteochondritis dissecans knee lesions after 6 and 12 months of nonoperative treatment.* Am J Sports Med, 2013. **41**(10): p. 2384-2391.

5. Cahill, B.R., M.R. Phillips, and N. Navarro, *The results of conservative management of juvenile osteochondritis dissecans using joint scintigraphy: a prospective study.* Am J Sports Med, 1989. **17**(5): p. 601-605.

6. Wall, E.J., J. Vourazeris, and G.D. Myer, *The healing potential of stable juvenile osteochondritis dissecans knee lesions.* J Bone Joint Surg Am, 2008. **90**(12): p. 2655-2664.

7. Eismann, E.A., et al., *Management strategies for osteochondritis dissecans of the knee in the skeletally immature athlete.* J Orthop Sports Phys Ther, 2014. **44**(9): p. 665-79.

8. *Arthritis: National Statistics*. 2015.

9. Tanna, S., *Osteoarthritis: Opportunities to addess pharmaceutical gaps*, in *Osteoarthritis*. 2004: World Health Organization.

10. Kapoor, M., et al., *Role of proinflammatory cytokines in the pathophysiology of osteoarthritis.* Nat Rev Rheumatol, 2011. **7**(1): p. 33-42.

11. Sellam, J. and F. Berenbaum, *The role of synovitis in pathophysiology and clinical symptoms of osteoarthritis.* Nat Rev Rheumatol, 2010. **6**(11): p. 625-35.

12. Robinson, W.H., et al., *Low-grade inflammation as a key mediator of the pathogenesis of osteoarthritis.* Nat Rev Rheumatol, 2016. **12**(10): p. 580-92.

13. Murphy, L. and C.G. Helmick, *The impact of osteoarthritis in the United States: A population-health perspective.* American Journal of Nursing, 2012. **112**(3).

14. Zhang, Y. and J.M. Jordan, *Epidemiology of Osteoarthritis.* Clin Geriatr Med, 2010. **26**(3): p. 355-69.

15. Lawrence, R.C., et al., *Estimates of the prevalence of arthritis and other rheumatic conditions in the United States. Part II.* Arthritis Rheum, 2008. **58**(1): p. 26-35.

16. Murphy, L., et al., *Lifetime risk of symptomatic knee osteoarthritis.* Arthritis Rheum, 2008. **59**(9): p. 1207-13.

17. Krasnokutsky, S., et al., *Current concepts in the pathogenesis of osteoarthritis.* Osteoarthritis Cartilage, 2008. **16 Suppl 3**: p. S1-3.

18. Afonso, V., et al., *Reactive oxygen species and superoxide dismutases: role in joint diseases.* Joint Bone Spine, 2007. **74**(4): p. 324-9.

19. Loeser, R.F., *Molecular Mechanisms of Cartilage Destruction: Mechanics, Inflammatory Mediators, and Aging Collide.* Arthritis Rheum, 2006. **54**(5): p. 1357-60.

20. Kim, H.A. and F.J. Blanco, *Cell death and apoptosis in osteoarthritic cartilage.* Curr Drug Targets, 2007. **8**(2): p. 333-45.

21. Blanco, F.J., et al., *Osteoarthritis chondrocytes die by apoptosis. A possible pathway for osteoarthritis pathology.* Arthritis Rheum, 1998. **41**(2): p. 284-9.

22. Ayral, X., et al., *Arthroscopic evaluation of chondropathy in osteoarthritis of the knee.* J Rheumatol, 1996. **23**(4): p. 698-706.

23. Ayral, X., et al., *Synovitis: a potential predictive factor of structural progression of medial tibiofemoral knee osteoarthritis -- results of a 1 year longitudinal arthroscopic study in 422 patients.* Osteoarthritis Cartilage, 2005. **13**(5): p. 361-7.

24. Goldring, S.R., *Alterations in periarticular bone and cross talk between subchondral bone and articular cartilage in osteoarthritis.* Ther Adv Musculoskelet Dis, 2012. **4**(4): p. 249-58.

25. Goldring, M.B. and S.R. Goldring, *Articular cartilage and subchondral bone in the pathogenesis of osteoarthritis.* Ann N Y Acad Sci, 2010. **1192**: p. 230-7.

26. Walsh, D.A., et al., *Angiogenesis in the synovium and at the osteochondral junction in osteoarthritis.* Osteoarthritis and Cartilage, 2007. **15**: p. 743-751.

27. Goldring, S.R., *Role of bone in osteoarthritis pathogenesis.* Med Clin North Am, 2009. **93**(1): p. 25-35, xv.

28. Sandell, L.J. and T. Aigner, *Articular cartilage and changes in arthritis. An introduction: cell biology of osteoarthritis.* Arthritis Res, 2001. **3**(2): p. 107-13.

29. Matyas, J.R., L.J. Sandell, and M.E. Adams, *Gene expression of type II collagens in chondro-osteophytes in experimental osteoarthritis.* Osteoarthritis Cartilage, 1997. **5**(2): p. 99-105.

30. Blom, A.B., et al., *Synovial lining macrophages mediate osteophyte formation during experimental osteoarthritis.* Osteoarthritis Cartilage, 2004. **12**(8): p. 627-35.

31. Blom, A.B., et al., *Crucial role of macrophages in matrix metalloproteinase-mediated cartilage destruction during experimental osteoarthritis: involvement of matrix metalloproteinase 3.* Arthritis Rheum, 2007. **56**(1): p. 147-57.

32. van Lent, P.L., et al., *Crucial role of synovial lining macrophages in the promotion of transforming growth factor beta-mediated osteophyte formation.* Arthritis Rheum, 2004. **50**(1): p. 103-11.

33. Grimm, N.L., et al., *Osteochondritis dissecands of the knee: Pathoanatomy, epidemiology, and diagnosis.* Clin Sports Med, 2014. **33**: p. 181-188.

34. Shea, K.G., et al., *Osteochondritis dissecans knee histology studies have variable findings and theories of ethiology.* Clin Orthop Relat Res, 2012. **471**(4): p. 1127-1136.

35. Yonetani, Y., et al., *Histological evaluation of juvenile osteochondritis dissecans of the knee: a case series.* Knee Surg Sports Traumatol Arthrosc, 2010. **18**: p. 723-730.

36. Schindler, O.S., *Osteochondritis dissecans of the knee.* Current Orthopaedics, 2007. **21**: p. 47-58.

37. Laor, T., et al., *Juvenile Osteochondritis Dissecans: Is it a growth disturbance of the secondary physis of the epiphysis?* Am J Reseach, 2012. **199**: p. 1121-1128.

38. *The diagnosis and treatment of osteochondritis dissecans: Guideline and evidence report*, in *AAOS Clinical Practice Guidelines Unit*. 2010, American Academy of Orthopaedic Surgeons.

39. Owens, J.B. and C. Lattermann, *Management of Osteochondritis Dissecans of the Knee*, in *Biologic Joint Reconstruction: Alternatives to arthroplasty*. 2009, Slack Incorporated.

40. Weiss, J.M., et al., *The Incidence of Surgery in Osteochondritis Dissecans in Children and Adolescents.* Orthop J Sports Med, 2016. **4**(3).

41. Sakata, K., et al., *Comparison between normal and loose fragment chondrocytes in proliferation and redifferentiation potential.* International Orthopaedics, 2012. **37**: p. 159-165.

42. O'Connor, M., et al., *Osteochondritis dissecans of the knee in children. A comparison of MRI and arthroscopic findings.* J Bone Joint Surg Br, 2002. **84**(2): p. 258–262.

43. Milewski, M.D., *Osteochondritis Dissecans: Diagnosis and Treatment Opetions for Atletes*. Clinicas Review Articles. 2014, Elsevier Health Sciences.

44. *ICRS Clinical Cartilage Injury Evaluation System*. 2000, International Cartilage Repair Society: http://www.cartilage.org/.

45. Kijowski, R., et al., *Juvenile versus adult osteochondritis dissecans of the knee: appropriate MR imaging criteria for instability.* Radiology, 2008. **148**(2): p. 571-8.

46. Robertson, W., B.T. Kelly, and D.W. Green, *Osteochondritis dissecans of the knee in children.* Current Opinion in Pediatrics, 2003. **15**: p. 38-44.

47. Erickson, B.J., et al., *Surgical management of osteochondritis dissecans of the knee.* Curr Rev Musculoskelet Med, 2013. **6**: p. 102-114.

48. Ganley, T.J., *Symposia: Treatment of Osteochondritis Dissecans in Children and Adolescents*, in *ISAKOS Congress*. 2013: Toronto, Canada.

49. Sanders, T.L., et al., *Nonoperative Management of Osteochondritis Dissecans of the Knee: Progression to Osteoarthritis and Arthroplasty at Mean 13-Year Follow-up.* Orthop J Sports Med, 2017. **5**(7).

50. Winthrop, Z., G. Pinkowsky, and W. Hennrikus, *Surgical treatment for osteochondritis dessicans of the knee.* Curr Rev Musculoskelet Med, 2015. **8**(4): p. 467-75.

51. Edmonds, E. and J. Polousky, *A review of knowledge in osteochondritis dissecans: 123 years of minimal evolution from Konig to the ROCK study group.* Clin Orthop Relat Res, 2013. **471**(4): p. 1118-26.

52. Aichroth, P., *Osteochondritis dissecans of the knee. A clinical survey.* J Bone Joint Surg Br, 1971. **53**(3): p. 440-7.

53. Hefti, F., et al., *Osteochondritis dissecans: a multicenter study of the European Pediatric Orthopedic Society.* J Pediatr Orthop B, 1999. **8**(4): p. 231-45.

54. Zanon, G., G. Di Vico, and M. Marullo, *Osteochondritis dissecans of the knee.* Joints, 2014. **2**(1): p. 29-36.

55. Pape, D., et al., *Disease-specific clinical problems associated with the subchondral bone.* Knee Surg Sports Traumatol Arthrosc, 2010. **18**(4): p. 448-62.

56. Enneking, W.F., *Clinical musculoskeletal pathology*. 3 ed. 1990: Florida: University of Florida Press.

57. Rogers, W.M. and H. Gladstone, *Vascular foramina and arterial supply of the distal end of the femur.* J Bone Joint Surg Am, 1950. **32 a**(4): p. 867-74.

58. Milgram, J.W., *Radiological and pathological manifestations of osteochondritis dissecans of the distal femur. A study of 50 cases.* Radiology, 1978. **126**(2): p. 305-11.

59. Uozumi, H., et al., *Histologic findings and possible causes of osteochondritis dissecans of the knee.* Am J Sports Med, 2009. **37**(10): p. 2003-8.

60. Petrie, P.W., *Aetiology of osteochondritis dissecans. Failure to establish a familial background.* J Bone Joint Surg Br, 1977. **59**(3): p. 366-7.

61. Mubarak, S.J. and N.C. Carroll, *Juvenile osteochondritis dissecans of the knee: etiology.* Clin Orthop Relat Res, 1981(157): p. 200-11.

62. Jeong, J.H., R. Mascarenhas, and H.S. Yoon, *Bilateral Osteochondritis Dissecans of the Femoral Condyles in Both Knees: A Report of Two Sibling Cases.* Knee Surg Relat Res, 2013. **25**(2): p. 88-92.

63. Mackie, T. and R.M. Wilkins, *Case report: Osteochondritis dissecans in twins: treatment with fresh osteochondral grafts.* Clin Orthop Relat Res, 2010. **468**(3): p. 893-7.

64. Woods, K. and I. Harris, *Osteochondritis dissecans of the talus in identical twins.* J Bone Joint Surg Br, 1995. **77**(2): p. 331.

65. Onoda, S., et al., *Osteochondritis dissecans of the knee in identical twins: a report of two cases.* J Orthop Surg (Hong Kong), 2012. **20**(1): p. 108-10.

66. Richie, L.B. and M.J. Sytsma, *Matching osteochondritis dissecans lesions in identical twin brothers.* Orthopedics, 2013. **36**(9): p. e1213-6.

67. Mei-Dan, O., et al., *Bilateral osteochondritis dissecans of the knees in monozygotic twins: the genetic factor and review of the etiology.* Am J Orthop (Belle Mead NJ), 2009. **38**(9): p. E152-5.

68. Gans, I., et al., *Identical osteochondritis dissecans lesions of the knee in sets of monozygotic twins.* Orthopedics, 2013. **36**(12): p. e1559-62.

69. Gornitzky, A.L., et al., *Osteochondritis Dissecans Lesions in Family Members: Does a Positive Family History Impact Phenotypic Potency?* Clin Orthop Relat Res, 2017. **475**(6): p. 1573-1580.

70. Barrie, H.J., *Hypertrophy and laminar calcification of cartilage in loose bodies as probable evidence of an ossification abnormality.* J Pathol, 1980. **132**(2): p. 161-8.

71. Barrie, H.J., *Hypothesis--a diagram of the form and origin of loose bodies in osteochondritis dissecans.* J Rheumatol, 1984. **11**(4): p. 512-3.

72. Trueta, J. and A. Trias, *The vascular contribution to osteogenesis. IV. The effect of pressure upon the epiphysial cartilage of the rabbit.* J Bone Joint Surg Br, 1961. **43-b**: p. 800-13.

73. Ytrehus, B., C.S. Carlson, and S. Ekman, *Etiology and pathogenesis of osteochondrosis.* Vet Pathol, 2007. **44**(4): p. 429-48.

74. Riddell, C., *Studies on the pathogenesis of tibial dyschondroplasia in chickens. III. Effect of body weight.* Avian Dis, 1975. **19**(3): p. 497-505.

75. Olstad, K., et al., *Transection of vessels in epiphyseal cartilage canals leads to osteochondrosis and osteochondrosis dissecans in the femoro-patellar joint of foals; a potential model of juvenile osteochondritis dissecans.* Osteoarthritis Cartilage, 2013. **21**(5): p. 730-8.

76. Pascual-Garrido, C., et al., *Viability of loose body fragments in osteochondritis dissecans of the knee. A series of cases.* Int Orthop, 2010. **34**(6): p. 827-831.

77. Skagen, P.S., et al., *Osteochondritis dissecans (OCD), an endoplasmic reticulum storage disease?: a morphological and molecular study of OCD fragments.* Scand J Med Sci Sports, 2011. **21**(6): p. e17-33.

78. Xu, M., et al., *Chondrocytes Derived From Mesenchymal Stromal Cells and Induced Pluripotent Cells of Patients With Familial Osteochondritis Dissecans Exhibit an Endoplasmic Reticulum Stress Response and Defective Matrix Assembly.* Stem Cells Transl Med, 2016. **5**(9): p. 1171-81.

79. Desjardin, C., et al., *Involvement of mitochondrial dysfunction and ER-stress in the physiopathology of equine osteochondritis dissecans (OCD).* Exp Mol Pathol, 2014. **96**(3): p. 328-38.

80. Thysen, S., F.P. Luyten, and R.J. Lories, *Targets, models and challenges in osteoarthritis research.* Dis Model Mech, 2015. **8**(1): p. 17-30.

81. Thote, T., et al., *Localized 3D analysis of cartilage composition and morphology in small animal models of joint degeneration.* Osteoarthritis and Cartilage, 2013. **21**(8): p. 1132-1141.

82. Wei, T., et al., *Analysis of early changes in the articular cartilage transcriptisome in the rat meniscal tear model of osteoarthritis: pathway comparisons with the rat anterior cruciate transection model and with human osteoarthritic cartilage.* Osteoarthritis Cartilage, 2010. **18**(7): p. 992-1000.

83. Appleton, C.T., et al., *Global analyses of gene expression in early experimental osteoarthritis.* Arthritis Rheum, 2007. **56**(6): p. 1854-68.

84. Endo, J., et al., *Comparative Analysis of Gene Expression between Cartilage and Menisci in Early-Phase Osteoarthritis of the Knee-An Animal Model Study.* J Knee Surg, 2017.

85. Willems, E., L. Leyns, and J. Vandesompele, *Standardization of real-time PCR gene expression data from independent biological replicates.* Anal Biochem, 2008. **379**(1): p. 127-9.

86. Hwang, S.G., et al., *Wnt-7a causes loss of differentiated phenotype and inhibits apoptosis of articular chondrocytes via different mechanisms.* J Biol Chem, 2004. **279**(25): p. 26597-604.

87. Lories, R.J. and F.P. Luyten, *Osteoimmunology: Wnt antagonists: for better or worse?* Nat Rev Rheumatol, 2009. **5**(8): p. 420-1.

88. Denhardt, D.T., et al., *Osteopontin as a means to cope with environmental insults: regulation of inflammation, tissue remodeling, and cell survival.* J Clin Invest, 2001. **107**(9): p. 1055-61.

89. Ryu, J.H., et al., *Hypoxia-inducible factor-2alpha regulates Fas-mediated chondrocyte apoptosis during osteoarthritic cartilage destruction.* Cell Death Differ, 2012. **19**(3): p. 440-50.

90. Cecil, D.L. and R. Terkeltaub, *Transamidation by transglutaminase 2 transforms S100A11 calgranulin into a procatabolic cytokine for chondrocytes.* J Immunol, 2008. **180**(12): p. 8378-85.

91. Yin, X., et al., *Tissue transglutaminase (TG2) activity regulates osteoblast differentiation and mineralization in the SAOS-2 cell line.* Braz J Med Biol Res, 2012. **45**(8): p. 693-700.

92. Dell'Accio, F., et al., *Activation of WNT and BMP signaling in adult human articular cartilage following mechanical injury.* Arthritis Res Ther, 2006. **8**(5): p. R139.

93. Dell'accio, F., et al., *Identification of the molecular response of articular cartilage to injury, by microarray screening: Wnt-16 expression and signaling after injury and in osteoarthritis.* Arthritis Rheum, 2008. **58**(5): p. 1410-21.

94. Leijten, J.C., et al., *Gremlin 1, frizzled-related protein, and Dkk-1 are key regulators of human articular cartilage homeostasis.* Arthritis Rheum, 2012. **64**(10): p. 3302-12.

95. Bluteau, G., et al., *Matrix metalloproteinase-1, -3, -13 and aggrecanase-1 and -2 are differentially expressed in experimental osteoarthritis.* Biochimica et Biophysica Acta, 2001: p. 147-158.

96. Rucklidge, G.J., G. Milne, and S.P. Robins, *Collagen type X: a component of the surface of normal human, pig, and rat articular cartilage.* Biochem Biophys Res Commun, 1996. **224**(2): p. 297-302.

97. Chevalier, X., *Fibronectin, cartilage, and osteoarthritis.* Semin Arthritis Rheum, 1993. **22**(5): p. 307-18.

98. Lust, G., N. Burton-Wurster, and H. Leipold, *Fibronectin as a marker for osteoarthritis.* J Rheumatol, 1987. **14 Spec No**: p. 28-9.

99. Perez-Garcia, S., et al., *Healthy and Osteoarthritic Synovial Fibroblasts Produce a Disintegrin and Metalloproteinase with Thrombospondin Motifs 4, 5, 7, and 12: Induction by IL-1beta and Fibronectin and Contribution to Cartilage Damage.* Am J Pathol, 2016. **186**(9): p. 2449-61.

100. Satkunananthan, P.B., et al., *In vivo fluorescence reflectance imaging of protease activity in a mouse model of post-traumatic osteoarthritis.* Osteoarthritis Cartilage, 2014. **22**(10): p. 1461-9.

101. Troeberg, L. and H. Nagase, *Proteases involved in cartilage matrix degradation in osteoarthritis.* Biochim Biophys Acta, 2012. **1824**(1): p. 133-45.

102. Chia, S.L., et al., *Fibroblast growth factor 2 is an intrinsic chondroprotective agent that suppresses ADAMTS-5 and delays cartilage degradation in murine osteoarthritis.* Arthritis Rheum, 2009. **60**(7): p. 2019-27.

103. Liu-Bryan, R. and R. Terkeltaub, *Emerging regulators of the inflammatory process in osteoarthritis.* Nat Rev Rheumatol, 2015. **11**(1): p. 35-44.

104. Yang, S., et al., *Hypoxia-inducible factor-2alpha is a catabolic regulator of osteoarthritic cartilage destruction.* Nat Med, 2010. **16**(6): p. 687-93.

105. Xu, Z., et al., *Cartilaginous Metabolomic Study Reveals Potential Mechanisms of Osteophyte Formation in Osteoarthritis.* J Proteome Res, 2017. **16**(4): p. 1425-1435.

106. Hashimoto, S., et al., *Development and regulation of osteophyte formation during experimental osteoarthritis.* Osteoarthritis Cartilage, 2002. **10**(3): p. 180-7.

107. Jenner, F., et al., *Differential Gene Expression of the Intermediate and Outer Interzone Layers of Developing Articular Cartilage in Murine Embryos.* Stem Cells Dev, 2014. **23**(16): p. 1883-98.

108. Cho, H.H., et al., *NF-kappaB activation stimulates osteogenic differentiation of mesenchymal stem cells derived from human adipose tissue by increasing TAZ expression.* J Cell Physiol, 2010. **223**(1): p. 168-77.

109. Hess, K., et al., *TNFalpha promotes osteogenic differentiation of human mesenchymal stem cells by triggering the NF-kappaB signaling pathway.* Bone, 2009. **45**(2): p. 367-76.

110. Nam, D., et al., *T-lymphocytes enable osteoblast maturation via IL-17F during the early phase of fracture repair.* PLoS One, 2012. **7**(6): p. e40044.

111. Sonomoto, K., et al., *Interleukin-1beta induces differentiation of human mesenchymal stem cells into osteoblasts via the Wnt-5a/receptor tyrosine kinase-like orphan receptor 2 pathway.* Arthritis Rheum, 2012. **64**(10): p. 3355-63.

112. Yeh, L.C., M.C. Zavala, and J.C. Lee, *Osteogenic protein-1 and interleukin-6 with its soluble receptor synergistically stimulate rat osteoblastic cell differentiation.* J Cell Physiol, 2002. **190**(3): p. 322-31.

113. Teeple, E., et al., *Animal models of osteoarthritis: challenges of model selection and analysis.* Aaps j, 2013. **15**(2): p. 438-46.

114. Goldring, M.B. and M. Otero, *Inflammation in osteoarthritis.* Curr Opin Rheumatol, 2011. **23**(5): p. 471-8.

115. Ren, T., Y. van der Merwe, and M.B. Steketee, *Developing Extracellular Matrix Technology to Treat Retinal or Optic Nerve Injury.* eNeuro, 2015. **2**(5).

116. Koob, T.J., et al., *Properties of dehydrated human amnion/chorion composite grafts: Implications for wound repair and soft tissue regeneration.* J Biomed Mater Res B Appl Biomater, 2014. **102**(6): p. 1353-62.

117. Koob, T.J., et al., *Biological properties of dehydrated human amnion/chorion composite graft: implications for chronic wound healing.* Int Wound J, 2013. **10**(5): p. 493-500.

118. Niknejad, H., et al., *Properties of the amniotic membrane for potential use in tissue engineering.* Eur Cell Mater, 2008. **15**: p. 88-99.

119. Sheikh, E.S., E.S. Sheikh, and D.E. Fetterolf, *Use of dehydrated human amniotic membrane allografts to promote healing in patients with refractory non healing wounds.* Int Wound J, 2014. **11**(6): p. 711-7.

120. Chevalier, X., et al., *Intraarticular injection of anakinra in osteoarthritis of the knee: a multicenter, randomized, double-blind, placebo-controlled study.* Arthritis Rheum, 2009. **61**(3): p. 344-52.

121. Kraus, V.B., et al., *Effects of intraarticular IL1-Ra for acute anterior cruciate ligament knee injury: a randomized controlled pilot trial (NCT00332254).* Osteoarthritis Cartilage, 2012. **20**(4): p. 271-8.

122. Gallagher, B., et al., *Chondroprotection and the prevention of osteoarthritis progression of the knee: a systematic review of treatment agents.* Am J Sports Med, 2015. **43**(3): p. 734-44.

123. Magnano, M.D., et al., *A pilot study of tumor necrosis factor inhibition in erosive/inflammatory osteoarthritis of the hands.* J Rheumatol, 2007. **34**(6): p. 1323-7.

124. Cho, H., et al., *Study of Osteoarthritis Treatment with Anti-Inflammatory Drugs: Cyclooxygenase-2 Inhibitor and Steroids.* Biomed Res Int, 2015. **2015**.

125. Verbruggen, G., *Chondroprotective drugs in degenerative joint diseases.* Rheumatology, 2006. **45**(2): p. 129-138.

126. Shi, C. and E.G. Pamer, *Monocyte recruitment during infection and inflammation.* Nat Rev Immunol, 2014. **11**(11): p. 762-74.

127. Zdrenghea, M.T., et al., *The role of macrophage IL-10/innate IFN interplay during virus-induced asthma.* Rev Med Virol, 2015. **25**(1): p. 33-49.

128. Fleetwood, A.J., et al., *Granulocyte-macrophage colony-stimulating factor (CSF) and macrophage CSF-dependent macrophage phenotypes display differences in cytokine profiles and transcription factor activities: implications for CSF blockade in inflammation.* J Immunol, 2007. **178**(8): p. 5245-52.

129. Jaguin, M., et al., *Polarization profiles of human M-CSF-generated macrophages and comparison of M1-markers in classically activated macrophages from GM-CSF and M-CSF origin.* Cell Immunol, 2013. **281**(1): p. 51-61.

130. Fleetwood, A.J., et al., *GM-CSF- and M-CSF-dependent macrophage phenotypes display differential dependence on type I interferon signaling.* J Leukoc Biol, 2009. **86**(2): p. 411-21.

131. Martinez, F.O., et al., *Transcriptional profiling of the human monocyte-to-macrophage differentiation and polarization: new molecules and patterns of gene expression.* J Immunol, 2006. **177**(10): p. 7303-11.

132. Lacey, D.C., et al., *Defining GM-CSF- and macrophage-CSF-dependent macrophage responses by in vitro models.* J Immunol, 2012. **188**(11): p. 5752-65.

133. Verreck, F.A., et al., *Phenotypic and functional profiling of human proinflammatory type-1 and anti-inflammatory type-2 macrophages in response to microbial antigens and IFN-gamma- and CD40L-mediated costimulation.* J Leukoc Biol, 2006. **79**(2): p. 285-93.

134. Mantovani, A., et al., *The chemokine system in diverse forms of macrophage activation and polarization.* Trends Immunol, 2004. **25**(12): p. 677-86.

135. Vannier, E., L.C. Miller, and C.A. Dinarello, *Coordinated antiinflammatory effects of interleukin 4: interleukin 4 suppresses interleukin 1 production but up-regulates gene expression and synthesis of interleukin 1 receptor antagonist.* Proc Natl Acad Sci U S A, 1992. **89**(9): p. 4076-80.

136. Cauli, A., G. Yanni, and G.S. Panayi, *Interleukin-1, interleukin-1 receptor antagonist and macrophage populations in rheumatoid arthritis synovial membrane.* Br J Rheumatol, 1997. **36**(9): p. 935-40.

137. Andersson, J., et al., *Lipopolysaccharide induces human interleukin-1 receptor antagonist and interleukin-1 production in the same cell.* Eur J Immunol, 1992. **22**(10): p. 2617-23.

138. Arend, W.P., et al., *Biological properties of recombinant human monocyte-derived interleukin 1 receptor antagonist.* J Clin Invest, 1990. **85**(5): p. 1694-7.

139. Arend, W.P. and B.P. Coll, *Interaction of recombinant monocyte-derived interleukin 1 receptor antagonist with rheumatoid synovial cells.* Cytokine, 1991. **3**(5): p. 407-13.

140. Bondeson, J., et al., *The role of synovial macrophages and macrophage-produced cytokines in driving aggrecanases, amtrix metalloproteinases, and other destructive and inflammatory responses in osteoarthritis.* Arthritis Research & Therapy, 2006. **8**(6).

141. Nasu, A., et al., *Genetically Matched Human iPS Cells Reveal that Propensity for Cartilage and Bone Differentiation Differs with Clones, not Cell Type of Origin.* PLOS ONE, 2013. **8**(1): p. e53771.

142. Brown, S.E., W. Tong, and P.H. Krebsbach, *The Derivation of Mesenchymal Stem Cells from Human Embryonic Stem Cells.* Cells Tissues Organs, 2008. **189**(1-4): p. 256-60.

143. Teramura, T., et al., *Induction of mesenchymal progenitor cells with chondrogenic property from mouse-induced pluripotent stem cells.* Cell Reprogram, 2010. **12**(3): p. 249-61.

144. Dominici, M., et al., *Minimal criteria for defining multipotent mesenchymal stromal cells. The International Society for Cellular Therapy position statement.* Cytotherapy, 2006. **8**(4): p. 315-7.

145. Mood, A.M., F.A. Graybill, and D.C. Boes, *Introduction to the Theory of Statistics*. 1974, New York: McGraw-Hill.

146. Council, N.R., *Appendix F: Construction of confidence intervals for mathematical combinations of random variables*. Regulating pesticides. 1980, Washington, D.C.: National Academies.

147. Cohen, J., *Statistical power analysis for the behavioral sciences. 2nd*. 1988, Hillsdale, NJ: erlbaum.

148. Hedges, L.V., *Olkin, 1.(1985). Statistical methods for meta-analysis.* Orlando, FL: Academic Pre55, 1990.

149. Toh, W.S., et al., *Differentiation and enrichment of expandable chondrogenic cells from human embryonic stem cells in vitro.* J Cell Mol Med, 2009. **13**(9b): p. 3570-90.

150. Chen, H., et al., *Runx2 Regulates Endochondral Ossification through Control of Chondrocyte Proliferation and Differentiation.* J Bone Miner Res, 2014. **29**(12): p. 2653-65.

151. Ramkisoensing, A.A., et al., *Human Embryonic and Fetal Mesenchymal Stem Cells Differentiate toward Three Different Cardiac Lineages in Contrast to Their Adult Counterparts.* PLOS ONE, 2011. **6**(9): p. e24164.

152. Bianco, P., P.G. Robey, and P.J. Simmons, *Mesenchymal stem cells: revisiting history, concepts, and assays.* Cell Stem Cell, 2008. **2**(4): p. 313-9.

153. Lin, C.S., et al., *Commonly Used Mesenchymal Stem Cell Markers and Tracking Labels: Limitations and Challenges.* Histol Histopathol, 2013. **28**(9): p. 1109-16.

154. Nassiri, F., et al., *Endoglin (CD105): a review of its role in angiogenesis and tumor diagnosis, progression and therapy.* Anticancer Res, 2011. **31**(6): p. 2283-90.

155. Anderson, P., et al., *CD105 (Endoglin)-Negative Murine Mesenchymal Stromal Cells Define a New Multipotent Subpopulation with Distinct Differentiation and Immunomodulatory Capacities.* 2013. **8**(10).

156. Yang, L., et al., *Multiple signals induce endoplasmic reticulum stress in both primary and immortalized chondrocytes resulting in loss of differentiation, impaired cell growth, and apoptosis.* J Biol Chem, 2005. **280**(35): p. 31156-65.

157. Kim, P.S. and P. Arvan, *Endocrinopathies in the family of endoplasmic reticulum (ER) storage diseases: disorders of protein trafficking and the role of ER molecular chaperones.* Endocr Rev, 1998. **19**(2): p. 173-202.

158. Hughes, A., et al., *Endoplasmic Reticulum Stress and Unfolded Protein Response in Cartilage Pathophysiology; Contributing Factors to Apoptosis and Osteoarthritis.* Int J Mol Sci, 2017. **18**(3).

159. Hamamura, K. and H. Yokota, *Stress to Endoplasmic Reticulum of Mouse Osteoblasts Induces Apoptosis and Transcriptional Activation for Bone Remodeling.* FEBS Lett, 2007. **581**(9): p. 1769-74.

160. Wu, J. and R.J. Kaufman, *From acute ER stress to physiological roles of the Unfolded Protein Response.* Cell Death And Differentiation, 2006. **13**: p. 374.

161. Cao, S.S. and R.J. Kaufman, *Unfolded protein response.* Current Biology, 2012. **22**(16): p. R622-R626.

162. Zamarbide, M., et al., *Phenyl acyl acids attenuate the unfolded protein response in tunicamycin-treated neuroblastoma cells.* PLoS One, 2013. **8**(8): p. e71082.

163. Ding, W.X., et al., *Differential effects of endoplasmic reticulum stress-induced autophagy on cell survival.* J Biol Chem, 2007. **282**(7): p. 4702-10.

164. Oslowski, C.M. and F. Urano, *Measuring ER stress and the unfolded protein response using mammalian tissue culture system.* Methods Enzymol, 2011. **490**: p. 71-92.

165. Audouard, C., et al., *Oocyte–Targeted Deletion Reveals That Hsp90b1 Is Needed for the Completion of First Mitosis in Mouse Zygotes.* PLOS ONE, 2011. **6**(2): p. e17109.

166. Zhu, G. and A.S. Lee, *Role of the Unfolded Protein Response, GRP78 and GRP94 in Organ Homeostasis.* J Cell Physiol, 2015. **230**(7): p. 1413-20.

167. Zenmyo, M., et al., *Gadd45beta expression in chondrosarcoma: a pilot study for diagnostic and biological implications in histological grading.* Diagn Pathol, 2010. **5**: p. 69.

168. Lindert, U., et al., *MBTPS2 mutations cause defective regulated intramembrane proteolysis in X-linked osteogenesis imperfecta.* Nat Commun, 2016. **7**: p. 11920.

169. Widmer, C., et al., *Molecular basis for the action of the collagen-specific chaperone Hsp47/SERPINH1 and its structure-specific client recognition.* Proc Natl Acad Sci U S A, 2012. **109**(33): p. 13243-7.

170. Tavakoli, T., et al., *Self-renewal and differentiation capabilities are variable between human embryonic stem cell lines I3, I6 and BG01V.* BMC Cell Biol, 2009. **10**: p. 44.

171. Féraud, O., et al., *Donor Dependent Variations in Hematopoietic Differentiation among Embryonic and Induced Pluripotent Stem Cell Lines.* PLoS One, 2016. **11**(3).

172. Sundelacruz, S., M. Levin, and D.L. Kaplan, *Comparison of the depolarization response of human mesenchymal stem cells from different donors.* Sci Rep, 2015. **5**: p. 18279.

173. Vitale, A.M., et al., *Variability in the Generation of Induced Pluripotent Stem Cells: Importance for Disease Modeling.* Stem Cells Transl Med, 2012. **1**(9): p. 641-50.

174. Vellanki, R.N., L. Zhang, and A. Volchuk, *OASIS/CREB3L1 is induced by endoplasmic reticulum stress in human glioma cell lines and contributes to the unfolded protein response, extracellular matrix production and cell migration.* PLoS One, 2013. **8**(1): p. e54060.

175. Lyon, R., et al., *Does extracorporeal shock wave therapy enhance healing of osteochondritis dissecans of the rabbit knee?: A pilot study.* Clin Orthop Relat Res, 2013. **471**: p. 1159-1165.

176. Pfeifer, C.G., et al., *Development of a large animal model of osteochondritis dissecans of the knee: A pilot study.* The Orthopaedic Journal of Sports Medicine, 2015. **3**(2).

177. Kon, E., et al., *How to treat osteochondritis dissecans of the knee: Surgical techniques and new trends.* The Journal of Bone and Joint Surgery, Inc., 2012. **94**.

178. Velez, R., et al., *A new preclinical femoral head osteonecrosis model in sheep.* Arch Orthop Trauma Surg, 2011. **131**: p. 5-9.

179. Conzemius, M.G., et al., *A new animal model of femoral head osteonecrosis: One that progresses to human-like mechanical failure.* Journal of Orthopaedic Research, 2006. **20**: p. 303-309.

180. Fan, M., et al., *Experimental animal models of osteonecrosis.* Rheumatol Int, 2011. **31**: p. 983-994.

181. Fondi, C. and A. Franchi, *Definition of bone necrosis by the pathologist.* Clin Cases Miner Bone Metab, 2007. **4**(1): p. 21-26.